MASS MOVEMENT PHENOMENA IN THE WESTERN SAN JUAN MOUNTAINS, COLORADO

A Thesis

by

KAYTAN ANAND KELKAR

Submitted to the Office of Graduate and Professional Studies of
Texas A&M University
in partial fulfillment of the requirements for the degree of

MASTER OF SCIENCE

Chair of Committee,	John R. Giardino
Committee Members,	John D. Vitek
	Franco Marcantonio
Head of Department,	Michael Pope

December 2017

Major Subject: Geology

ABSTRACT

Mass movement is an integral part of the evolution of hillslope morphology, which poses a potential hazard to human activity in mountainous terrain. The San Juan Mountains of southwestern Colorado have an ongoing legacy of slope instability as a result of a complex geologic setting compounded by high-relief topography. Although, landslide studies in the area have focused on the documentation of triggers for slope failure and field mapping, inadequate investigation of components responsible for susceptibility to mass movement still exists. The area was last extensively mapped for mass movement deposits during the 1970s, since then landslide studies have not been undertaken. Therefore, this leads one to ask major questions pertaining to the risk from mass movement in the San Juan Mountains: What are the major components that cause slopes to fail in the San Juan Mountains? And what is the distribution of surficial phenomena, which indicate potential hazards from slope failure?

The aforementioned questions were addressed by fulfilling the following objectives: 1) Identify various components associated with slope failure in the San Juan Mountains; 2) Map areas susceptible to mass movement; and 3) Map features of mass movement in the area. To accomplish these objectives, a 3D Geographic Information Systems (GIS)-based weighted overlay approach was utilized to map susceptibility to landslides. The weighted overlay method was applied in two-phases, including a heuristic approach and a Principal Component Analysis (PCA) technique. This weighted overlay integrated six terrain variables: slope and slope length, aspect, geology,

vegetation cover, and soil drainage. A surficial geomorphological map at a scale of 1:3,000 was constructed, to map the surficial extent of geomorphic phenomenon in the region.

The findings of this study suggests that: 1) Aspect (48%), slope (34%), and geology (9%) have the greatest relative weighted influence on slope failure, 2) the San Juan Mountains are experiencing a general uniform rate of erosion, 3) East and west-facing slopes have the greatest areal coverage and increase the likelihood of high and very high susceptibility to landslides, 4) Class 2 slopes (22.01°- 44°) have the greatest areal coverage also increasing the likelihood for high and very high susceptibility to landslides, 5) Class 2, 3, and 4 slopes are highly correlated to high susceptibility, classes 3 and 4 are highly correlated to very high susceptibility 6) Areas within 50 m from roads are highly susceptible to landslides, 7) Talus and landslide deposits are the most widespread surficial deposits in the area 8) Mapped landforms demarcate the extents of former glaciation of the western San Juan Mountains.

With growing anthropogenic influence in the area, human-induced modification of steep slopes is occurring. A study such as this, combining emerging geospatial, visualization, heuristic, deterministic, and statistical techniques will improve landslide prediction in mountain terrain.

DEDICATION

I dedicate this thesis to my grandparents, mother, and father, Anand Kelkar, who passed away before its completion. He instilled positive virtues which have greatly influenced my upbringing. His teachings have taught me the value of a well-rounded education and to remain a righteous person. Babasaheb, every moment spent with you has been a gift. I will always be indebted to my both grandfathers, Narayanrao Walavalkar and Govind Kelkar, from who I have learned that there is no substitute for hard work. My sincerest Namaskars to all of you.

ACKNOWLEDGEMENTS

I am grateful to my committee chair Dr. Giardino for his immense support and providing me the essential foundations of the discipline of Geomorphology. I thank my committee members, Dr. Vitek and Dr. Marcantonio for their valuable guidance and resourceful inputs throughout this learning process. I would also like to thank Dr. Steve Johnson, who is in charge of the Immersive Visualization Center for his assistance with 3 dimensional data modeling. Thanks also goes to Amy Price, Caitlin Carter, Anastasia Fedotova, Daniel McGinty and Fernando Pachuca for their assistance with fieldwork. Special thanks to Shubek Thapa, Taylor Rowley, Panshu Zhao, and Raquel Granados Aguilar for their patience and advice in GIS and remote sensing. I thank my research colleagues within the High Alpine and Arctic Research Program (HAARP) and the department for their collaborative efforts.

I thank the Department of Geology and Geophysics at Texas A&M University for its continued support throughout the course of my master's education.

Finally, thank you to my mother for her patience, relentless love, and encouragement during this difficult phase in my life.

CONTRIBUTORS AND FUNDING SOURCES

This thesis was supported by the thesis committee comprising, chair Dr. John R. Giardino, and committee members Dr. John D. Vitek and Dr. Franco Marcantonio.

All work for this thesis was funded individually by the student without outside financial contributions.

NOMENCLATURE

ASTER	Advanced Spaceborne Thermal and Emission and Reflection Radiometer
CDOT	Colorado Department of Transportation
DEM	Digital Elevation Model
GIS	Geographic Information Systems
IGU	International Geographical Union
LANDSAT	Formerly Earth Resources Technology Satellite
NDVI	Normalized Difference Vegetation Index
NDWI	Normalized Difference Water Index
NRCS	Natural Resources Conservation Service
PC	Principal Component
PCA	Principal-Component-Analysis
SGU	Subcommission on Geomorphological Mapping
TLS	Terrestrial Laser Scanning
USGS	United States Geological Survey

TABLE OF CONTENTS

Page

LIST OF FIGURES

Page

LIST OF TABLES

Page

CHAPTER I

INTRODUCTION

Mass movement is an integral part of the evolution of hillslope morphology, which poses a potential hazard to human activity in mountains terrain. Hence, the identification and quantification of risk from mass movement is key to saving lives and safeguarding economic interests in mountainous environments. The complex geologic setting and rugged topography of the San Juan Mountains are prone to slope failure. Climate change and increased human development are modifying the equilibrium conditions of relatively steep former ice-contact slope deposits and potentially increase frequencies of mass movement in the area.

The San Juan Mountains are located in southwestern Colorado and encompass an area of ~1,615 km^2 (Figure 1). Composed primarily of volcanic rocks over shales, limestones, and sandstones, the San Juan Mountains were extensively glaciated during the Pleistocene. As a result of this glaciation in concert with active slope forming processes, slopes in the area are over-steepened and are prone to mass movement.

Problem Statement

Mass movement and fluvial incision are the two major processes occurring in the San Juan Mountains. Howe (1909) was the first to call attention to the widespread occurrence of landslides in the San Juan Mountains. Landslide studies (Varnes, 1949; Armstrong and Armstrong, 1977; Luedke and Burbank, 1977, Joachim, 1986) in the area

conducted over the past century have established the occurrence of diverse types of mass movement, but, unfortunately do not convey the imminent risk that can affect the current population. Reconnaissance hazard mapping was initiated in the 1970s. During this time, mass movement deposits surrounding major towns were mapped to provide the data for enforcement of guidelines for development (Ives et al., 1976; Ives and Bovis, 1978; Ives and Krebs, 1978). Since then, focus on mapping of the present-day extent of mass movement deposits in the San Juan Mountains has been ignored. The lack of interest in the geomorphic processes that operate in the region created a major void in understanding where and why slopes fail.

The slopes in the San Juan Mountains are steep and predisposed to various types of mass movement, which leads one to ask the following questions: What are the major components that cause slopes to fail in the San Juan Mountains? And what is the distribution of surficial phenomena, which indicate potential hazards from slope failure?

Objectives and Hypothesis

To determine the major components that contribute to unstable slopes in the San Juan Mountains, the objectives of this thesis are summarized in the following:

1. Identify the various components associated with slope failure in the San Juan Mountains.
2. Map the areas susceptible to mass movement in the area.
3. Map features of mass movement in the area.

Thus the main hypothesis for this study is:

H_1: A combination of slope angle and length, aspect, geology, soil drainage, and vegetation cover create unstable slope conditions.

H_0: A combination of slope angle and length, aspect, geology, soil drainage, and vegetation cover do not create unstable slope conditions.

By stating the said objectives and hypothesis, it provides the reader a progression of the scientific method used to answer the research question. This hypothesis was tested using the Landslide-Susceptibility equation defined in the methodology in Chapter II (Avtar et al., 2011).

Description of Thesis

This thesis presents a model of susceptibility to landslides and a surficial geomorphological map of the western San Juan Mountains. Whereas, Chapter I provides the introduction outlining the research problem, the additional two chapters are written to address and fulfill the said objectives.

The framework of this thesis varies from a standard thesis, Chapters II and III are formatted as two separate papers for the purpose of publication. Chapter II is formatted for publication in the journal *Geomorphology*. This chapter examines the role of each terrain parameter contributing to slope failure in the region. Chapter III is written in the format of the *Journal of Maps.* Chapter III provides the distribution and extent of mass movement deposits and landforms indicative of the periglacial regime and extensive glaciation of the San Juan Mountains.

CHAPTER II

THE OCCURRENCE AND SUSCEPTIBILITY TO MASS MOVEMENTS IN THE WESTERN SAN JUAN MOUNTAINS, COLORADO*

Synopsis

The San Juan Mountains are located in southwestern Colorado and encompass an area of ~1,615 km^2 (Figure 1). Composed primarily of volcanic rocks over shales, limestones, and sandstones, the San Juan Mountains were severely glaciated during the Pleistocene. As a result of this glaciation in concert with active slope forming processes, slopes in the area are over-steepened and are prone to mass movement.

Mass movement is the active down-slope movement of rock, vegetation, or debris driven by gravity. This mass movement is triggered by a combination of precipitation, seismic activity, and human-induced changes to the landscape (Iverson, 2000; Larsen, 2008; Khan et al., 2013; Sidle et al., 2014 Collins and Jibson, 2015). Various types of mass movement contribute to the evolution of hillslope morphology characterized *via* the downward displacement of material, which is a potential natural hazard for humans and the built environment. Subsequent, widespread landslide activity has resulted in injuries, fatalities, and infrastructure damage (Schuster, 1996; Highland,

* Part of this chapter is reprinted with permission from "The Occurrence and Susceptibility to Mass Movement in the Western San Juan Mountains, Colorado: A 3-D Mapping Approach" by Kelkar, K.A., and Giardino, J.R., 2017. Landslides: Putting Experience, Knowledge and Emerging Technologies into Practice: Proceedings of the 3rd North American Symposium on Landslides, Association of Environmental and Engineering Geologists Special Publication, 27, p.949-957, 2017 by Association of Environmental and Engineering Geologists.

1998; Petley, 2012). Recently, landslide inventories and determination of potential landslide risk have gained attention. Thus, mapping the distribution of landslides, identification of slope instability, and prediction of slope failure, serve vital roles in saving lives and protecting infrastructure.

Introduction

Past landslide studies have mapped landslide susceptibility employing various approaches, ranging from heuristic, deterministic to statistical techniques (Van Westen et al., 2006; Regmi et al., 2010; Meten et al., 2015). The heuristic approach relies on the *a priori* knowledge of the investigator to make estimations of past as well as potential slope instability. The deterministic techniques, however, facilitate the calculation of factors of safety by considering such parameters as slope, structural geology, and soil-moisture content (Zhu et al., 2014). The statistical approach uses statistical computation of the influence of specific variables contributing to slope instability to assess susceptibility. Studies comparing deterministic and statistical models suggest the latter provides improved accuracy for assessing susceptibility to mass movement (Yilmaz, 2009; Cervi et al., 2010). Therefore, a study of susceptibility of mass movement which combines the aforementioned methods will enhance the prediction of mass movement.

Current research uses Geographic Information Systems (GIS) to successfully map spatial distribution of risk of mass movement at large scales (Regmi et al., 2010; Aplarslan, 2011; Yusof and Pradhan, 2014; Sadr et al., 2014). Advancement in GIS technology has expedited capture, storage, mapping, monitoring, modeling, and management of remotely-sensed data. A GIS application allows a researcher to designate

a hierarchal-weighted assignment to identify the individual role of various factors responsible for landslide propagation (Regmi et al., 2010; Sadr et al., 2014). In addition, GIS functions provide a flexible scale to integrate weighted influence for specific terrain parameters that conveniently highlight landslide-prone areas (Pradhan et al., 2010; Meten et al., 2015). Although, GIS has been widely used to delineate risk associated with landslides worldwide, no GIS-based mass-movement-susceptibility study has been undertaken in the San Juan Mountains. In addition to identifying the components of mass movement in the San Juan Mountains, a comprehensive model for susceptibility to landslides needs to be developed to address increased sporadic mass movement.

Study Area

The study area encompasses eight USGS quadrangles: Ridgway, Dallas, Mount Sneffels, Ouray, Telluride, Ironton, Ophir, and Silverton located in southwestern Colorado (Figure 1). This section of the San Juan Mountains is situated west of the continental divide within the Southern Rocky Mountains physiographic province (Thornbury, 1965). The study area extends north-south from Silverton to Ridgway (N 38˚09’ 10”, W 107˚45’ 21” to N 37˚48’ 44”, W 107˚39’ 52”) and east-west from Telluride to Silverton (N 37˚56’ 50”, W 107˚51’ 34” to N 37˚48’ 40” to W 107˚39’ 33”). Access to the region is *via* the San Juan Skyway consisting of U.S. Highways 62, 145, and 550, respectively. Hiking trails and county roads provide access to the backcountry.

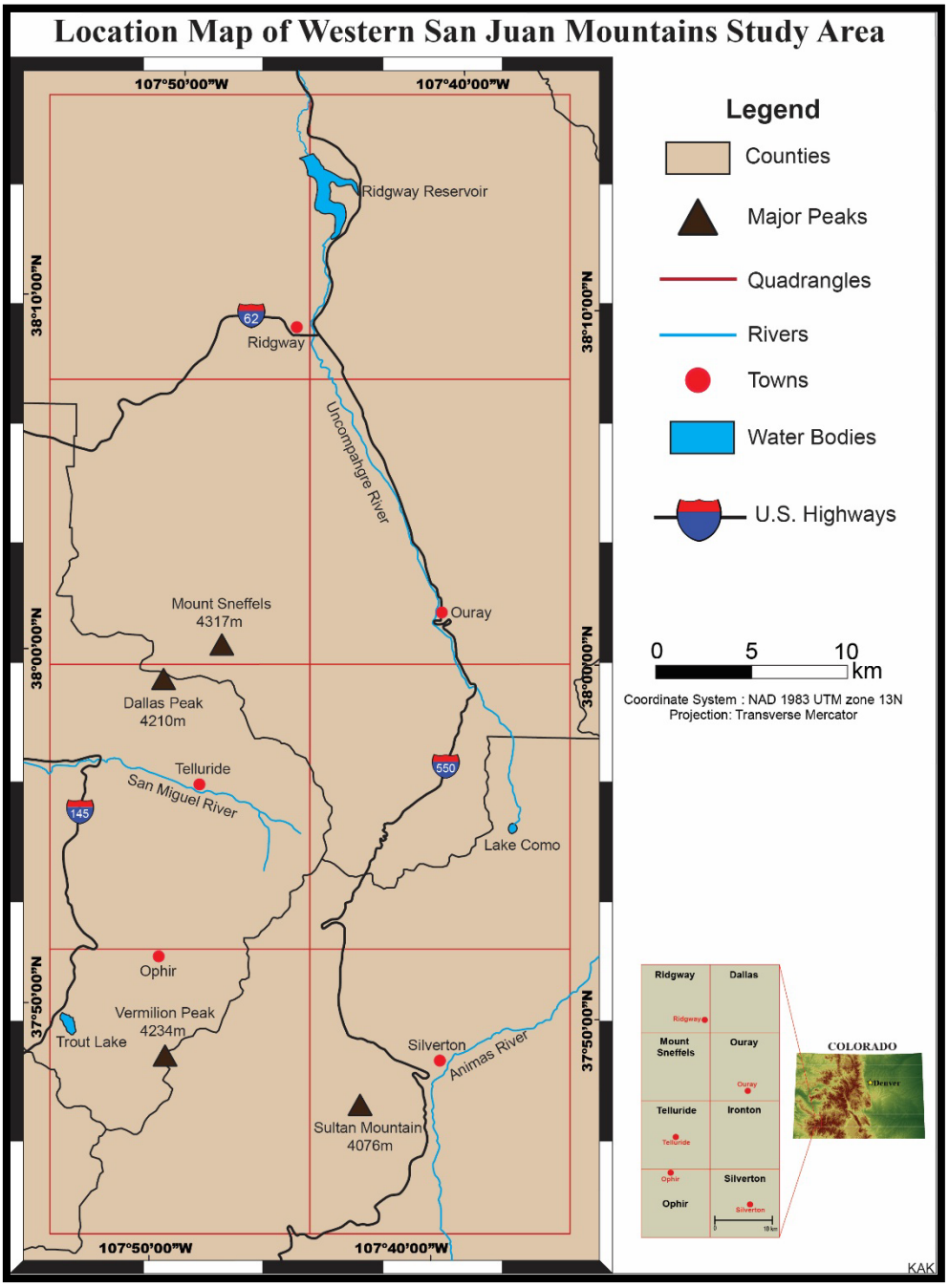

Figure 1: Location of study area.

Geology and Geomorphology

The study area ranges from forested slopes in the lower sections to bare rugged rock slopes above tree line. The San Juan Mountains are drained by the Animas, San Miguel, and Uncompahgre Rivers. Elevations within the study area range from 2,050 m at the Ridgway Reservoir to 4,317 m at the summit of Mount Sneffels. Hillslope morphology varies from small gently rolling hills to steep mountainous terrain. Dominant geomorphic features include rocky hills, glaciated and incised valleys, river valleys, floodplains, talus, colluvium, landslides, avalanche tracks and cones, rock glaciers, fens and alps, and various glacial erosional and depositional landforms.

The present-day landscape of the western San Juan Mountains is the result of orogeny, extensive volcanism, glacial erosion, fluvial activity, and mass movement (Cerveny and Blair, 1997). Ongoing fluvial activity has created deep canyons in the area and floodplains in Ouray, Silverton, Ridgway, and Telluride. Two lithologies dominate the study area: 1) Tertiary igneous rocks, which consist of massive floes, breccia, and rhyolitic tuff and 2) Cretaceous sedimentary rocks, which include limestone, shale, siltstone, and sandstone (Luedke and Burbank, 1962; Burbank and Luedke, 1964; Burbank and Luedke, 1966; Hail, 1989; Steven and Hail, 1989; Luedke, 1996; Luedke and Burbank, 2000). The volcanic lithology is based on massive lava and pyroclastic flows whereas the sedimentary rocks are remnants of an ancient seaway (Figure 2) (Moore, 2004). The advance of Quaternary glaciers eroded the landscape and formed various erosional and depositional landforms.

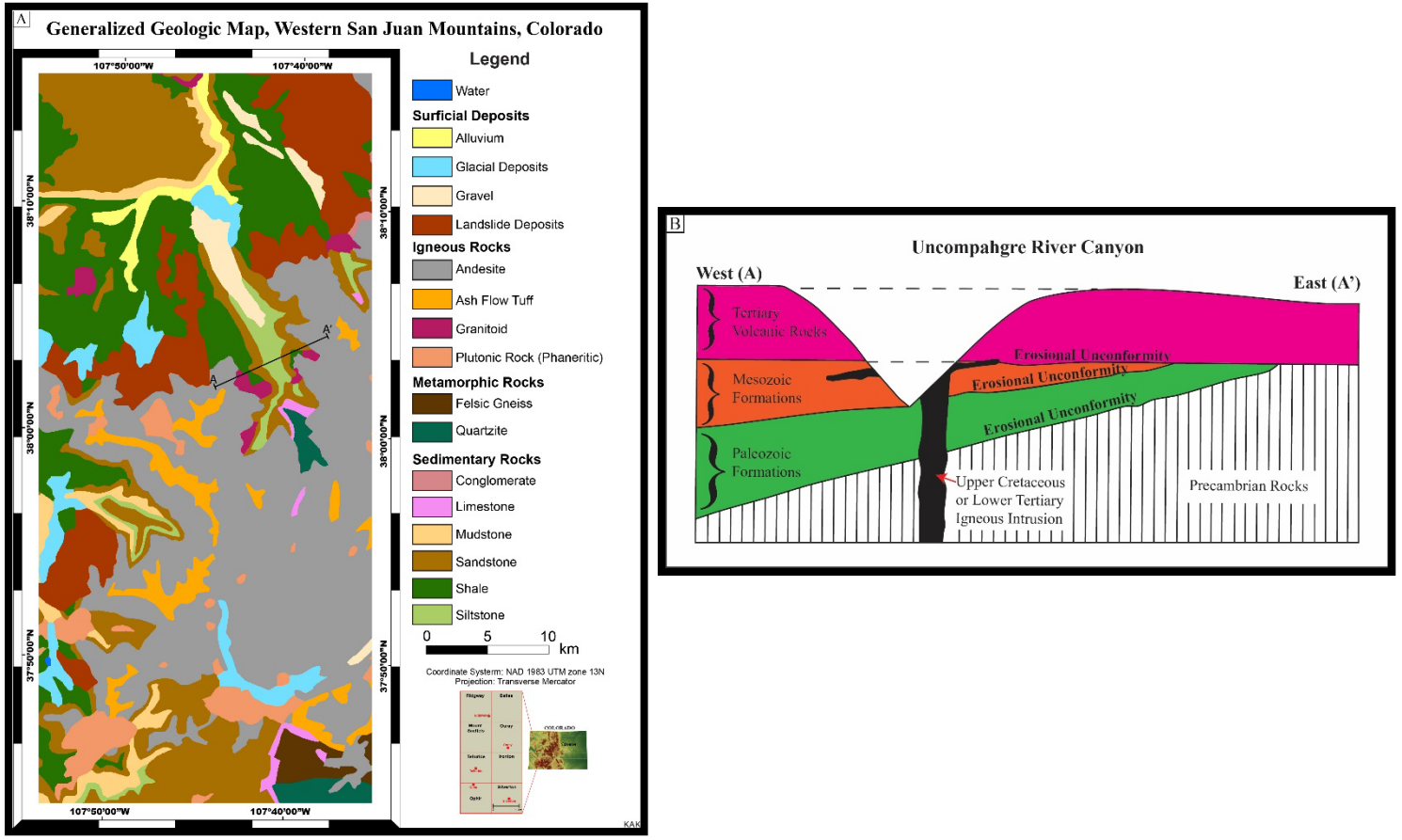

Figure 2: A) Lithologies observed in the study area. B) Generalized cross-section of the geology (Reprinted from Moore, 2004).

Pleistocene landslide deposits, originating from local bedrock, occur throughout the area; flood plains and valley train deposits fill valley floors in the study area (Mather, 1957). Mass movement, ranging from talus, landslides, debris flows to snow avalanches continue to shape the topography of the San Juan Mountains (Figure 3).

Figure 3: Mass-movement deposits. A) Rockfall activity at cliffs overlooking Telluride, Black Bear Pass Summit Trail. The red circle denotes dislodged rocks, impact zone is highlighted in white, and talus is encircled in black (8/16/15). B) A large landslide deposit in close proximity to the Horsetheif Trail, Ouray (8/11/15) C) Debris flow on Skyrocket Creek, Ouray, highlighted in red (8/10/15).

The glacial history of the western San Juan Mountains has set the stage for slope instability in the area. During the Last Glacial Maximum, a large ice-cap covered the landscape of the San Juan Mountains, and the various valleys were filled with alpine glaciers. These glaciers were responsible for many ice-contact slope deposits in the valleys (Atwood and Mather, 1932; Guido et al., 2007; Carrara, 2011). Climatic warming led to deglaciation, which facilitated glacial erosion and deposition imprinting the present geomorphic landscape.

Climate and Vegetation

Local climate in the study area varies from semi-arid to subalpine-alpine regimes. Annual average temperatures range from -4°C to 13.5°C based on 1982-2005 data from Telluride, Ouray, Ridgway, and Silverton climatic stations (Western Regional Climate Center, 2015). Precipitation occurs as rain in the summer and snow in the winter (Toney and Anderson, 2006). Summer monsoonal precipitation originates from convective storms. Average annual precipitation and average snowfall is 558 mm and 3,450mm respectively, based on 1982-2005 data for Telluride, Ouray, Ridgway, and Silverton climate stations (Western Regional Climate Center, 2015).

Vegetation in the study area consists of grasses, sedges, hedges, mosses, and mixed conifer forests. Land use in the study area includes urban, agricultural land, rangeland, forests, water bodies, wetlands, barren land, and perennial snow.

Anthropogenic Impact

The regional economy heavily relies on tourism. As a result, the growing number of tourists, recreationalists, and permanent residents choose to inhabit the area even with the risk from mass movement. Although, the major towns are confined to valley floors, proposed expansion is compelling people to construct structures on steep slopes with potential liability. (Figure 4). Subsequent development involves excavation of slopes and removal of slope support which creates unstable conditions. Furthermore, recreationalists traversing rugged mountain terrain face the risk of encountering dangers of landslides. All activities lead to a greater anthropogenic pressure on the landscape of the San Juan Mountains.

Figure 4: The red oval denotes houses built of steeper slopes in close proximity to Ouray (8/14/15).

Methodology

Identifying landslide-prone areas using a combination of heuristic, deterministic, and statistical methods required development of a multifaceted approach. The methodology consisted of two phases to improve the mapping of susceptibility to landslides in the western San Juan Mountains. A weighted-overlay ARCGIS® module was employed for a two phased assessment of susceptibility to landslides: 1) heuristic-based approach; and 2) Principal-Component-Analysis (PCA) based approach. The PCA function in ENVI® software was implemented to conduct a Principal-Component-Analysis of the relative weights for each terrain parameter. The susceptibility to mass movement was mapped using categories of very high, high, moderate, and low as adopted from Jenks' classification (Jenks and Caspall, 1971).

To answer the research question, six terrain components were integrated using geospatial methods to determine the relative influence in the propagation of mass-movement: slope angle, slope length, aspect, geology, soil drainage, and vegetation cover (Table 1).

Table 1: Data used to identify components of slope instability for this study.

Terrain Parameter	Data Type	Data Source
Slope Angle and Slope Length	Raster	DEM
Aspect	Raster	DEM
Geology	Vector (Polygon)	USGS
Surface Roughness	Raster	DEM
Soil Drainage	Vector (Polygon)	NRCS
NDWI	Raster	LANDSAT
NDVI	Raster	LANDSAT
Roads	Vector (Line)	CDOT

* CDOT: Colorado Department of Transportation, DEM: Digital Elevation model, LANDSAT: formerly Earth Resources Technology Satellite, NRCS: Natural Resources Conservation Service, USGS: United States Geological Survey.

GIS-Weighted Overlay

The GIS-weighted overlay method entailed the following steps:

- Each spatial layer was assigned a weight, as percentage for relative influence for slope failure.
- Each spatial layer was mapped to a common suitability scale. Where, 0 was areas not prone to landsliding and 1 was areas prone to landsliding.
- All spatial layers were overlaid to produce a map of susceptibility to landslides.

This multi-criterion weighted-overlay method is expressed as follows:

$$LS = \sum\left[(W_{sl}) \times (R_{sl}) + (W_{sg}) \times (R_{sg}) + (W_{sa}) \times (R_{sa}) + (W_{ge}) \times (R_{ge}) + (W_{vg}) \times (R_{vg}) + (W_{sd}) \times (R_{sd})\right] \quad (1)$$

where, *LS* is landslide susceptibility, *W* is weight of parameter, *R* is rank of the parameter, *sl* is slope angle, *sg* is slope length, *Sa* is aspect, *ge* is geology, *vg* is vegetation cover, and *sd* is soil drainage (Avtar et al., 2011).

The framework for geospatial techniques is based on the Digital Elevation Model (DEM) of the study area. An ASTER DEM with 10 meter solution and conforming to the North American Datum of 1983 was obtained from (https://viewer.nationalmap.gov/basic). In the interest of uniformity for remote-sensing analysis, each spatial layer was prescribed to the coordinate system, NAD 1983 Universal Transverse Mercator Zone 13 North and a cell size of 10 x 10 meters.

Slope Angle and Slope Length

Slope gradient is a significant factor influencing the propagation of landslides. Logically, steeper slopes were classified as having a greater ability to initiate landslides as compared to gentler slopes. The spatial distribution of slope is fundamental to quantifying risk from landslides. Slope angles were derived in radians from the DEM.

The normalization of study area slope was generated using the following:

$$\frac{Sin\ (Slope)}{180\ \times\ \pi} = (0,1) \quad (2)$$

where, *sin* is the Sine of slope angle, and π is 3.1417.

On completion of the slope map, slope was reclassified in four classes for analysis: 1) class 1 (0°- 22°); 2) class 2 (22.01°- 44°); 3) class 3 (44.01°- 66°); and 4) class 4 (66.01°- 90°).

Slope length was calculated using the flow length function in ARCGIS® once the data for slope angle were obtained. It is implied slopes that are steeper and shorter have a greater risk potential to affect human life and infrastructure than slopes that are relatively flat. Thus, longer and less steep slopes in the area were designated a lower risk potential. Slope length is considered as a frictional coefficient defined in the following equation:

$$F_{cof} = \frac{Slope\ Angle}{Slope\ Length} \quad (3)$$

where, F_{cof} is Frictional Component.

Aspect

The directional component of slope can substantially affect susceptibility to landslides because as aspect varies contrasting micro-climatic conditions and slope energy conditions, are created, which can regulate the occurrence of slope failure. Thus, drier south-facing slopes lack vegetation cover are prone to landsliding, as compared to vegetated north-facing slopes, which enhance soil moisture and potential saturation.

Slope aspect was calculated in radians from the DEM using the aspect function in ARCGIS®. The normalization of aspect from 0 to 360̊ was used by evaluating aspect *via* a fuzzy-exponential decay function represented in the following equation:

$$[Sin\left(\frac{Aspect}{2}\right)] \quad (4)$$

where, *sin* is Sine of *aspect* divided by two.

After preparation of the normalized aspect map, aspect was further reclassified into cardinal and primary inter-cardinal directions for evaluation of directional slope components. These directions were: north, northeast, east, southeast, south, southwest, west, and northwest.

Vegetation Cover

Vegetation is a significant variable, which can moderate the initiation of landslides. Roots in highly vegetated areas bind the soil very similar to rebar in concrete and reduce the chances for displacement of debris. To delineate vegetation cover, The Normalized Difference Vegetation Index (NDVI) was used (Bannari et al., 1995). The NDVI was calculated from LANDSAT Band 4 (red) and LANDSAT Band 5 (near infrared) remote-sensed data expressed as:

$$NDVI = \frac{\text{LANDSAT Band 5} - \text{LANDSAT Band 4}}{\text{LANDSAT Band 5} + \text{LANDSAT Band 4}} \quad (5)$$

Soil Drainage

Saturated soils in mountain sides aid in slopes exceeding specific geomorphic thresholds, which can result in slope instability. Data for soil drainage are from the

Natural Resources Conservation Service (NRCS) digital-soil-map shapefile (https://gdg.sc.egov.usda.gov). Poorly drained soils that result in unstable conditions were reclassified as areas prone to movement. Soil drainage for the PCA-based landslide model was replaced by the Normalized Difference Water Index (NDWI) (McFeeters, 1996). NDWI as expressed:

$$NDWI = \frac{LANDSAT\ Band\ 3 - LANDSAT\ Band\ 5}{LANDSAT\ Band\ 3 + LANDSAT\ Band\ 5} \quad (6)$$

Geology and Surface Roughness

The likelihood of slope instability is related to rock strength. Lithologies more resistant to weathering have a lower probability of contributing to the propagation of landslides. Geologic spatial data were acquired from a USGS digital-geology shapefile for each geologic unit (https://mrdata.usgs.gov/geology/state/state.php?state-CO). Sedimentary and igneous lihtologies in the study area were reclassified, and the rank is based on rock strength for susceptibility to landslides. For the PCA-based landslide model, the geology layer was replaced by a surface-roughness layer (Hobson, 1972). To provide a quantitative measure of strength of lithology, it was assigned rippability values corresponding to values based on the Caterpillar© D8R ripper classification (Caterpillar© Tractor Company, 2000), which was calculated using block statistics and the raster calculator function in ARCGIS® as:

$$Surface\ Roughness = \frac{\sqrt{\left(\sum_{i=1}^{n} xi\right)^2 + \left(\sum_{i=1}^{n} yi\right)^2 + \left(\sum_{i=1}^{n} zi\right)^2}}{n} \quad (7)$$

where, *xi* is *sin* (s) * *cos*(a), *yi* is *sin*(s) * *sin*(a), *zi* is *cos*(s), s is slope gradient and a is aspect (Hobson, 1972).

Rippability is the measure of soil or rock ease of excavation by mechanical excavation categorized as rippable, marginal, and non-rippable. The degree of rippability is derived from seismic wave velocities corresponding to the performance of the Caterpillar© D8R ripper for respective rock types (Figure 5). Physical characteristics of readily rippalble sedimentary rocks are: frequent planes of weakness, weathering, brittleness, low strengths, and low seismic velocities.

Properties such as massive, crystalline, high strengths, and high seismic velocities of igneous and metamorphic rocks are non-rippable (Caterpillar© Tractor Company, 2000).

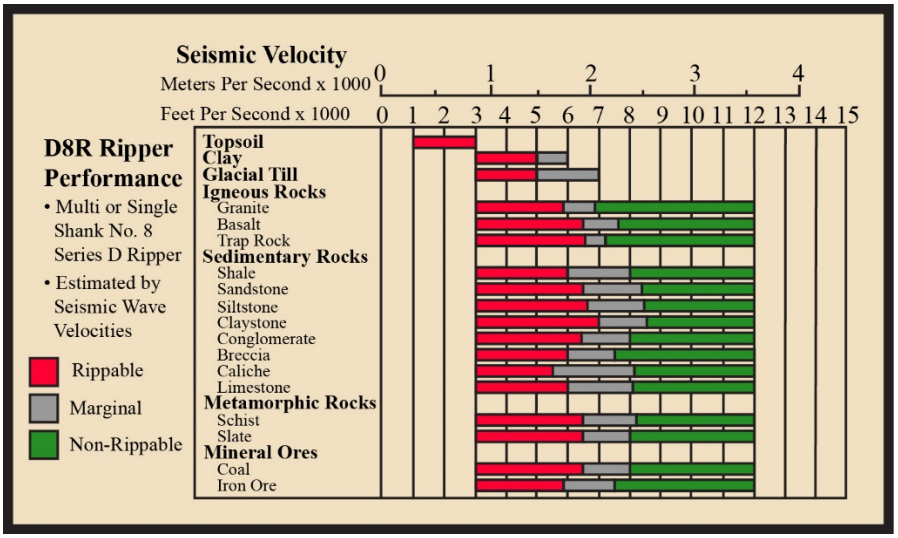

Figure 5: The corresponding lithologic rippability values based on seismic wave velocities (Reprinted from Caterpillar® Tractor Company, 2000).

Normalization of Data

Normalization of data was necessary to ensure consistent values for factors, within each terrain parameter which may not cause slope failure. The normalization process precedes the overlaying of all terrain variables to produce a reliable map of susceptibility to landslides. All spatial layers were normalized to a common suitability scale of 0-1 using the following equation: (Pradhan et al., 2010):

$$\frac{(R - Rmin)}{(Rmax - Rmin)} \tag{8}$$

Distance to Roads

Road construction in mountain terrain put areas adjacent to mountain roads at risk from slope failure. Unstable conditions near mountain roads is compounded by the loss of slope support from excavation of mountainsides and pulsation caused by passing by vehicles (Ayalew and Yamagashi, 2005; Mittal et al., 2008). Distance to infrastructure is represented by roads (i.e., paved highways, unpaved roads, and local unpaved roads) from the Colorado Department of Transportation (CDOT) shapefile. To examine distance to roads, road buffers with 50 meter increments (50-250 m) were created to identify the proximity of susceptibility to mass movement along roadsides.

Results and Discussion

Comparison of Heuristic and PCA-Based Landslide Models

Landslides in mountain environments are widespread natural hazards characterized as being highly mobile and catastrophic. Predicting the occurrence of landslides in mountain terrain is challenging because of the sporadic and spatially discontinuous occurrence of landslides (Huggel et al., 2012; Stoffel et al., 2014). As per the heuristic definition, such techniques heavily rely on the best-judgement criteria of the investigator to determine factors contributing to slope instability. Consequently, individual subjectivity of governing parameter weight is not conducive for data reproducibility (Yilmaz, 2009). Although, the application of heuristic techniques is popular in the scientific community (Kayastha et al., 2013; Schleier et al., 2014; Youssef et al., 2015), reliability of heuristic data is questionable.

Potential weights for landsliding based on *a priori* reasoning were designated for each terrain parameter in the weighted overlay (Figure 6). This approach provides a basic perspective of susceptibility to landslides in the San Juan Mountains (Figure 7).

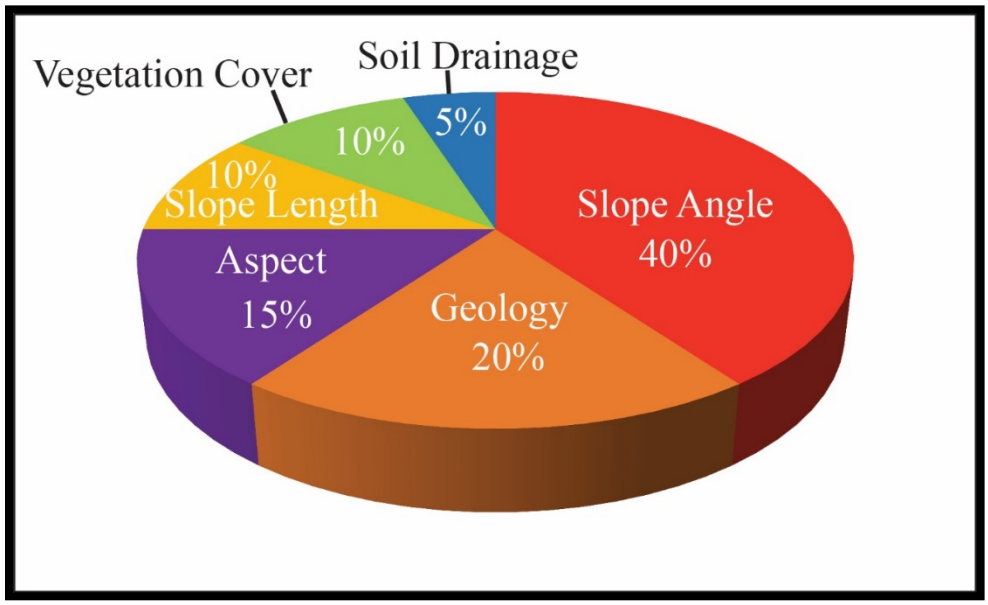

Figure 6: Heuristic weight-percent influence for each respective parameter (Reprinted with permission from Kelkar and Giardino, 2017).

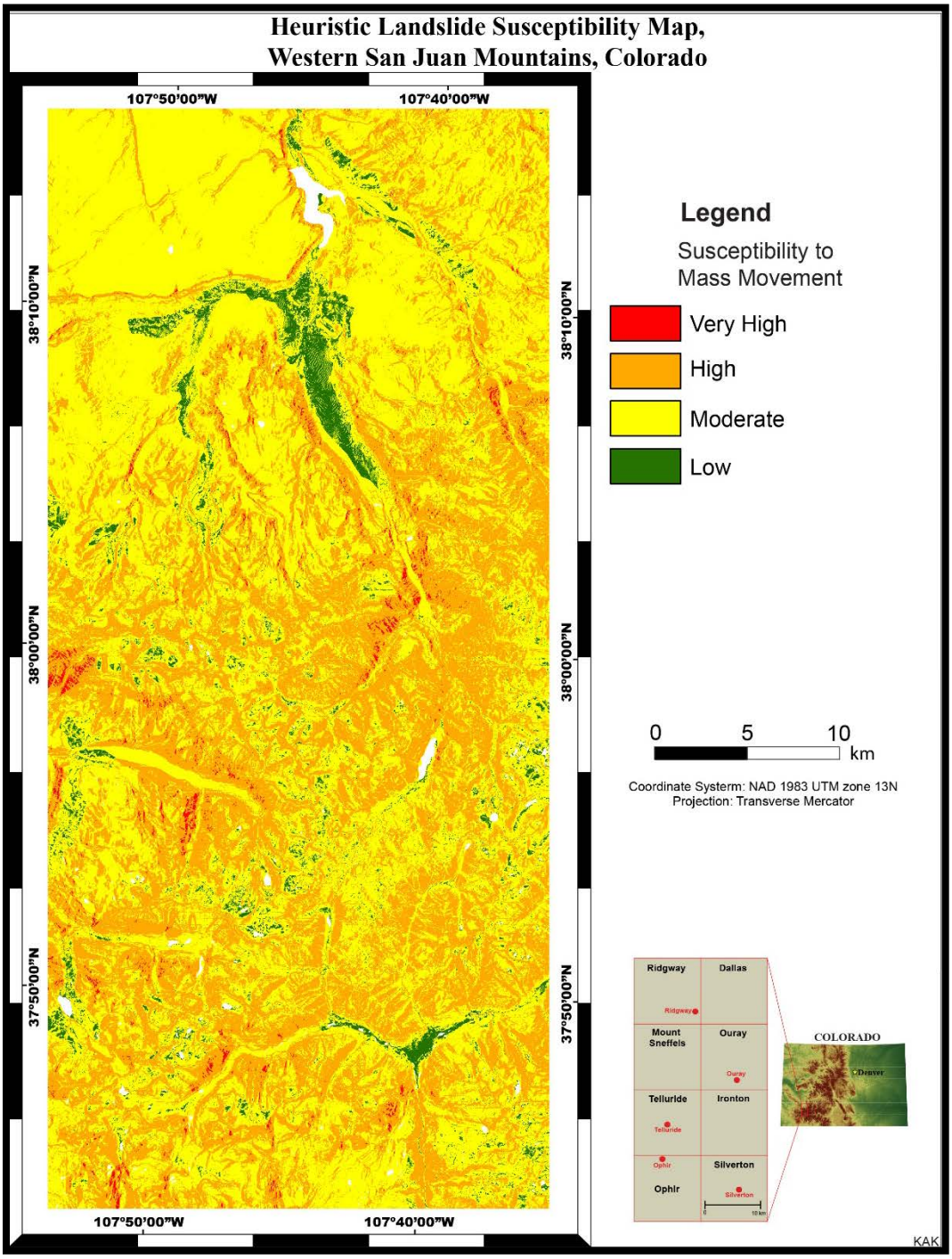

Figure 7: Map of heuristic susceptibility to mass movement. Note: water bodies are omitted (Reprinted with permission from Kelkar and Giardino, 2017)

The visual inspection of the map for heuristic susceptibility to landslides suggests inconsistency in susceptibility designations. Lack of detailed geospatial information for geology and soil drainage generated an unreliable mapping of susceptibility. The reclassification of geologic units, based on rational thresholds for weathering of lithology, provided subjective geospatial data (Table 2). Also, soil drainage comprised a generalized digital shapefile with inadequate detailed data. Yilmaz (2009) emphasized a significant drawback of the heuristic method, which applies to basic types of mass-movement and uniform, intrinsic datasets.

Figure 7 displays discrepancies observed for the map of heuristic susceptibility to landslides. For instance, the bottom of formerly glaciated valleys with nearly flat topography have a low likelihood of initiating landslides, but these areas were mapped as moderate susceptibility. The top of Loghill Mesa (norther section of map), consisting of relatively low-relief lacking the topography to cause slope failure, is predominantly classified as moderate susceptibility. Regardless, areas consisting of near flat topography indicate low susceptibility to landslides. On the contrary, cliffs adjacent to Ouray and Telluride are not mapped as very high susceptibility, yet such steep mountain slopes predisposed to rockfall lack appropriate susceptibility classifications.

Table 2: Heuristic-based ranking devised for geology.

Lithology	Rank	Mass Movement Potential
Alluvium	0.1	Low
Gravel	0.1	Low
Glacial Deposits	0.2	Low
Granitoid	0.4	Moderate
Plutonic Rock	0.4	Moderate
Andesite	0.5	Moderate
Felsic Gneiss	0.5	Moderate
Quartzite	0.5	Moderate
Ash Flow Tuff	0.6	Moderate
Limestone	0.7	High
Siltstone	0.8	High
Sandstone	0.8	High
Conglomerate	0.8	High
Shale	0.9	High
Mudstone	0.9	High
Landslide Deposits	1	High
Water	Omitted	Not Applicable

Because of the drawbacks in the heuristic model for susceptibility to landslide, a refined evaluation was necessary. To counteract the limitations encounters through the heuristic approach, a PCA-based model was constructed. PCA is a multivariate mathematical procedure which transforms a number of possibly correlated variables into a smaller number of uncorrelated variables or principal components (Pearson, 1901). Additionally, reduction of the parameter subsets provides maximum variance for components to identify factor loading (Bishop, 1995; Komac, 2006).

In the past couple of decades, landslide studies have shifted focus to data-driven statistical models using bivariate and multivariate methodologies (Carrara, 1983; Baeza and Corominas, 2001; Nandi and Shakoor, 2010). The advent of readily available large-scale computation has facilitated the analysis of regional spatial data, often produced with a PCA approach. Crosta and Agliardi (2013), and Shahabi et al., (2015) have applied PCA successfully to investigate landside vulnerability in the European Alps and Zab Basin, Iran, respectively. The efficiency of a PCA-based methodology is best summarized by Sabokbar et al., (2014 page 15) as a "method of decreasing dimensionality and characteristics that delineate multivariate samples for identify spatial patterns." In effect, the investigator can study the influence of each chosen factor contributing to slope instability. Likewise, variances obtained for principal components assist in distinguishing the greater impact of a respective parameter compared to other inserted variables. PCA method requires no *a priori* knowledge of the landslide-related variables, eliminating human-induced error when determining relative influence on

landslide susceptibility. Thereby, for this study, a PCA method is assumed to refine the assessment of landslide susceptibility in the San Juan Mountains.

Upon completion of the PCA procedure, six principal components were generated indicative of factor loading for slope failure with PC1 as the greatest factor loading and PC6 as lowest factor loading. Of the produced principal components, factor loading was observed as follows: PC1 is aspect, PC2 is slope angle, PC3 is surface roughness, PC4 is NDVI, PCA5 is slope length, and PC6 is NDWI (Figure 8).

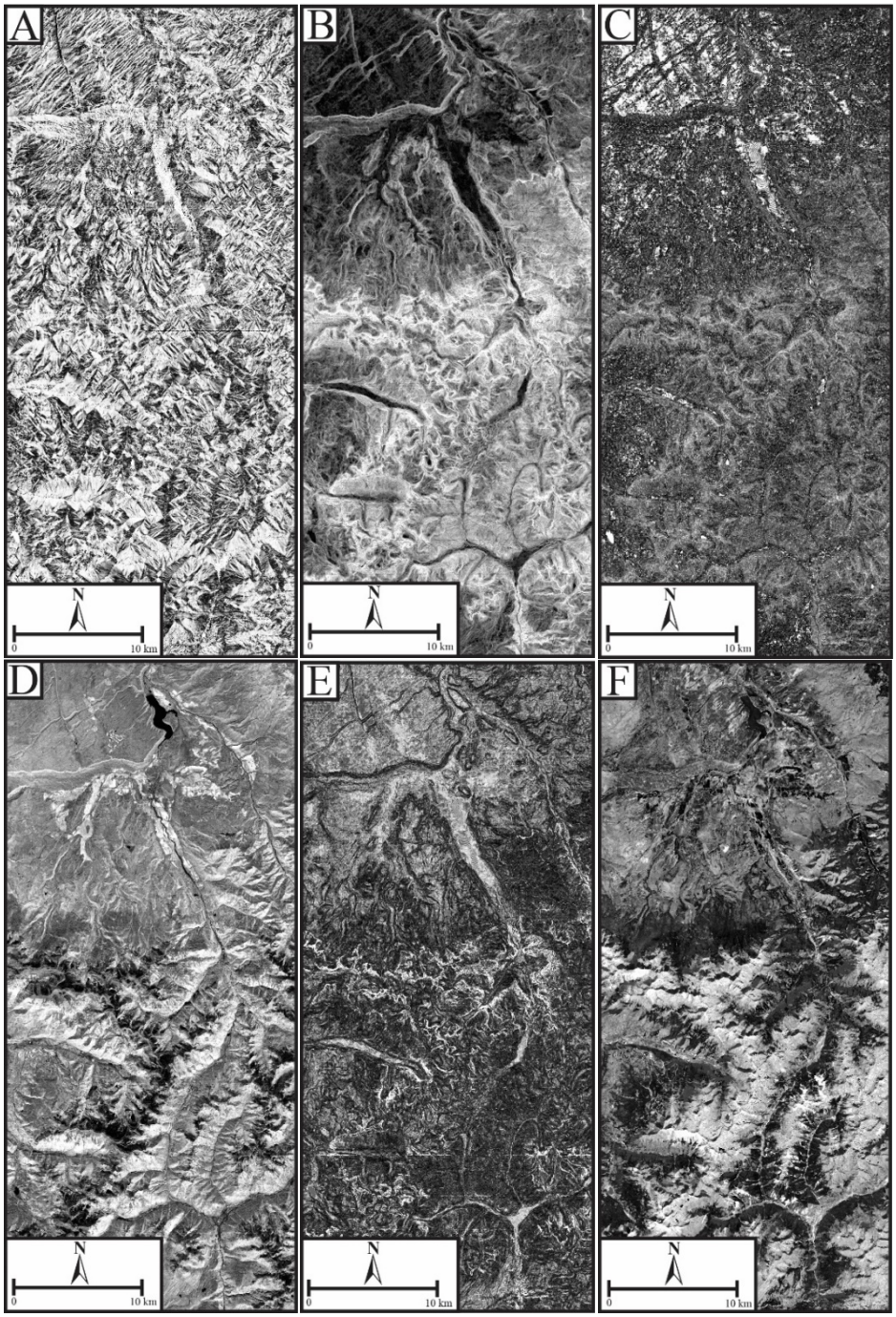

Figure 8: Images produced on completion of PCA procedure. A) Aspect; B) Slope Angle; C); Surface Roughness (Geology); D) NDVI; E) Slope Length; and F) NDWI (soil drainage).

Table 3 shows Eigenvalues representative of factor loading for each terrain parameter (Table 3). Contrary to the heuristic-based weight percent influences which ranked slope angle, geology, and aspect as the main components of slope failure, PCA-based aspect accounts for the greatest variance at 48% for landslide propagation. PCA-based slope angle and surface roughness (i.e., geology) have the second and third greatest variance on slope failure, respectively (Figure 9). Vegetation cover, slope length, and soil drainage rank, in this order, for least influence on slope failure for heuristic and PCA-based landslide assessment.

Table 3: Extracted Eigenvalues based on PCA.

Spatial Parameter	Eigenvalue
Aspect	0.100378
Slope Angle	0.071562
Surface Roughness (Geology)	0.019301
NDVI	0.016035
Slope Length	0.001291
NDWI (Soil Drainage)	0.000516

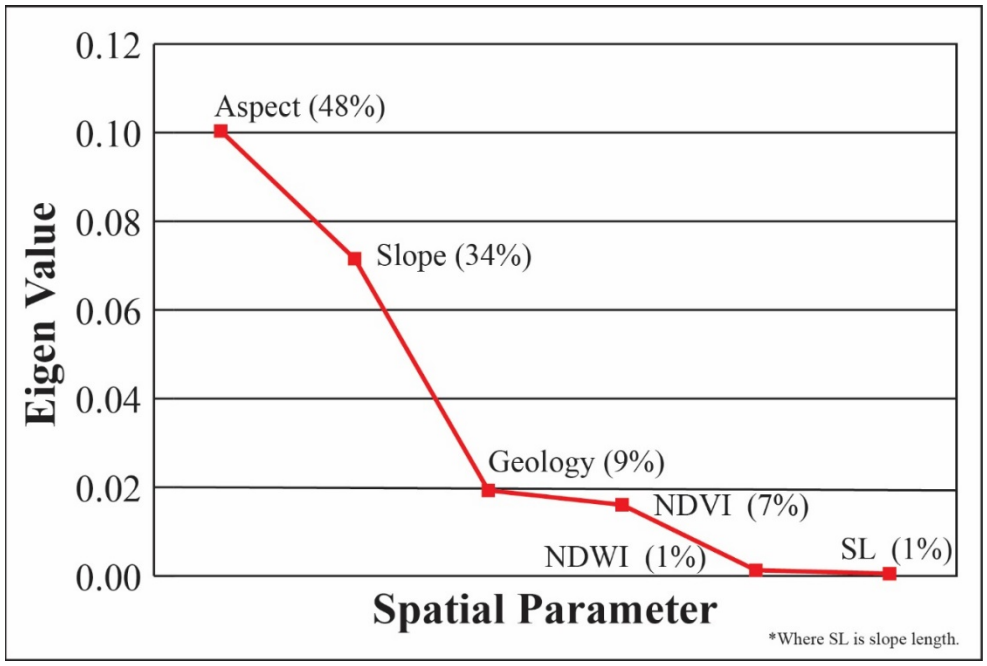

Figure 9: A scree plot displaying the calculated relative weight-percentages for PCA.

Insertion of PCA-weight influences in a weighted-overlay produces a more robust pixel-based map of susceptibility to mass-movements (Figure 10). The PCA-based map of susceptibility to landslides presents comprehensive coverage of areas which may propagate landslides mapped as high to very-high susceptibility to landslides. Biases observed in the heuristic susceptibility to landslides map include a small spatial extent for very high and low susceptibility to landslides. These biases are addressed using the PCA technique (Figure 11). The PCA method mapped greater area for low and very high susceptibility, and smaller area for moderate and high susceptibility in comparison to the heuristic approach. Both approaches correspond however, to substantial areal coverage for moderate and high susceptibility to landslides.

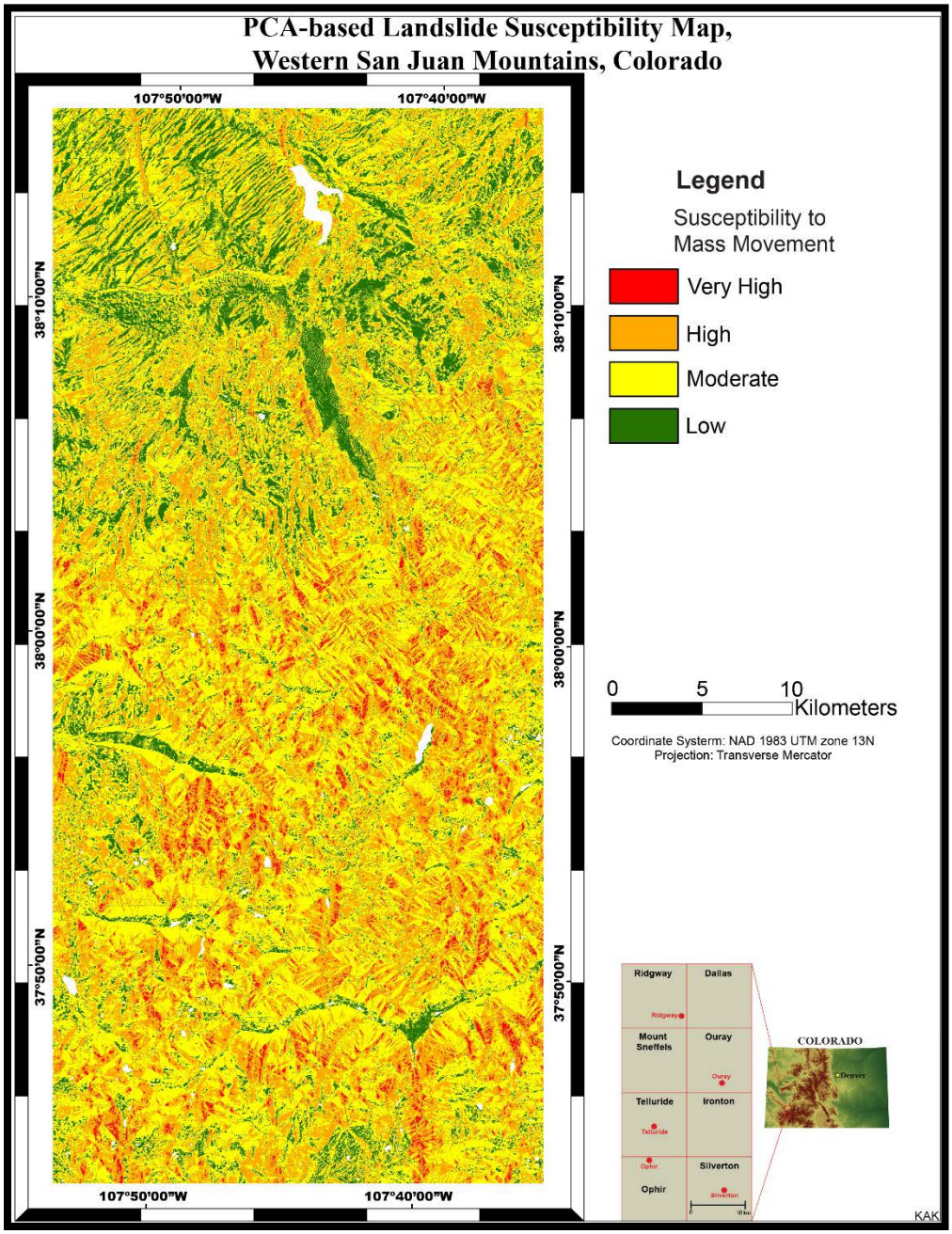

Figure 10: PCA-based susceptibility to mass movement map. Note: water bodies are omitted (Reprinted with permission from Kelkar and Giardino, 2017).

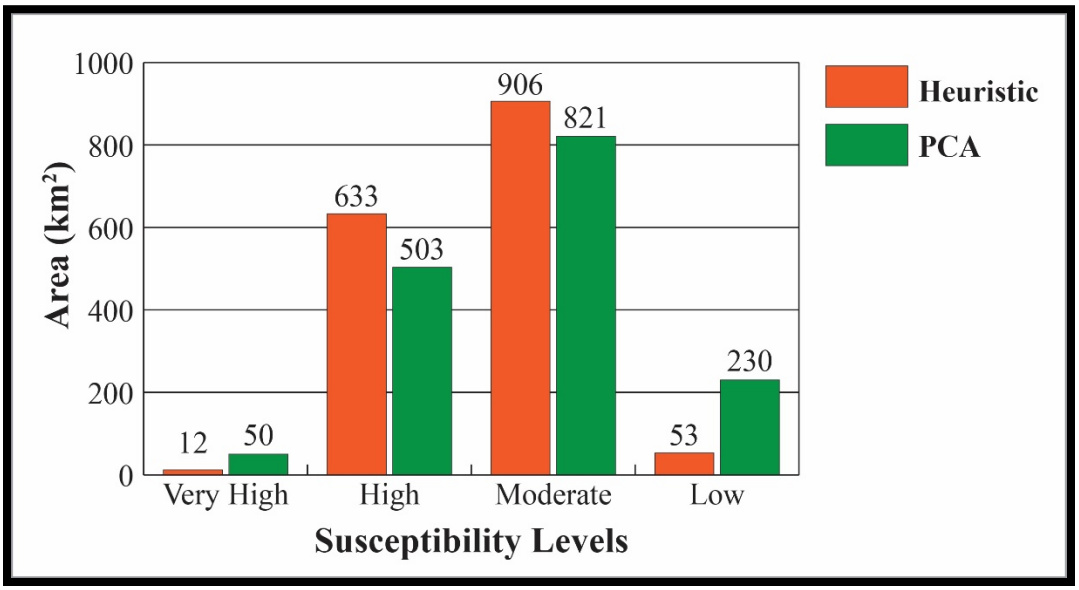

Figure 11: The areal coverage for each susceptibility class for the heuristic and PCA method.

Table 4 displays the correlation of the six interpolated spatial variables via a correlation matrix (Table 4). Aspect has strong negative correlations with slope angle, NDVI, and geology, respectively. The inter-relatedness can be associated with micro-climatic conditions on differing slopes faces in alpine regions. Aspect plays an import role in regulating precipitation, moisture retention, and insulation on slopes. As a fundamental erosive agent, less precipitation means less material is transported downslope affecting surface roughness. Inadvertently, the gradual undercutting of slope alters slope angle generating surface roughness. Additionally, the intensity of precipitation received on slopes influences vegetation cover and soil drainage.

Slope angle exhibits a positive correlation of 0.932620 and 0.372324 with slope length and soil drainage, respectively. Increased slope gradient results in shorter slope length, as opposed to gentler slopes creating greater slope lengths. Subsequently, steeper slopes facilitate drainage of water content in soils. Slope angle has a negative correlation of -0.430622 and -0.265550 with NDVI and surface roughness. Because vegetation growth is sparse on highly steep slopes, accelerated erosion impacts the smoothness of slope surfaces.

Table 4 shows surface roughness (i.e. geology) having negative correlations with soil drainage and slope length. The degree of surface roughness affects seepage of soil moisture, rougher slopes will inhibit runoff from soil drainage as opposed to smoother slopes.

NDVI has a negative correlation of -0.410717 and -0.367737 with slope length and soil drainage, respectively. Logically, soil drainage determines the availability of water for vegetation growth. The lack of soil development on steeper slopes (shorter slope length) does not provide favorable conditions for the growth of vegetation.

Table 4: Correlation matrix of six input spatial parameters

Correlation Matrix	Aspect	Slope Angle	Geology (SRF)	NDVI	Slope Length	NDWI (Soil Drainage)
Aspect	**1**	-0.001370*	-0.018824*	-0.062207*	0.001370	0.001105
Slope Angle	-0.001370	**1**	-0.265550*	-0.430622*	0.932620*	0.372324*
Geology (SRF)	-0.018824	-0.265550	**1**	0.224044	-0.256848*	-0.318635*
NDVI	-0.062207	-0.430622	0.224044	**1**	-0.410717*	-0.367737*
Slope Length	0.001370	0.932620	-0.256848	-0.410717	**1**	0.324149
NDWI (Soil Drainage)	0.001105	0.372324	-0.318635	-0.367737	0.324149	**1**

*Significant values.

Hypsometric Analysis

The hypsometric curve was first devised as a way to study areal extent at different elevations, and this analysis is a valuable tool in the interpretation of landscape evolution (Strahler, 1952; Schumm, 1956). This method provides a comprehensive perspective of the landscape. Recently, disciplines including tectonics, fluvial hydrology and earth surface studies have implemented hypsometric analysis at regional scales (Pena et al., 2009).

A hypsometric curve was derived from the DEM of the study area (Figure 12). The hypsometric curve has an overall linear trend. Although a linear trend suggests a uniform rate of erosion for the San Juan Mountains, minor convexity and concavity are shown. The concave profile at 2,100 m is linked with deposition of sediment from regional drainage. On closer inspection, a concave profile was observed at the central portion of the curve encompassing 3,000 m to 3,500 m elevation. This concavity is the result of erosional processes at higher elevations displayed in the convex structure of the hypsometric curve at ~ 4,000 m. Mass movement and denudation processes at higher elevations supply debris that occupies numerous cirque basins.

This hypsometric curve presents the spatial extent of varying elevations. Nearly, 50 % of the study area is at an elevation of 3,000 m to 4,317 m. 30 % of the area is situated between 2,500 m to 3,000 m. The remaining elevation below 2,500 m covers 20% of the region.

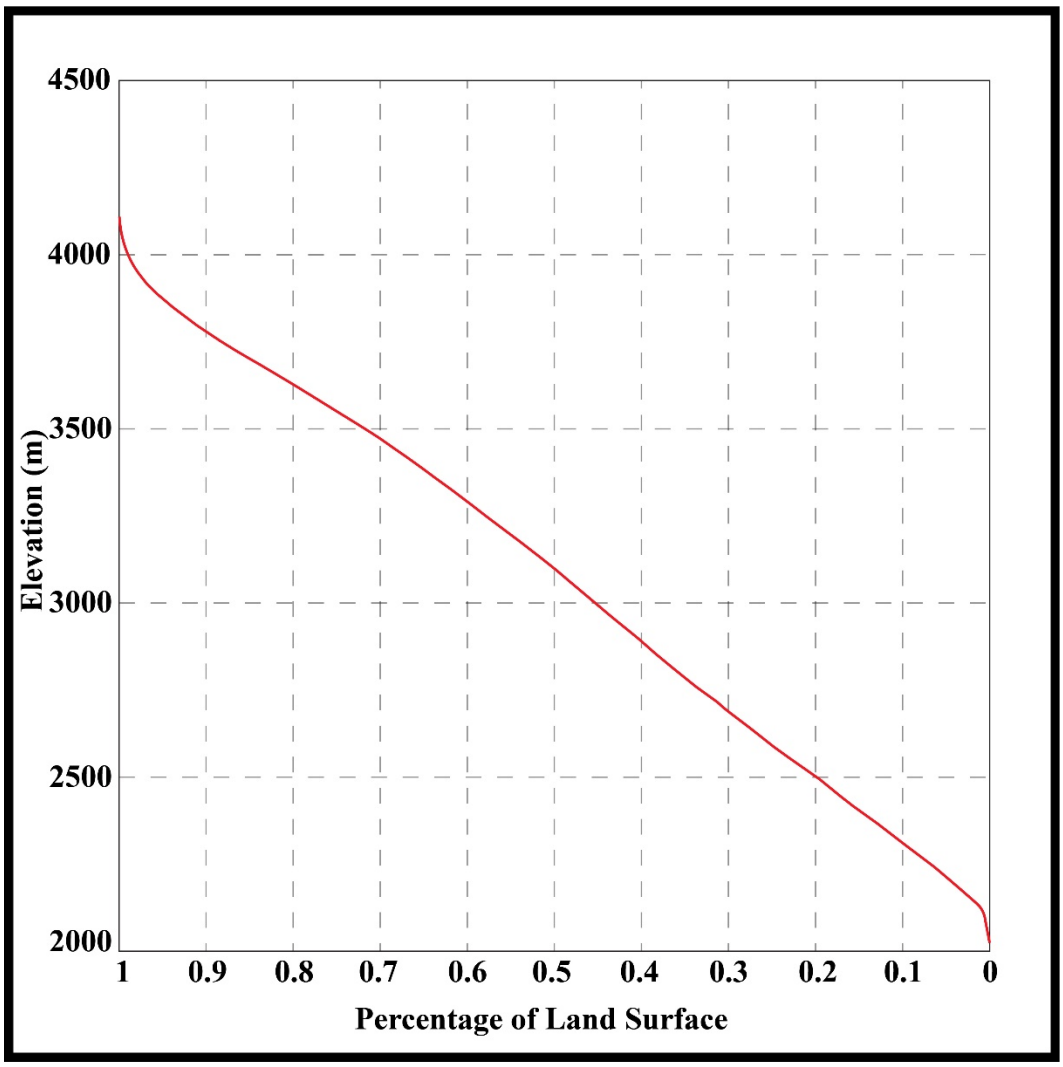

Figure 12: Hypsometric curve of the eight quadrangles encompassing the western San Juan Mountains.

Areal Coverage for Aspect

The dominant role of aspect with regard to the susceptibility to landslides was established in the previous section of this thesis. Diverse aspect sets the stage for varied climatic and energy conditions on the respective slopes. Solar radiation influences moisture retention and vegetation altering micro-climates in alpine regions.

To determine the role of aspect on landslide susceptibility in the western San Juan Mountains, areal coverage of each susceptibility class within cardinal and inter-cardinal directions were calculated (Figure 13). The areal coverage percentages for each slope direction area: north: 12.63%, northeast: 14.90%, east: 12.56%, southeast: 9.98%, south: 9.89%, southwest: 11.17%, west: 13.75%, and northwest: 13.44% (Figure 14).

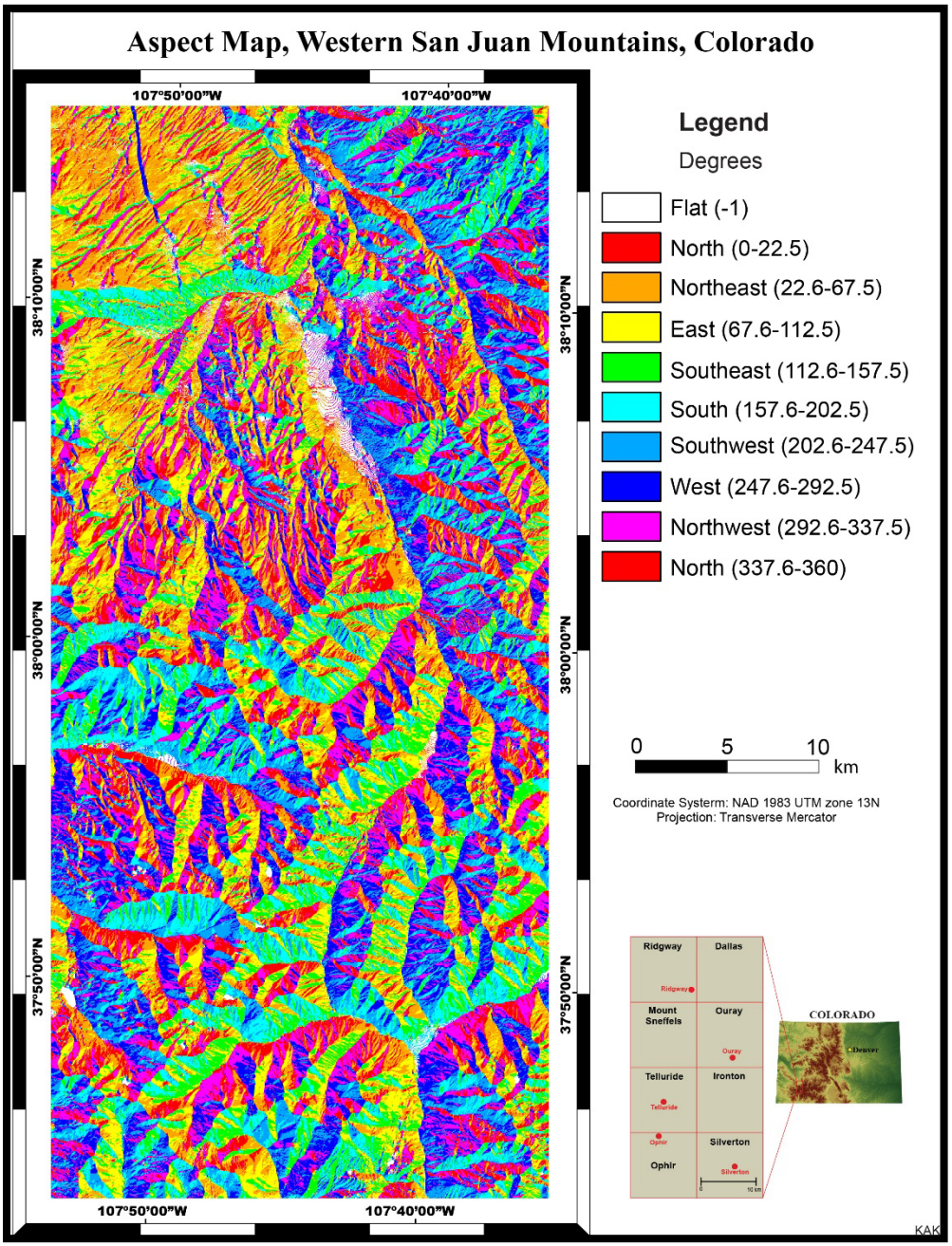

Figure 13: The reclassification of aspect for the western San Juan Mountains.

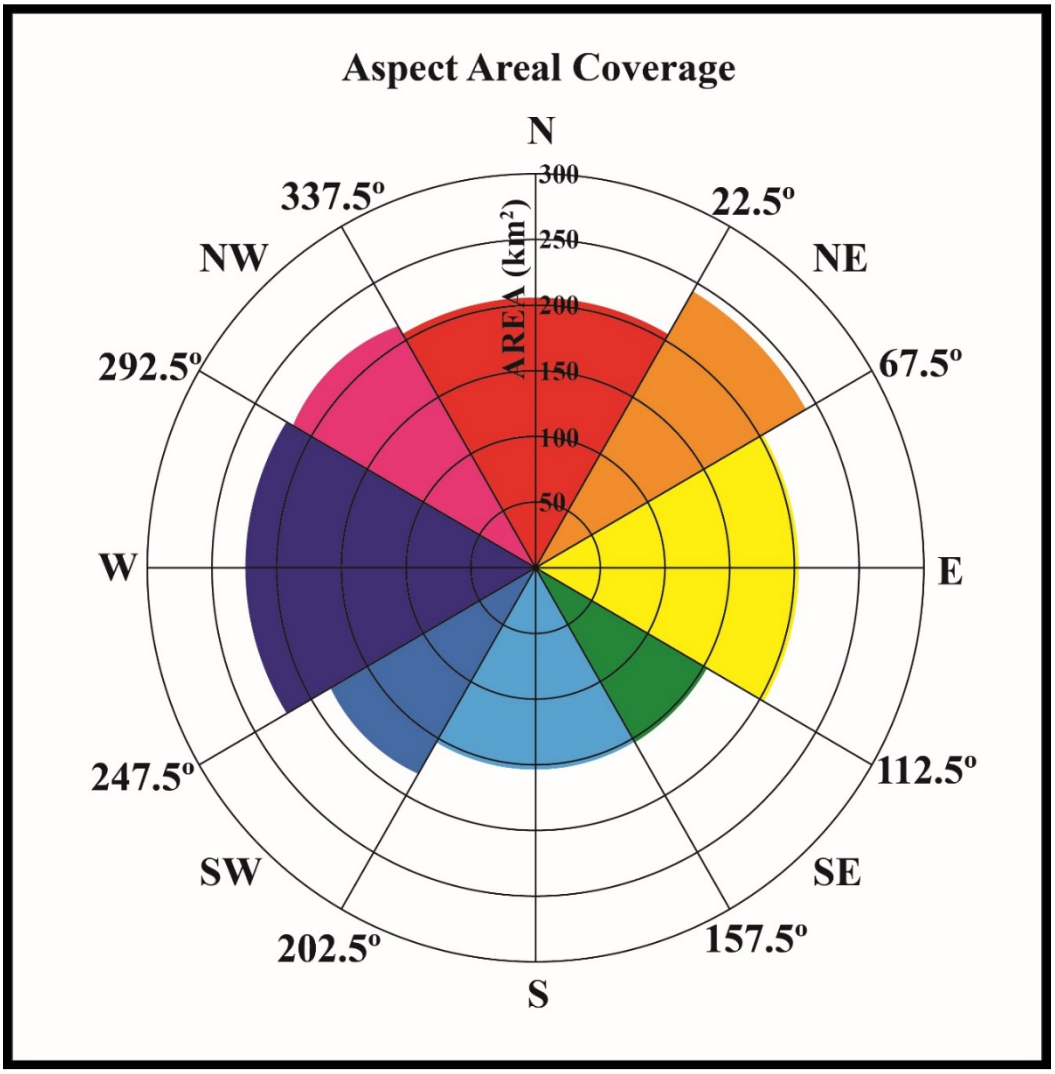

Figure 14: Northeast (240.74 km^2) and West (222.22 km^2) facing slopes cover the largest extent of the region.

North-facing slopes and south-facing slopes were determined to have the greatest areal coverage for low susceptibility covering 71 km^2 and 52.49 km^2, respectively (Figure 15 A). Alpine regions in the North Hemisphere have wetter north-facing slopes in comparison to south-facing slopes. It can be inferred that mesic north-facing slopes in the western San Juan Mountains are not saturated to the point of directly causing slope

failure. Moisture rich environments facilitate vegetation growth which in turn binds soils, minimizing landslide propagation. Dry south-facing slopes in the San Juan Mountains do not exceed the respective strength thresholds.

Moderate susceptibility to landslides is observed on all slope faces (Figure 15 B). Northeast, northwest, and southwest-facing slopes cover majority of moderate susceptibility pixels constituting 160.43 km^2, 140.28 km^2 and, 117.75 km^2, respectively.

The majority of high susceptibility to landslide pixels occur on east and west-facing slopes (Figure 15 C, D). West-facing slopes account for 165.83 km^2 and east-facing slopes 149.85 km^2 for high susceptibility, respectively. The very high susceptibility landslide pixels are only situated on west and east-facing slopes. West and east-facing slopes cover 27.13 km^2 and 22.61 km^2 of very high susceptibility landslide pixels, respectively.

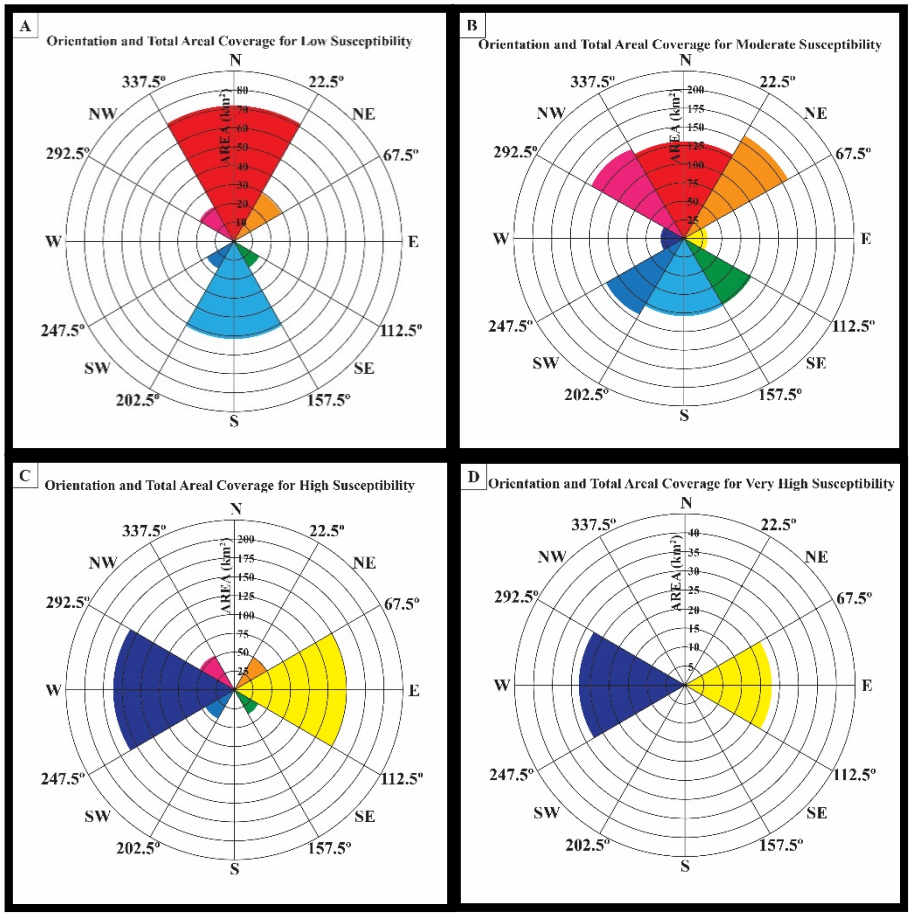

Figure 15: Landslide susceptibility pixel area coverage for aspect orientations. A) Low susceptibility; B) Moderate Susceptibility; C) High susceptibility; and D) Very high susceptibility.

Although, this thesis has established aspect orientations susceptible to landslides, the climatic conditions present on all aspects was not examined. A potential major variable affecting west and east-facing slopes is solar radiation, which in effect controls specific variables. Solar radiation regulates evapotranspiration, type of vegetation, retention of soil moisture, and snow thickness. Progressively, east and west-facing slopes will experience contrasting climatic conditions depending on the path of solar radiation. Thus, west-facing slopes are expected to remain warmer than east-facing slopes through a 24 hour duration. Persistence of greater snowpacks on eastern-facing slopes can be assumed which creates variable moisture conditions.

Areal Coverage for Slope Angle

The map of slope angle was categorized into four classes: 1) class 1 (0°- 22°); 2) class 2 (22.01°- 44°); 3) class 3 (44.01°- 66°); and 4) class 4 (66.01°- 90°) (Figure 16). The following are calculated areal coverages of the study area: class 1: 55.58%; class 2: 40.09%; class 3: 4.23%; and class 4: 0.085%. The areal extent of each class of slope angle was compared to each susceptibility class within the PCA-based landslide map.

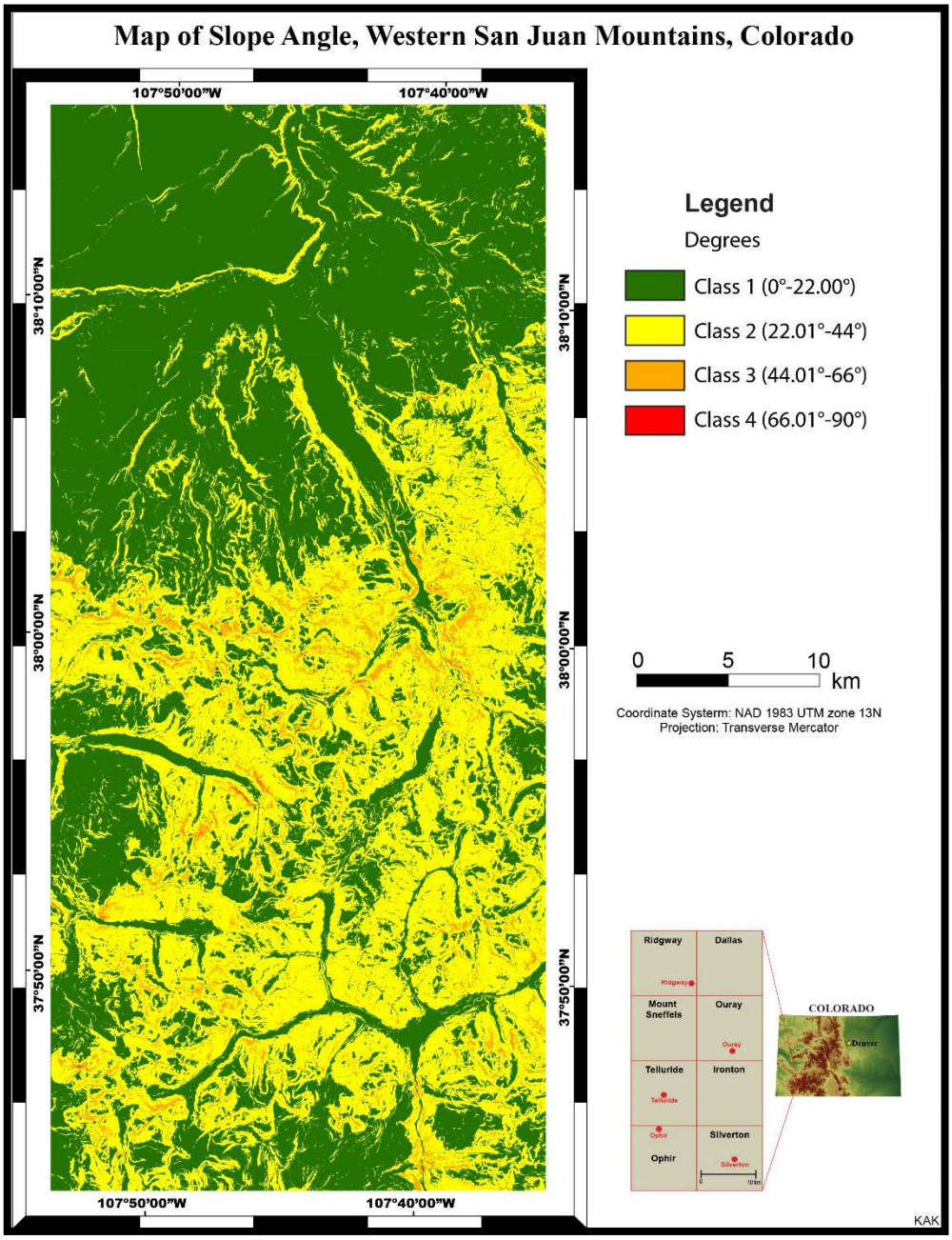

Figure 16: Slope classes 1 and 2 dominate the study area.

Class 1 and class 2 slopes encompass areas with low susceptibility to landslides, accounting for 229.56 km^2 and 1.15 km^2 (Figure 17 A).

Moderate susceptibility to landslide pixels were present within all four slope classes. The areal coverage for moderate susceptibility was 458.69 km^2, 335.29 km^2, 26.38 km^2, and 0.68 km^2 for slope classes 1-4, respectively (Figure 17 B).

For high susceptibility to landslide pixels, all slope classes were mapped. The areal coverage for slope classes 1-4 were: 199.41 km^2, 273.22 km^2, 29.57 km^2, and 0.55 km^2, respectively (Figure 17 C).

All slope classes were mapped for very high susceptibility to landslides. The areal extent for each class was: 1.37 km^2, 37.43 km^2 12.43 km^2, and 0.21 km^2 for slope classes 1-4, respectively (Figure 17 D).

Overall, the rose diagrams display a general agreement with hypothesized landslide risk correlating to slope gradient. Of the four slope classes, class 2 slopes (22.01°- 44°) contribute to moderate, high and very high susceptibility to landslides. Class 1 slopes (0°- 22°) are responsible for high susceptibility, also. Anthropogenic development must be avoided near slopes with class 2, 3, and 4 slope gradients. Although, class 1 slopes are favorable for structures, 0°- 22° slopes within high susceptibility to landslide areas should not be ignored. This analysis demonstrates that an intermittent danger exists from landslide activity in the western San Juan Mountains.

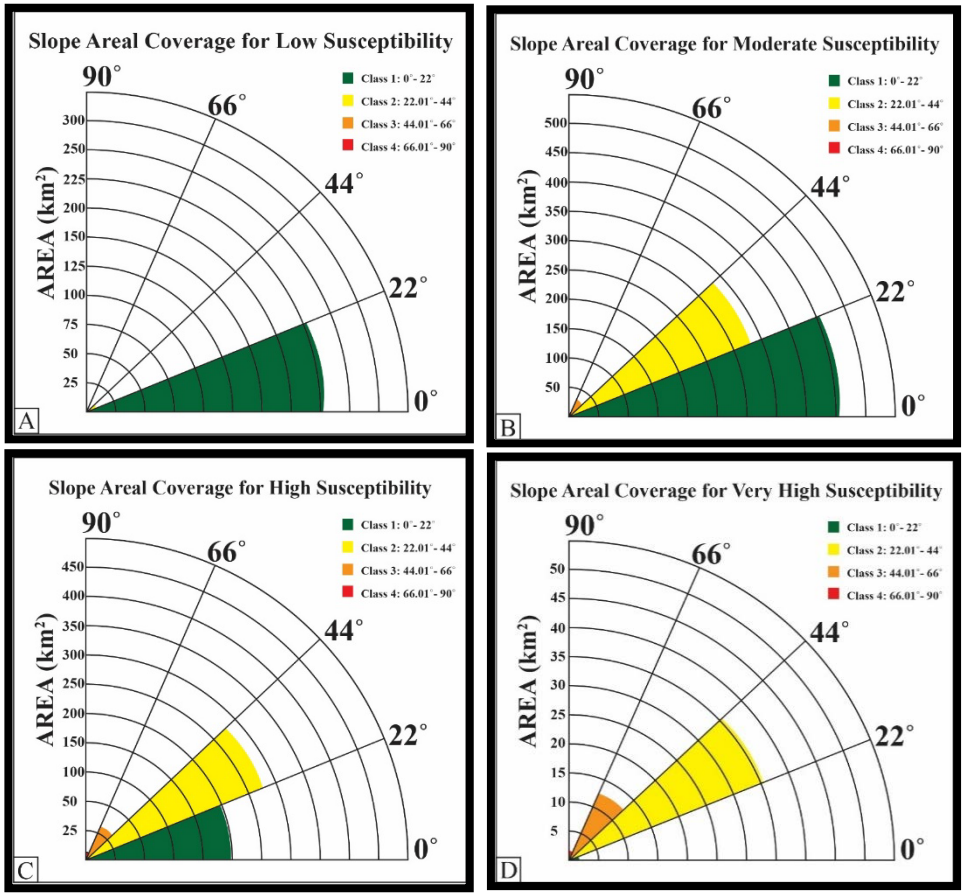

Figure 17: Slope areal coverage for susceptibility classes. A) Low susceptibility; B) Moderate susceptibility; C) High susceptibility; and D) Very high susceptibility.

Frequency Ratio Analysis for Aspect and Slope Angle

Based on the areal coverage for aspect and slope angle for each susceptibility level, frequency ratios were computed to validate the role of said parameters in potential slope instability. The frequency ratio approach is a practical applied probability method widely used to forecast future slope failures (Lee and Min, 2001; Lee et al., 2004). In the interest of landslide vulnerability, it is imperative to determine the correlation between susceptible areas and the specific components of factors responsible for landslides in the San Juan Mountains. If the frequency value approaches or exceeds 1, that implies a higher correlation, whereas, a value less than 1 approaching 0 suggests a lower correlation (Ram Mohan et al., 2011; Demir et al., 2015). Frequency ratio is expressed as (Erner and Duzgun, 2010):

$$FR = \frac{PS}{PC} \tag{9}$$

Where, *FR* is frequency ratio, *PS* is percentage of area covered of susceptibility level examined, and *PC* is percentage of area covered of respective parameter class.

The following are frequency ratio values obtained for aspect (Table 5, 6, 7, 8) and for slope angle (Table 9, 10, 11, 12) correlating to each susceptibility level. The total area of the aspect and slope angle spatial layer; and susceptibility layer mapped is 1615.28 km^2 and 1604 km^2, respectively.

Table 5: North, northeast, south, and northwest aspect orientations have the highest correlation to low susceptibility.

Class	Area of class (km^2)	Percentage of area in class (%; PC)	Area of LS (km^2)	Percentage of LS area (%; PS)	Frequency Ratio
Flat	26.64	1.649	22.95	1.43	0.867
North	204	12.62	71	4.426	0.350
Northeast	240.74	14.90	29.06	1.811	0.121
East	202.84	12.55	0.207	0.012	0.001
Southeast	161.31	9.986	15.68	0.977	0.097
South	159.9	9.899	52.49	3.272	0.330
Southwest	180.39	11.16	16.69	1.040	0.093
West	222.22	13.75	0.187	0.011	0.0008
Northwest	217.24	13.44	22.42	1.397	0.103

*Where LS is low susceptibility.

Table 6: Northeast, south, southwest, north, and northwest aspect orientations have the greatest correlation to moderate susceptibility.

Class	Area of class (km^2)	Percentage of area in class (%; PC)	Area of MS (km^2)	Percentage of MS area (%; PS)	Frequency Ratio
Flat	26.64	1.649	1.07	0.066	0.040
North	204	12.62	131.9	8.223	0.651
Northeast	240.74	14.90	160.4	10	0.671
East	202.84	12.55	29.25	1.823	0.145
Southeast	161.31	9.986	105.6	6.587	0.659
South	159.9	9.899	106.6	6.647	0.671
Southwest	180.39	11.16	117.7	7.314	0.657
West	222.22	13.75	27.96	1.743	0.126
Northwest	217.24	13.44	140.2	8.745	0.650

*Where MS is moderate susceptibility.

Table 7: East and west aspect orientations have the greatest correlation to high susceptibility.

Class	Area of class (km^2)	Percentage of area in class (%; PC)	Area of HS (km^2)	Percentage of HS area (%; PS)	Frequency Ratio
Flat	26.64	1.649	0.002	0.0001	0.00007
North	204	12.62	0.174	0.010	0.0008
Northeast	240.74	14.90	49.67	3.096	0.207
East	202.84	12.55	149.85	9.342	0.743
Southeast	161.31	9.986	39.15	2.440	0.244
South	159.9	9.899	0.117	0.007	0.0007
Southwest	180.39	11.16	44.52	2.775	0.248
West	222.22	13.75	165.83	10.33	0.751
Northwest	217.24	13.44	53.43	3.331	0.247

*Where HS is high susceptibility.

Table 8: East and west aspect orientations have the highest correlation to very high susceptibility.

Class	Area of class (km^2)	Percentage of area in class (%; PC)	Area of VHS (km^2)	Percentage of VHS area (%; PS)	Frequency Ratio
Flat	26.64	1.649	0	0	0
North	204	12.62	0.0003	0.00002	0.000001
Northeast	240.74	14.90	0.098	0.006	0.0004
East	202.84	12.55	22.61	1.409	0.112
Southeast	161.31	9.986	0.064	0.004	0.0004
South	159.9	9.899	0.0002	0.00001	0.000001
Southwest	180.39	11.16	0.1	0.006	0.0005
West	222.22	13.75	27.12	1.691	0.123
Northwest	217.24	13.44	0.092	0.005	0.0004

*Where VHS is very high susceptibility.

Table 9: Class 1 slopes are responsible for low susceptibility.

Class	Area of class (km^2)	Percentage of area in class (%; PC)	Area of LS (km^2)	Percentage of LS area (%; PS)	Frequency Ratio
0°-22°	897.9	55.58	229.5	14.31	0.257
22.01°-44°	647.6	40.09	1.152	0.071	0.001
44.01°-66°	68.39	4.233	0.0004	0.00002	0.000006
66°-90°	1.368	0.084	0	0	0

*Where LS is low susceptibility.

Table 10: Class 2 slopes have the highest correlation to moderate susceptibility.

Class	Area of class (km^2)	Percentage of area in class (%; PC)	Area of MS (km^2)	Percentage of MS area (%; PS)	Frequency Ratio
0°-22°	897.9	55.58	458.6	28.59	0.514
22.01°-44°	647.6	40.09	335.3	20.90	0.521
44.01°-66°	68.39	4.233	26.38	1.644	0.388
66°-90°	1.368	0.084	0.608	0.379	0.448

*Where MS is moderate susceptibility.

Table 11: Class 2, 3, and 4 slopes are all correlated to high susceptibility.

Class	Area of class (km^2)	Percentage of area in class (%; PC)	Area of HS (km^2)	Percentage of HS area (%; PS)	Frequency Ratio
0°-22°	897.9	55.58	199.41	12.43	0.223
22.01°-44°	647.6	40.09	273.22	17.03	0.424
44.01°-66°	68.39	4.233	29.57	1.843	0.435
66°-90°	1.368	0.084	0.551	0.034	0.408

*Where HS is high susceptibility.

Table 12: Class 3 and 4 slopes are all correlated to very high susceptibility.

Class	Area of class (km^2)	Percentage of area in class (%; PC)	Area of VHS (km^2)	Percentage of VHS area (%; PS)	Frequency Ratio
0°-22°	897.9	55.58	0.203	0.012	0.0002
22.01°-44°	647.6	40.09	37.43	2.333	0.058
44.01°-66°	68.39	4.233	12.43	0.774	0.183
66°-90°	1.368	0.084	0.208	0.012	0.153

* Where VHS is very high susceptibility.

Lithologic Conditions

The implementation of lithologic factors in landslide studies is vital to delineate areas prone to mass movement. Lithology subject to weathering poses a threat to human endeavors near steep slopes. The identification of lithologic strength serves as a measure for the degree of weathering vital to determine geomorphic thresholds on slopes. For this purpose, the Caterpillar© rippability index provides a standard to quantify erosion of bedrock. Geologic interpretations generally involve a level of subjectivity; the application of the rippability index also solely rests on the decisions of the researcher.

To identify the role of geology for the initiation of mass movement, the rippability index refined the heterogeneous geology of the study area for spatial analysis. Figure 18 displays that mean surface roughness broadly decreases from surficial deposits to sedimentary lithology and igneous/metamorphic lithology. Gravel (0.415) has the highest surface roughness for surficial deposits. For sedimentary strata, sandstone (0.286) and siltstone (0.188) have the highest and lowest mean surface roughness. Felsic gneiss (0.175) has a higher mean surface roughness than quartzite (0.150) mapped in the area. Igneous rocks, andesite (0.160) and granitoid (0.227) were classified for lowest and high mean surface roughness values respectively. The overall trend indicates that higher average surface roughness is present for lithology more prone to weathering, as opposed to crystalline rock. Another factor possibly impacting values of surface roughness is the transport and deposition of surficial deposits leading to irregular surfaces. In-situ crystalline bedrock that has undergone minimal weathering consists of smoother

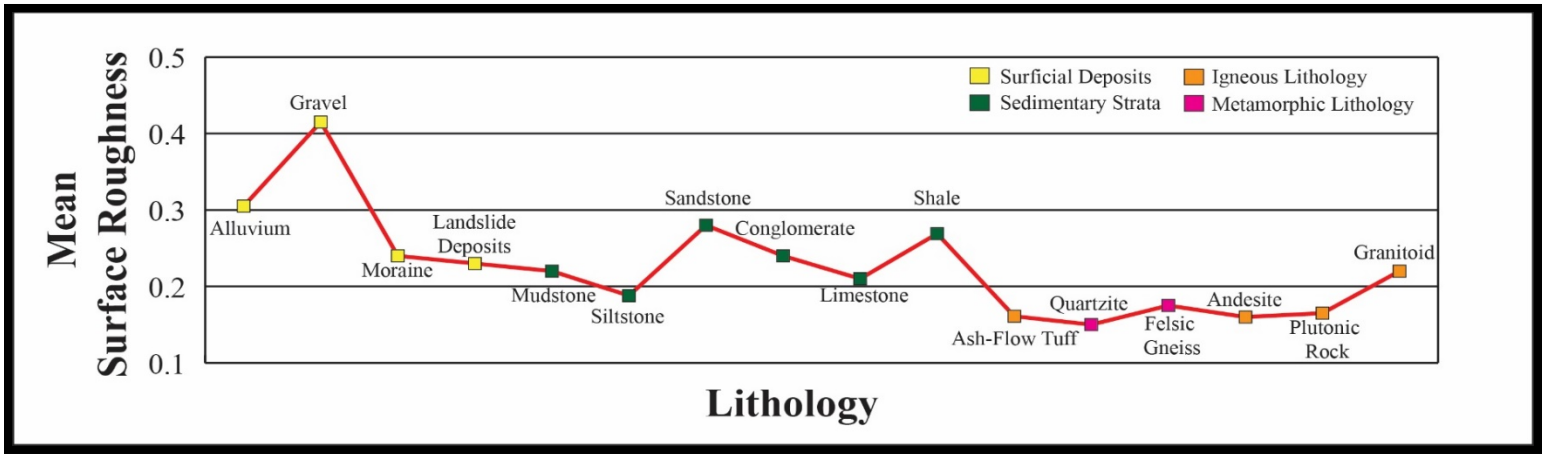

Figure 18: Surficial deposits have the highest average surface roughness for all lithology observed.

surfaces.

Lithology Weathering Factors

Rock forming processes and the exposure of bedrock to the elements, gradually leads to the weathering of lithology. Several factors including, planes of weaknesses, jointing, interbedding and vegetation growth affect the durability of bedrock (Figure 19). Frequent field observations and monitoring of problematic lithology is required to recognize unstable slopes. Studies show that lithologic variation is a major cause for undercutting of slopes leading to an increased potential for rockfall (Vanderwater et al., 2005; Santi et al., 2009).

The potential for mass movement in the San Juan Mountains is driven by volcanic lithologies overlying weaker sedimentary formations. Fieldwork documented the presence of the aforementioned factors responsible for the physical weathering of bedrock. Site specific studies in the San Juan Mountains which focus on weaker outcrops prone to erosion are needed.

Figure 19: Interbedded shale and limestone observed in the Hermosa Formation of the Perimeter Trail, Ouray (8/14/15). Field notebook is 15 cm wide.

Susceptibility to Mass Movement from Roads

Increased anthropogenic activity in mountainous terrain can cause accelerated slope instability (Figure 20). Excavation of mountainsides, and additional widening of roads can cause undercutting and removal of slope support. The vibrations from passing cars can also trigger slope instability (Ayalew and Yamagashi, 2005; Mittal et al., 2008).

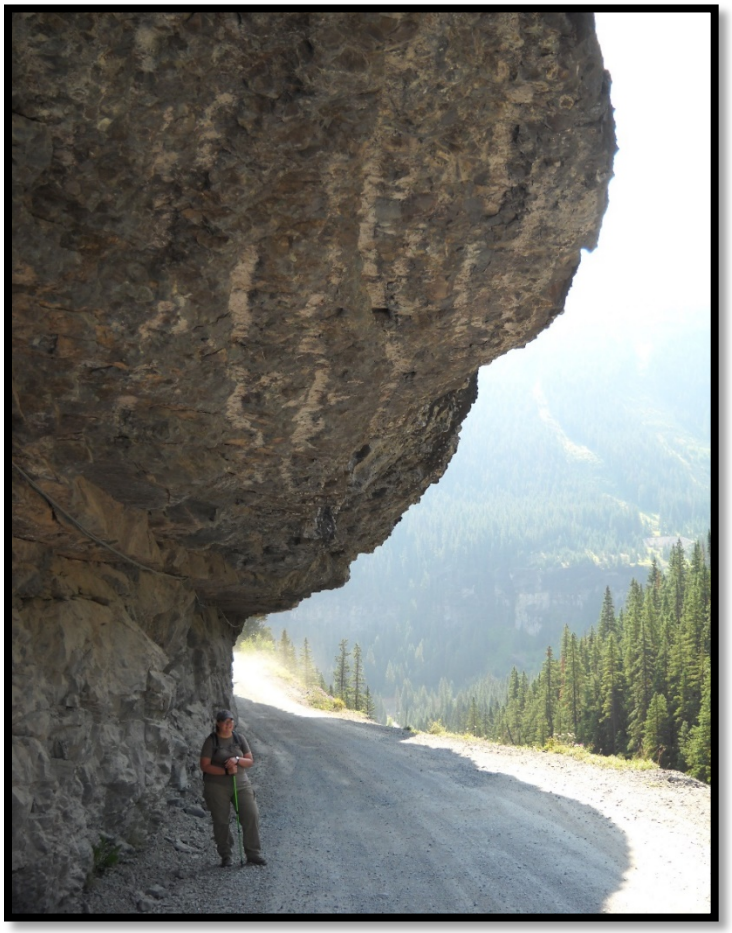

Figure 20: The access road to Camp Bird Mine near Ouray is significantly undercut (8/21/15).

Colorado Highway 550, 145 and mountains road in the area are susceptible to landslides. GIS analysis has established that a high potential for mass movement exists in close proximity to roads in the region (Figure 21). Colorado Highway 550 was closed for more than a month in January 2014, as the result of a rockslide that blocked the highway and prevented travel between Ouray and Silverton. Repair work and the reinforcement of crib walls cost $ 4.9 million (Colorado Department of Transportation, 2016). With an increase in year-round residents, greater influx of tourists, and

recreationalists traversing high mountain roads a heighten risk occurs of encountering the dangers of landslide activity on roads in the region.

Sites of potential damage to roads were mapped by measuring the buffer distance to roads for the proximity to the four categories of susceptibility to landslides (Figure 22). Predominantly, a considerably greater number of potential points for damage to roads were mapped for the PCA method. This is a result of an extensive pixel-based PCA model for susceptibility to landslides, as opposed to the lack of site specific mapping within the heuristic model. For the PCA based model, low, moderate, and high susceptibility to landslides graphs show a decrease in the number of points progressively from 50 m to 250 m road buffers. A general upward trend of increase in sites for potential damage is observed for the very high susceptibility landslide graph for the PCA method. A decreasing trend is observed for the number of points for potential damage for hazard from low susceptibility. For moderate and very high susceptibility, however, an increase in potential points for hazard to roads from 50m to 250 m is observed. Lastly, the number of points in the high susceptibility graph do not display variability in the number of potential sites for infrastructural damage.

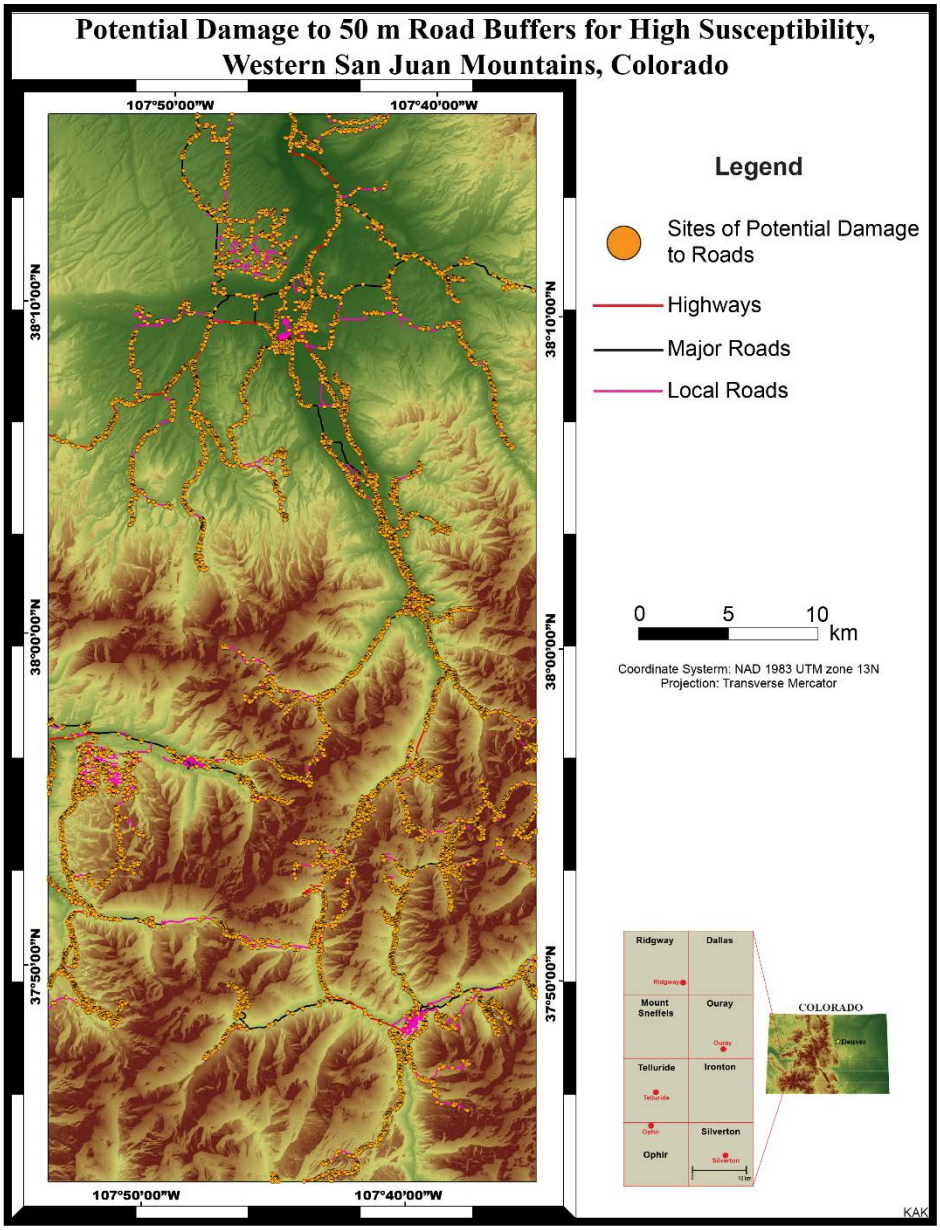

Figure 21: A total 3,906 points for potential hazard to roads were mapped for the PCA method at 50 m buffers.

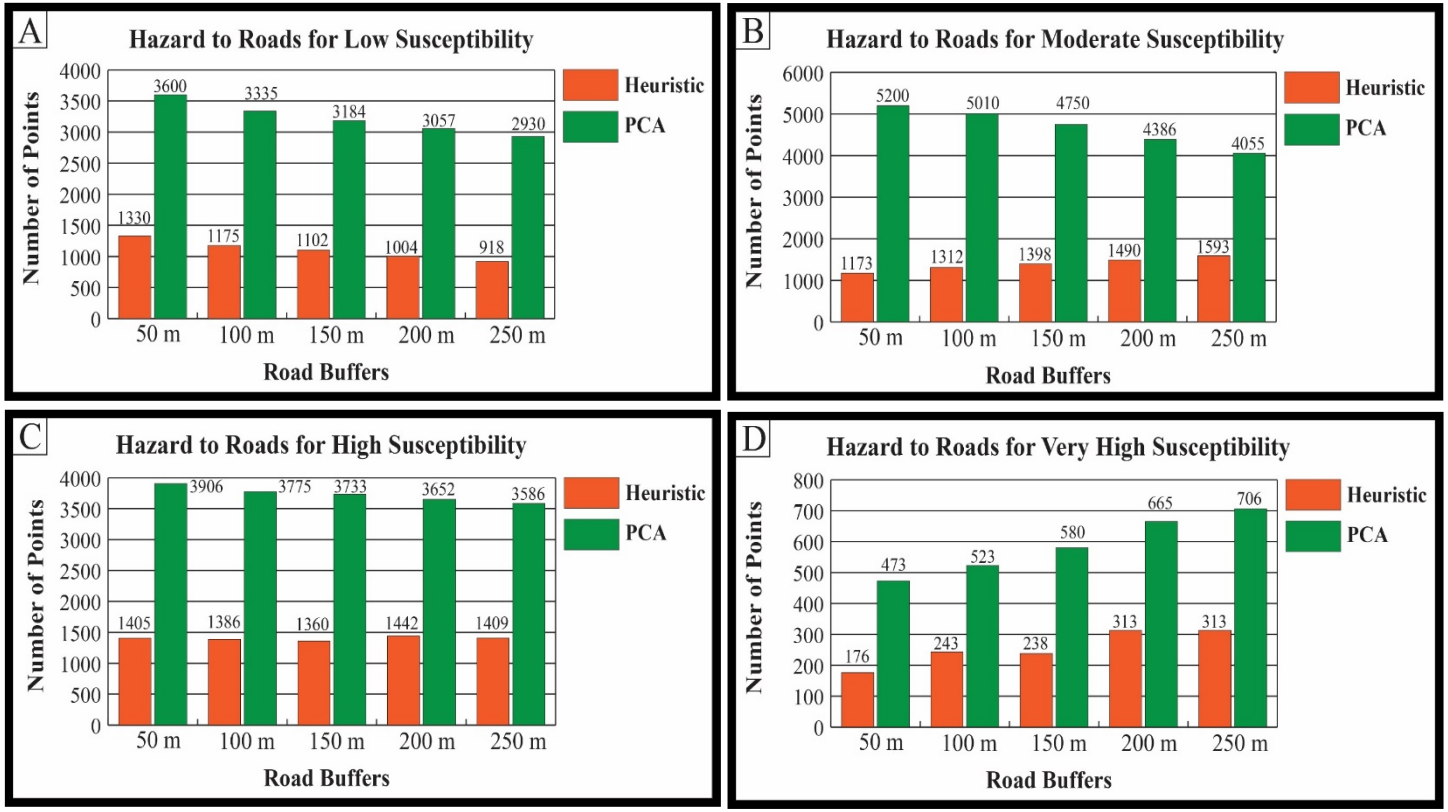

Figure 22: Bar graphs showing the number of points per road buffers for susceptibility classes. A) Low susceptibility; B) Moderate susceptibility; C) High susceptibility; and D) Very high susceptibility.

3-D Model of Susceptibility to Landslides

3-D visualization is a valuable tool in numerous scientific disciplines. Technological advances in software have enabled geoscientists to implement novel techniques to visualize landscapes and geomorphic systems. The use of 3-D visualization in modeling landslides has progressed considerably in the past decade (Teza et al., 2007; Barbarella et al., 2015). Immersive visualization of heuristic and PCA-based susceptibility to landslide maps is provided in separate supplementary videos. Furthermore, integration of emerging geospatial methods, utilizing GIS and 3- dimensional modeling, will enhance the prediction of landslides (Gigli et al., 2014; Warrick and Ritchie, 2017).

Figure 23 is an interactive 3-D model of the PCA-based map of susceptibility to landslides. The 3-D module was prepared in ArcScene® software and projected in 3-dimensions at the Immersive Visualization Center (IVC) at Texas A&M University. This virtual model presents the viewer an opportunity to visualize landslide occurrence with respect to the topography of the San Juan Mountains.

This 3-D landslide model has numerous practical applications. 3-D visualization allows the viewer to maneuver the model accordingly to interpret highly vulnerable slopes. A virtual fly-by of the study area provides the layperson a dynamic true-to-life perspective of an active landscape (Figure 24). This model serves as a valuable educational resource to those who have difficulty in visualizing landscapes and pertinent geomorphic processes. This visualization is provided in a supplementary video. Furthermore, this model can be applied to inform residents and regional planners to promote best land-use practices in a dynamic landscape. This work serves as a standard for future landslide studies to build a framework to improve landslide prediction in the San Juan Mountains.

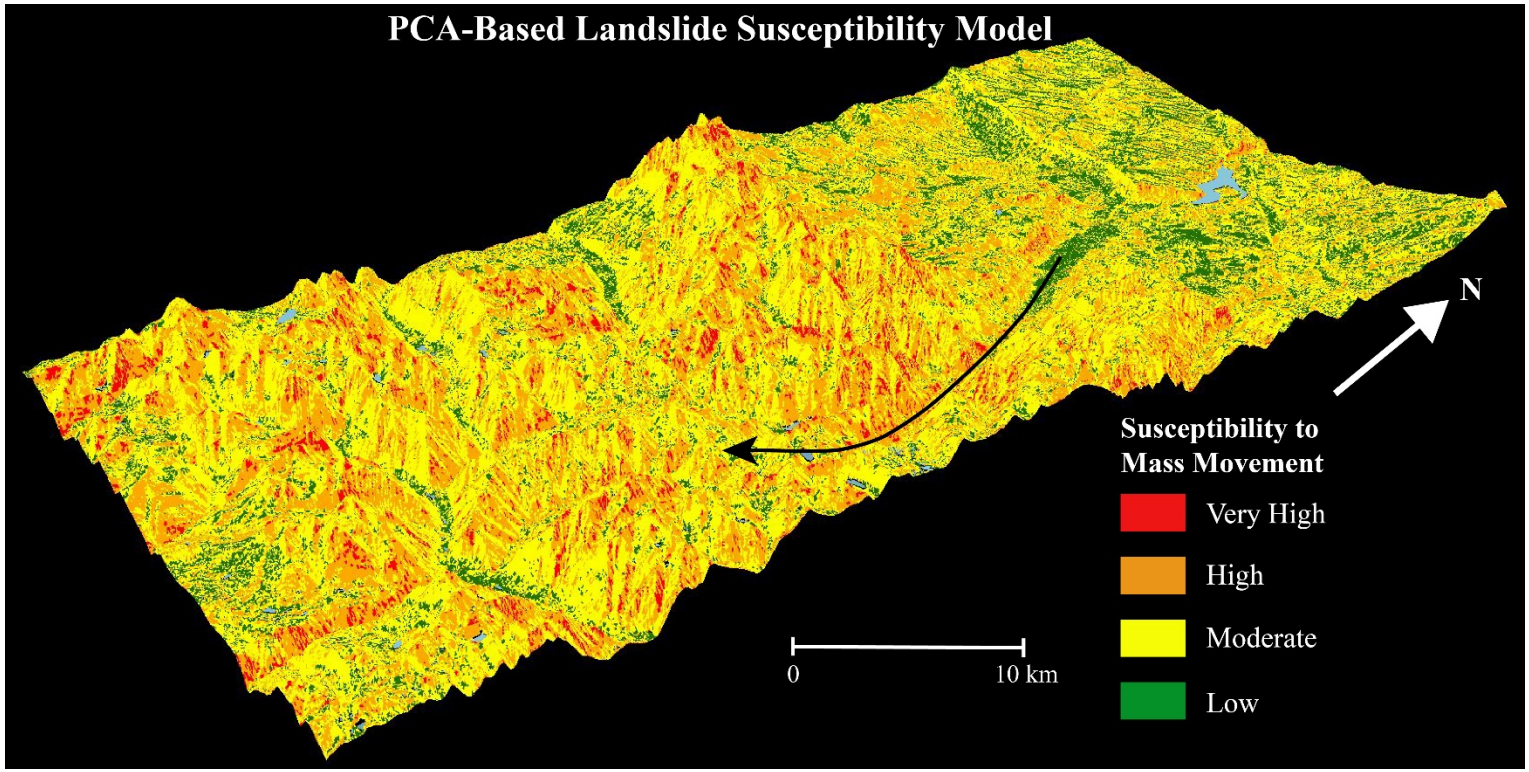

Figure 23: A 3-D perspective of the PCA-based susceptibility to landslide map. The black arrow denotes the path of the fly-by pictured in the following figure (Reprinted with permission from Kelkar and Giardino, 2017).

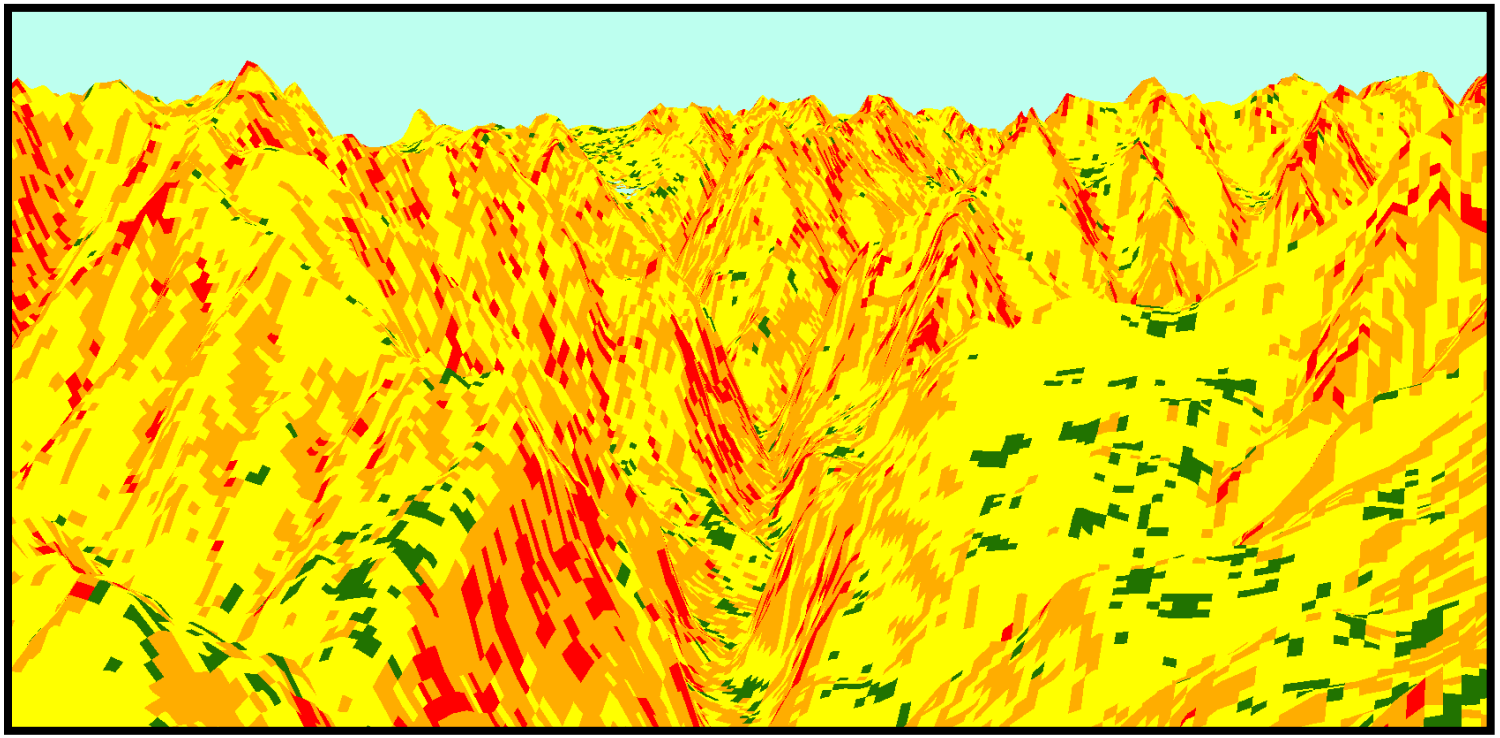

Figure 24: A screenshot of a fly-by heading south through the former glaciated valley near Ouray.

Conclusion

Mass movement is constantly altering the landscape of the San Juan Mountains. With an increasing number of year-round residents and recreationalists choosing to inhabit the region even with the risk from mass movement, the likelihood of a major catastrophic event is increasing. The public must be made aware to understand the hazards associated with a dynamic landscape. Hence, the prediction of mass movements is crucial to protecting lives and preventing damage to infrastructure. This study has developed a cost effective; accurate method to evaluate the potential for mass movement in mountain terrain. Improved interpretation of mass movement is vital to avoid life-threatening conditions and safeguard economic interests in the San Juan Mountains. Based on the analyses of the data, the following conclusions can be offered:

1) Aspect, slope angle, and geology have the greatest relative weighted influence on slope failure in the San Juan Mountains.
2) The western San Juan Mountains are experiencing a general uniform rate of erosion based on hypsometric analysis.
3) East and west-facing slopes have the greatest areal coverage increasing the likelihood of high and very high susceptibility to landslides.
4) Class 2 slopes (22.01°- 44°) have the greatest areal coverage also increasing the likelihood for high and very high susceptibility to landslides.
5) Class 2, 3, and 4 slopes are highly correlated to high susceptibility, classes 3 and 4 are highly correlated to very high susceptibility.

6) Surficial deposits have the greatest mean surface roughness off all lithologic units.
7) Areas within 50 m from roads are highly susceptible to landslides.
8) Using a combination of heuristic, deterministic, and statistical approaches will improve landslide prediction.

CHAPTER III

GEOMORPHIC PHENOMENA OF THE WESTERN SAN JUAN MOUNTAINS, COLORADO

Synopsis

Mass movement is a recurrent phenomenon in the rugged topography of the western San Juan Mountains, Colorado. Debris flows, landslides, and snow avalanches pose a significant threat to human life and infrastructure in the area. In this study, the surficial geomorphology of the western San Juan Mountains was mapped at a scale of 1:3,000 to determine the spatial distribution of phenomena which potentially pose hazards from slope failures.

The study area encompasses the USGS quadrangles: Ridgway, Dallas, Mount Sneffels, Ouray, Telluride, Ironton, Ophir, and Silverton covering an area of approximately 1,615 km^2. Mapped surficial landforms were categorized as 1) glacial landforms; 2) glaciofluvial landforms; 3) fluvial and water; 4) gravitational landforms; 5) morphological components; 6) outcrop geology; and 7) periglacial landforms. Mapping was completed using a combination of field mapping and air-photo interpretation. Talus and landslide deposits are the dominant landforms in the area. This map provides a detailed understanding of the landscape evolution of the San Juan Mountains. Furthermore, this valuable resource will assist in future geomorphological studies and land-use planning.

Introduction

The San Juan Mountains are situated in southwestern Colorado and encompass ~ 1,615 km^2. Composed primarily of volcanic strata overlaying shales, limestones, and sandstones, the San Juan Mountains were extensively glaciated during the Pleistocene. As a result of glaciation and subsequent slope processes, slopes in the area are over steepened and prone to mass movement.

Geomorphology is an illustrative discipline, often expressed through mediums such as sketches, photographs, block diagrams, and maps which display the evolution of landforms. Geomorphological maps serve as a visual representation of: 1) landforms, 2) surficial deposits, 3) geomorphic processes and, 4) chronology of geomorphic processes (Demek, 1972; Vitek et al., 1996; Henaff, 2011; Otto and Smith, 2013). Geomorphology was first developed by W. M. Davis (1909) and G. K. Gilbert (1877) to explain how processes- shaped landforms. During the early 20^{th} century, geomorphological mapping was initiated at site-specific, and generalized regional-scale landform interpretations (Fenneman, 1931; Reisz, 1962; Hayden et al., 1986). Following World War II, interest in geomorphological mapping intensified particularly in Europe. European geomorphologists shifted focus from mapping individual features to mapping comprehensive regional-scale geomorphology to highlight factors driving landscape change (Hayden et al., 1986; Verstappen, 2011). This development in geomorphology prompted numerous countries including France, Germany, Switzerland, and Poland to commence detailed nation-wide mapping at scales from 1:10,000 to 1:100,000 (Annaheim, 1956; Klimaszewski, 1956; Galon, 1962; Klimaszewski, 1963). As a result

of a greater number of maps being drafted in the various European countries, differences in ideologies, methodologies, and compatibility of map applications emerged. In addition to these challenging differences faced by the geomorphology community, the use of diverse symbols further complicated the use and interpretation of geomorphological maps by the international community.

The International Geographical Union (IGU) Subcommission on Geomorphological Mapping (SGM) convened in Krakow, Poland, in 1962 to establish a standardized set of guidelines for modern geomorphological mapping (Hayden et al., 1986; Klimaszewski, 1982). A standard legend for international use was approved in subsequent SGM meetings (Gellert, 1968; Bashenina, 1972; Demek, 1972; Gellert and Scholz, 1974). Unfortunately, modern geomorphological cartography, however, is still restrained because of continuing diverse techniques and applications.

Today numerous applications of geomorphological maps exist, which are based on the objective of the cartographer for an intended audience. Dramis et al., (2011) summed up the concise role of geomorphic mapping with their simple statement: “the importance of geomorphological maps has increased progressively.” The utilization of geomorphological maps has gradually evolved from providing spatial distribution of landforms to a provisional tool for fundamental investigation in various environmental disciplines: ecology, forestry, and pedology (Panizza, 1978; Cooke and Doornkamp, 1990; Brunsden, 2003). In recent years, geomorphological maps have become essential for engineers, urban planners, risk managers, and land conservationalists studying

growing anthropogenic pressures on landscapes (Gustavsson et al., 2006; Griffiths and Abraham, 2008; Henaff, 2011).

The methodologies available to produce geomorphological maps have progressively advanced because of technological advances. The preparation of modern maps involve three stages: pre-mapping, field mapping, and digitization (Knight et al., 2011). Specific tasks for each stage of mapping vary depending on the aim of the cartographer. To conduct successful field mapping, pre-mapping tasks such as obtaining satellite imagery, topographic/geologic maps, and interpreting air-photos of the study area are necessary. Field mapping, though a time-consuming strenuous task, provides unparalleled access to topography by first-hand observations in the field. Subsequent field reconnaissance consists of drafting field maps of observed landforms by traversing the region, notetaking, field photography, and collecting Global Positioning System (GPS) locations (Otto and Smith, 2013). The accuracy of field mapping is determined by the experience-level associated with landform interpretation of the field mapper, and presence of surficial features (Sahlin and Glasser, 2008; Rose and Smith, 2008; Wilson, 2009).

Prior to the advent of Geographic Information Systems (GIS), geomorphological maps were traditionally hand-drafted. A range of emerging digitization programs compatible with high-resolution satellite data, and remote-sensed data have facilitated the preparation of more detailed geomorphological maps (Blomdin et al., 2016; Lardeux et al., 2016; Lindholm and Heyman 2016). In addition, GIS functions provide the investigator an efficient medium of mapping, modeling, monitoring, and managing

relevant data to construct geomorphological maps. Thus, a mapping study integrating the aforementioned approaches will consolidate the evaluation of data in the construction of maps of the surficial geomorphology in the San Juan Mountains.

A growing number of communities inhabit unstable slopes. These settlement locations are driven, in part, by dramatic population growth (Petley, 2010). Unfortunately, forecasting slope failures is a challenge geomorphologists face because of the episodic and spatially discontinuous occurrences. Recent studies (Claessens et al., 2007; Hearn and Hart, 2011; Martinez-Grana et al., 2016) combine various geomorphological mapping techniques to delineate the spatial extent of mass-movement features to promote best land-use practices.

The preliminary assessment of unstable slopes world-wide is well recorded based on accounts of ground displacements. Additionally, long-term monitoring of slopes is required. Thus, geomorphological mapping of features characteristic of unstable conditions coupled with on-site field investigations facilitates international landslide inventories (Galli et al., 2008; Frodella et al., 2014; Gorum et al., 2017). Although, the stated approach has been used extensively worldwide, mass movement studies in the San Juan Mountains lack a comprehensive geomorphological map, which highlights the features associated with actual and potential slope failures.

Mass movement is constantly modifying the landscape of the San Juan Mountains. This dynamic situation begs the question: what is the distribution of surficial phenomena, which indicate potential hazards from slope failure?

Objective

The goal of this research is to determine the major components that contribute to unstable slopes in the San Juan Mountains by mapping the features of mass movement in the San Juan Mountains.

Study Area

The study area encompasses eight USGS quadrangles: Ridgway, Dallas, Mount Sneffels, Ouray, Telluride, Ironton, Ophir, and Silverton located in southwestern Colorado (Figure 25). This section of the San Juan Mountains is situated west of the continental divide within the southern Rocky Mountains physiographic province (Thornbury, 1965). The study area extends north south from Silverton to Ridgway (N 38˚09’ 10”, W 107˚45’ 21” to N 37˚48’ 44”, W 107˚39’ 52”) and east west from Telluride to Silverton (N 37˚56’ 50”, W 107˚51’ 34” to N 37˚48’ 40” to W 107˚39’ 33”). Access to the region is *via* the San Juan Skyway consisting of U.S. Highways 62, 145, and 550, respectively. Hiking trails and county roads provide access to the backcountry.

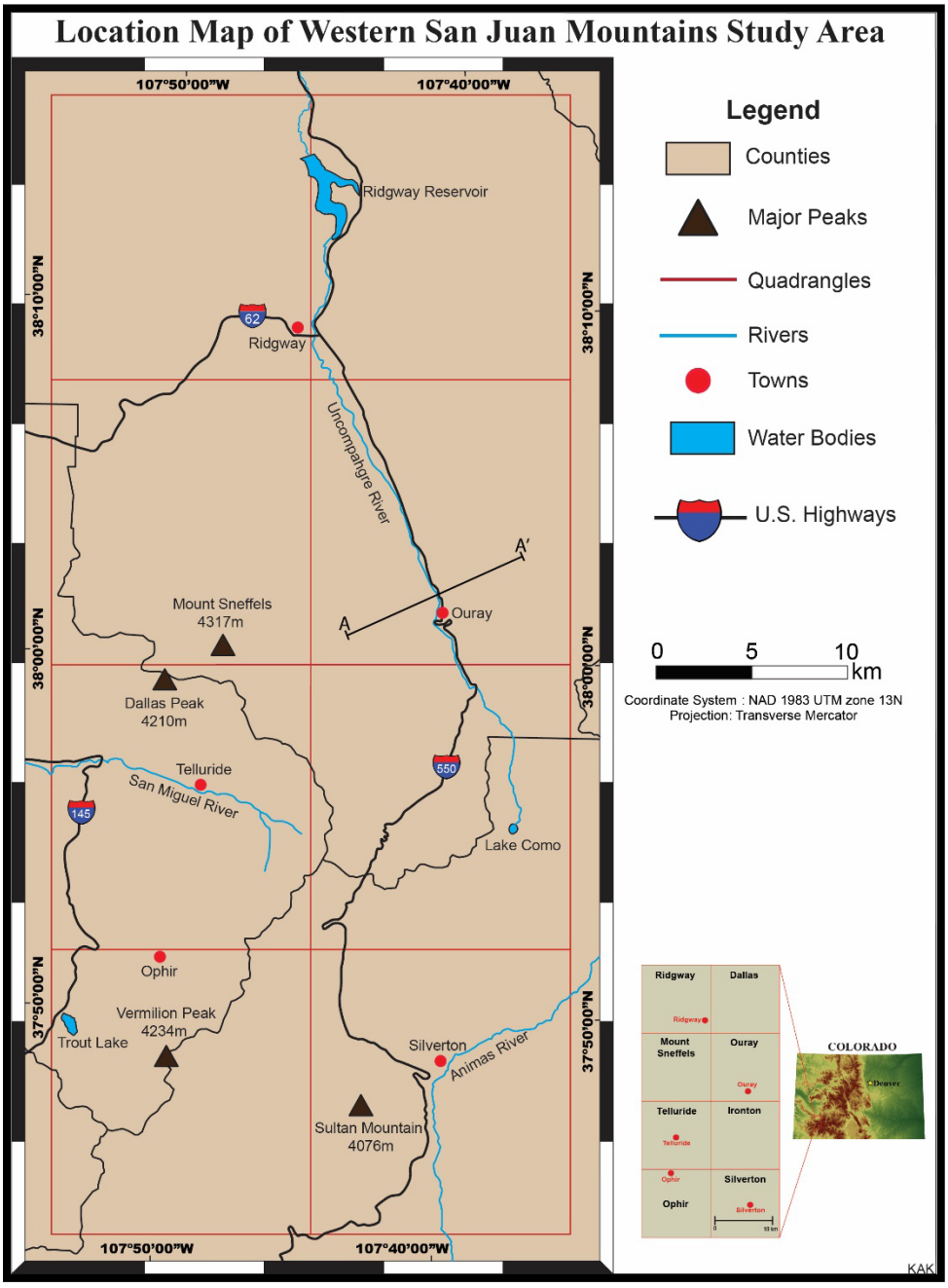

Figure 25: Location and extent of study area. The A to A' transect shows the location of the generalized geologic cross-section in figure 28.

Geology and Geomorphology

The study area ranges from forested slopes in the lower sections to bare, rugged rocky slopes above tree-line. The San Juan Mountains are drained by the Animas, San Miguel, and Uncompahgre Rivers. Elevations within the study area range from 2,050 m at the Ridgway Reservoir to 4,317 m at the summit of Mount Sneffels (Figure 26). Hillslope morphology varies from small gently rolling hills to steep mountainous terrain. Dominant geomorphic features include rocky hills, glaciated and incised valleys, floodplains, landslides, avalanche tracks and cones, streams and rivers, rock glaciers and various glacial erosional and depositional landforms.

The present-day landscape of the western San Juan Mountains is the result of orogeny, extensive volcanism, glacial erosion, fluvial and mass movement processes (Cerveny and Blair, 1997) (Figure 27). The study area is composed primarily of two lithologies: 1) Tertiary igneous rocks, which consist of massive flows, breccia, and rhyolitic tuffs, and 2) Cretaceous sedimentary rocks, which include limestone, shale, siltstone, and sandstone (Luedke and Burbank, 1962; Burbank and Luedke, 1964; Burbank and Luedke, 1966; Hail, 1989; Steven and Hail, 1989; Luedke, 1996; Luedke and Burbank, 2000; Moore, 2004).

The volcanic lithology is primarily massive lava and pyroclastic flows; whereas, the sedimentary rocks are remnants of an ancient seaway (Figure 28) (Moore, 2004). Episodic uplift of the region during the Mesozoic has resulted in the deformation and faulting of the lithology (Cerveny and Blair, 1997). The advance of Quaternary glaciers eroded the landscape and formed various erosional and depositional glacial landforms.

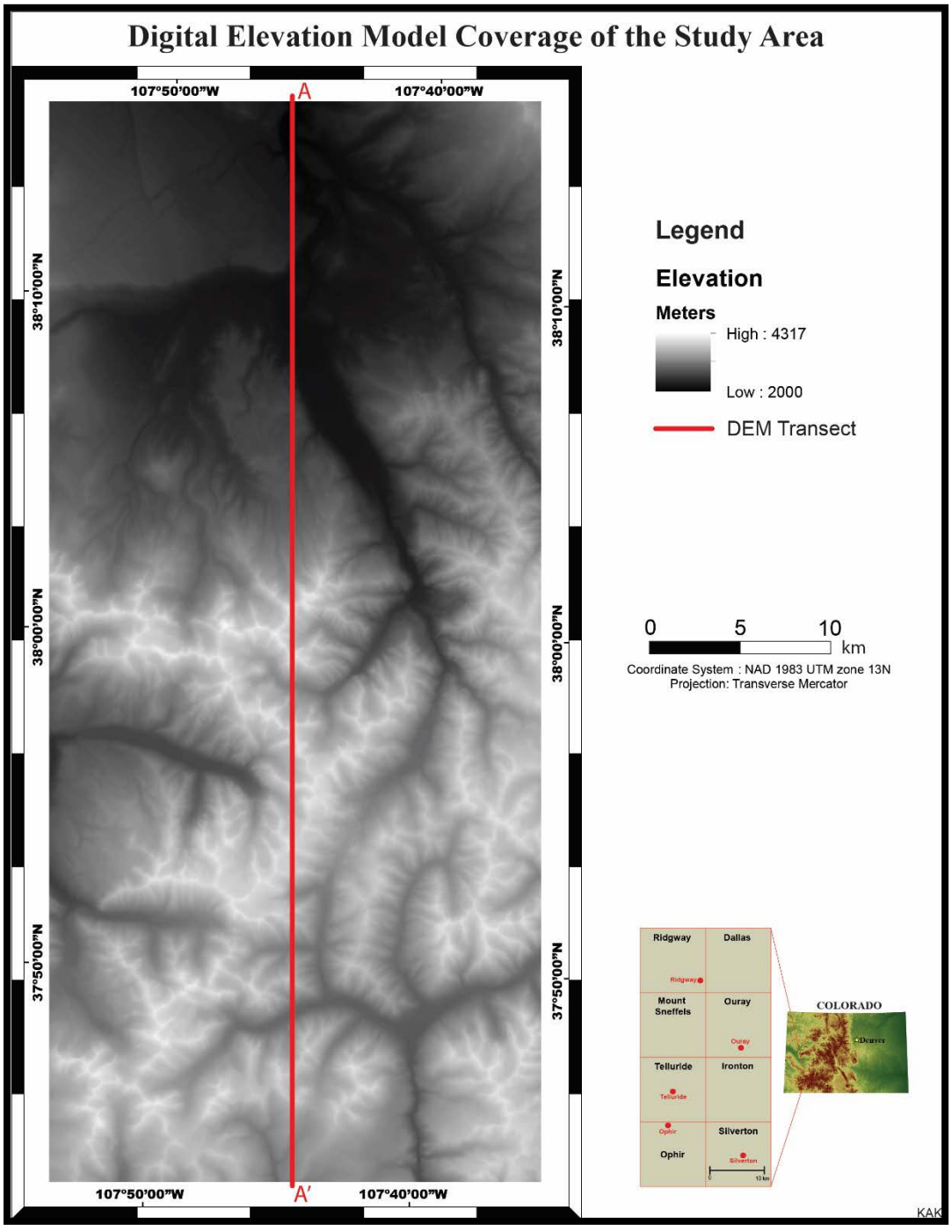

Figure 26: Moderate to high topography of the San Juan Mountains.

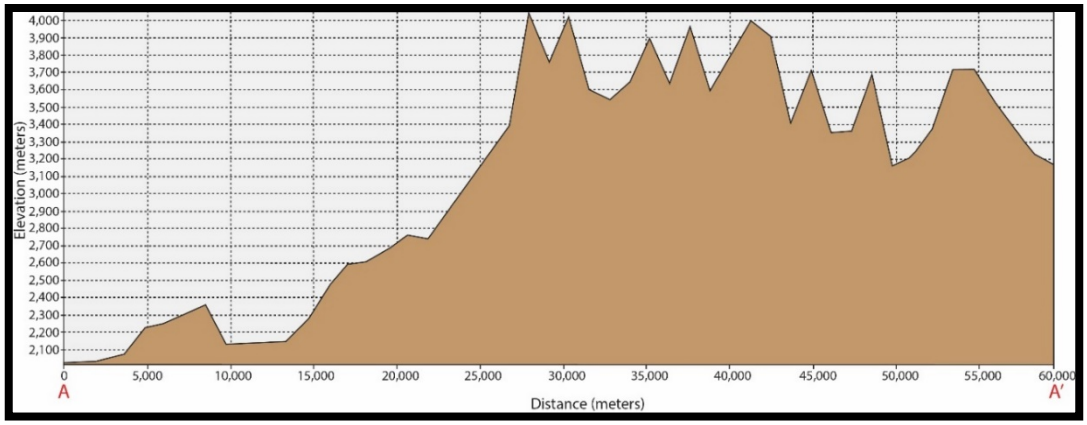

Figure 27: Elevation profile of the A-A' transect.

Pleistocene landslide deposits, originating from local bedrock, occur throughout the area, and Quaternary alluvium fills the valley floors in the study area (Mather, 1957). Mass movement, ranging from talus, landslides, debris flows to snow avalanches, continue to shape the topography of the San Juan Mountains.

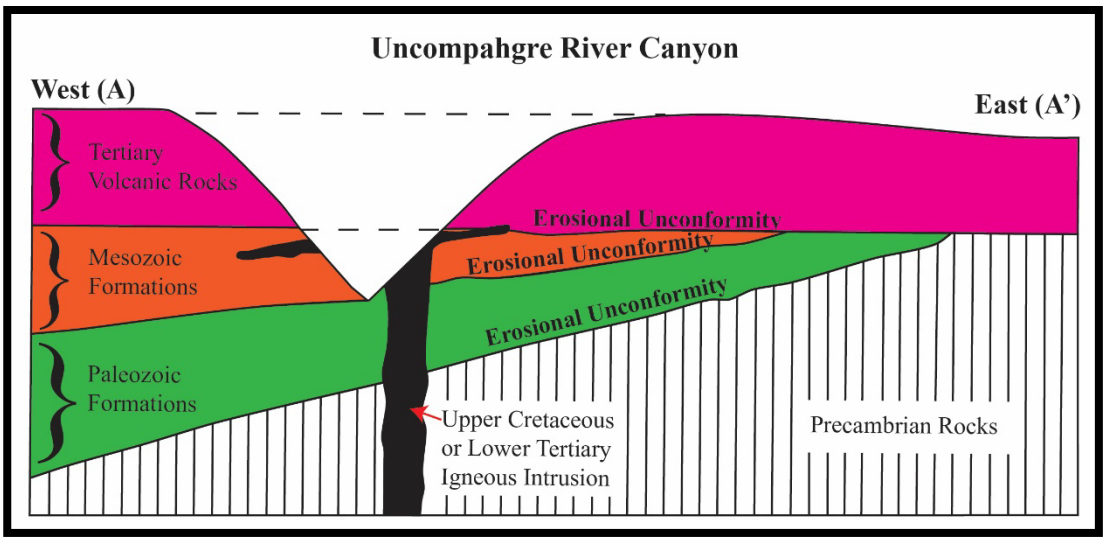

Figure 28: Generalized geologic cross-section of the study area (Reprinted from Moore, 2004).

The glacial history of the western San Juan Mountains has set the stage for slope instability in the area. During the Last Glacial Maximum, a large ice cap covered the San Juan Mountains, and numerous valleys were filled with alpine glaciers. These glaciers provided support for many ice-contact slope deposits in the valleys (Atwood and Mather, 1932; Guido et al., 2007; Carrara, 2011). Recession to a state of deglaciation facilitated glacial erosion and deposition that had a strong imprint on the present geomorphic landscape (Figure 29). A simulation of deglaciation is provided in a supplementary video.

Figure 29: Numerous U-shaped valleys indicative of glacial erosion are present in the San Juan Mountains (8/08/15).

Since the end of glaciation, mass movement is another major process operating in the San Juan Mountains. Howe (1909) was the first to call attention to the widespread occurrence of landslides in the San Juan Mountains. Landslide studies in the area conducted over the past century have established the occurrence of diverse types of mass movement, but, unfortunately, do not convey the imminent risk that can affect the current built environments and population (Varnes, 1949; Armstrong and Armstrong, 1977; Luedke and Burbank, 1977; Joachim, 1986).

Reconnaissance hazard mapping was initiated in the 1970s. During this time, mass movement deposits surrounding major towns were mapped to provide the data necessary to enforce guidelines for development (Ives et al., 1976; Ives and Bovis, 1978; Ives and Krebs, 1978). Since then, a focus on mapping of the present-day extent of mass movement deposits in the San Juan Mountains has been nearly absent. The lack of interest in the geomorphic processes that operate in the region created a major void in understanding where and why slopes fail in the San Juan Mountains.

Methodology

The methodology for this study consisted of: 1) field mapping; 2) digitizing; 3) interpretation; and 4) construction of field maps.

Field mapping was based on USGS geologic maps at 1:24,000 (Luedke and Burbank, 1962; Burbank and Luedke, 1964; Burbank and Luedke, 1966; Hail, 1989; Steven and Hail, 1989; Luedke, 1996; Luedke and Burbank, 2000) and Google Earth® imagery scans at 1:3,000 to map features observed in the field. Specific landforms were mapped on the imagery.

On completion of fieldwork, digitization of the geomorphological map was conducted using ArcMap 10.3® software. The final geomorphic map was constructed at 1:3,000 by interpreting digital geologic maps in kml-file format and satellite imagery available on the world imagery option in ArcMap 10.3®. Additional, analysis of Google Earth® imagery was undertaken to visualize landforms in three-dimensions, which were not accessed during fieldwork.

Morphology was mapped as polygons representing the spatial extent of each specific type of landform using the ArcMap® digitization tool (Stroeve et al., 2013; Lardeux et al., 2016). Ridges were mapped as lines, using symbols proposed by Demek (1972). Areal coverage of each respective type of landform was calculated in ArcMap 10.3®. Supplementary map components were drafted using Adobe Illustrator CC®.

Results and Discussion

Landforms were mapped into eight categories: 1) glacial landforms; 2) glaciofluvial landforms; 3) fluvial and water; 4) gravitational landforms; 5) morphological components; 6) outcrop geology; 7) periglacial landforms; and 8) cultural features (Figure 30). Each category of landform was derived from the respective origin of the landform. A 3-D visualization of the geomorphological map is available as a supplementary video.

Several glacial deposits were identified in the study area. The only ground moraine identified is in the vicinity of Trout Lake. This ground moraine sits in flat topography, consisting of Quaternary glacial till (Luedke and Burbank, 1962). The extent of Pleistocene lateral moraines, comprised of unconsolidated to consolidated poorly sorted sediment ranging from clay to boulders, were identified and mapped (Leudke, 1996) (Figure 31). Former ice-contact slope deposits which are prone to potential future slope failure were mapped as lateral moraines. Several recessional moraines within cirque basins were mapped, also (Figure 32); the recessional moraines consist of glacial till.

Larger recessional moraines derived from the Uncompahgre Glacier were identified adjoining the mesa near Ridgway (Carrara, 2011). Terminal moraines classified in the area, establish the foremost extent of former Pleistocene glaciers (Luedke, 1996). In total two terminal moraines were mapped. First, the terminal moraine of the Uncompahgre Glacier indicates the northernmost periphery of glacial advance in the study area. The other terminal moraine is situated in Telluride near the Society Turn locality (Giardino per. comm. 2016). Unfortunately, no present-day field observations are possible of this terminal moraine because it was excavated in the 1990s for construction of Earthworks.

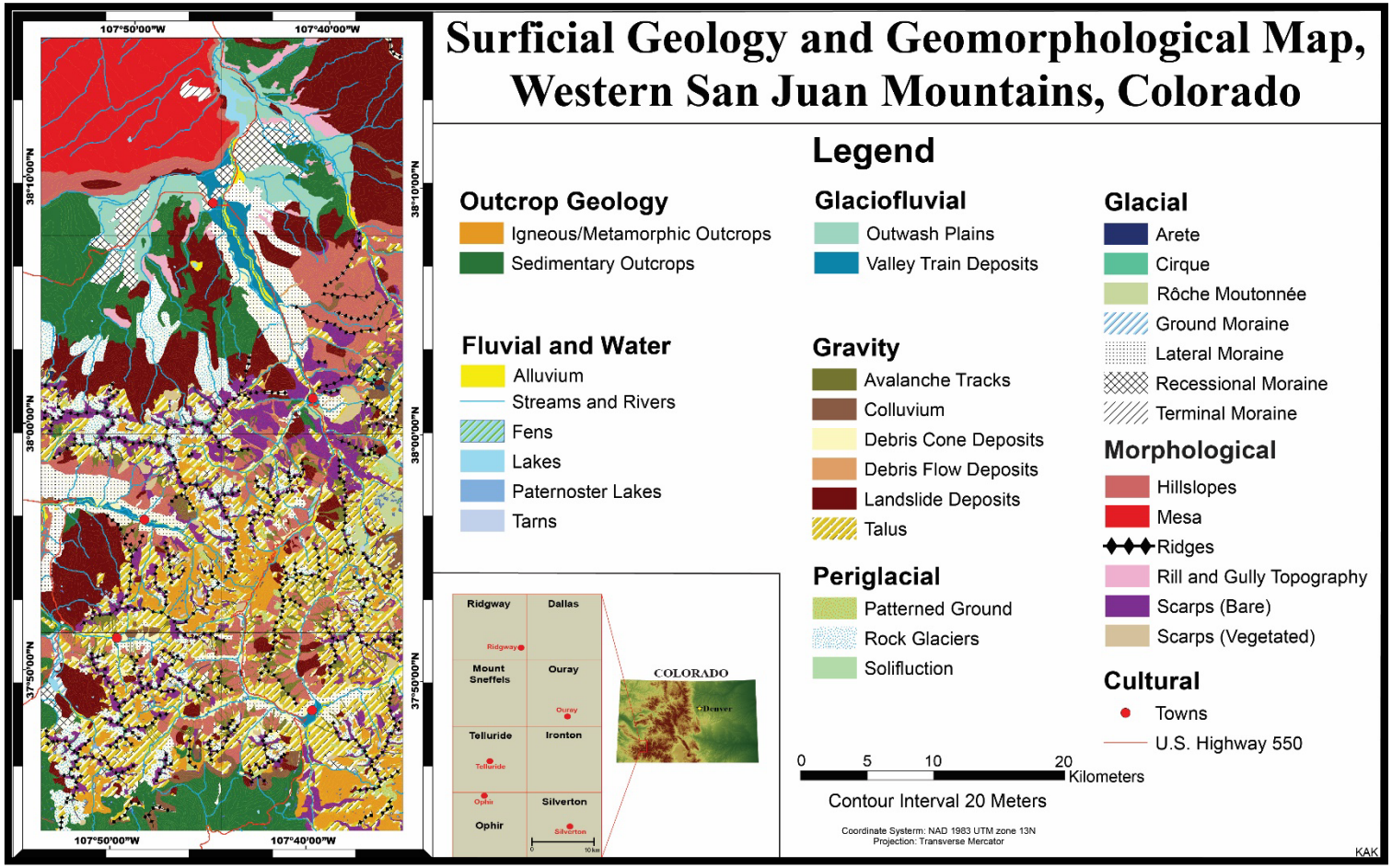

Figure 30: Composite map of surficial deposits and geomorphic phenomena in the western San Juan Mountains.

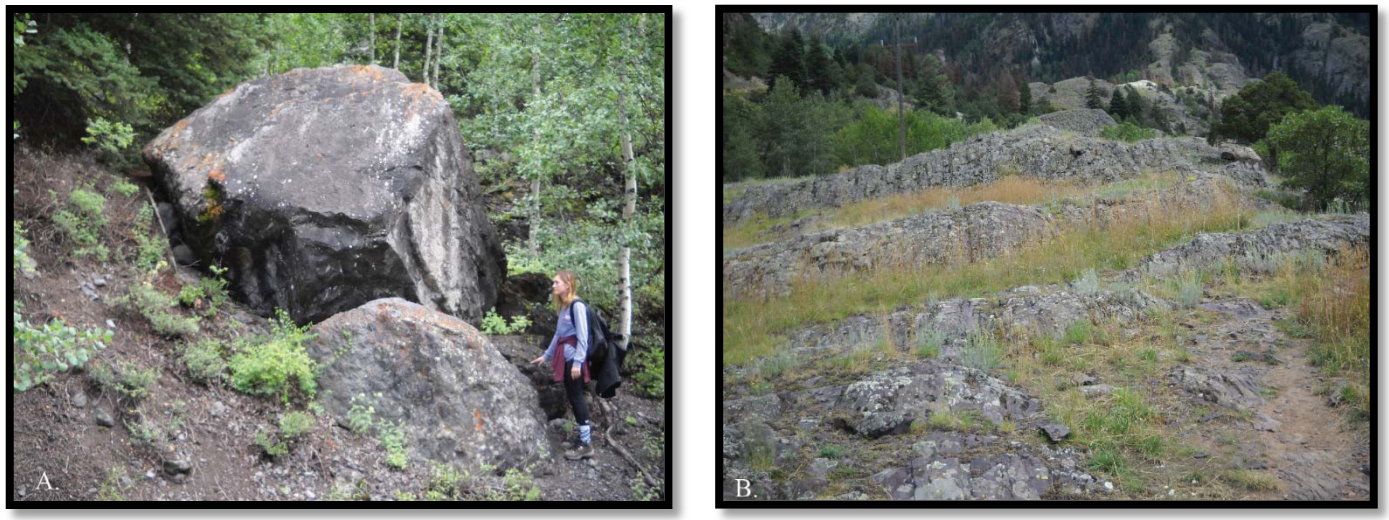

Figure 31: A) Glacial erratic, Alpine Loop Trail (08/08/15); B) Rôche Moutonnée on Leadville Limestone, South of Ouray (08/14/15).

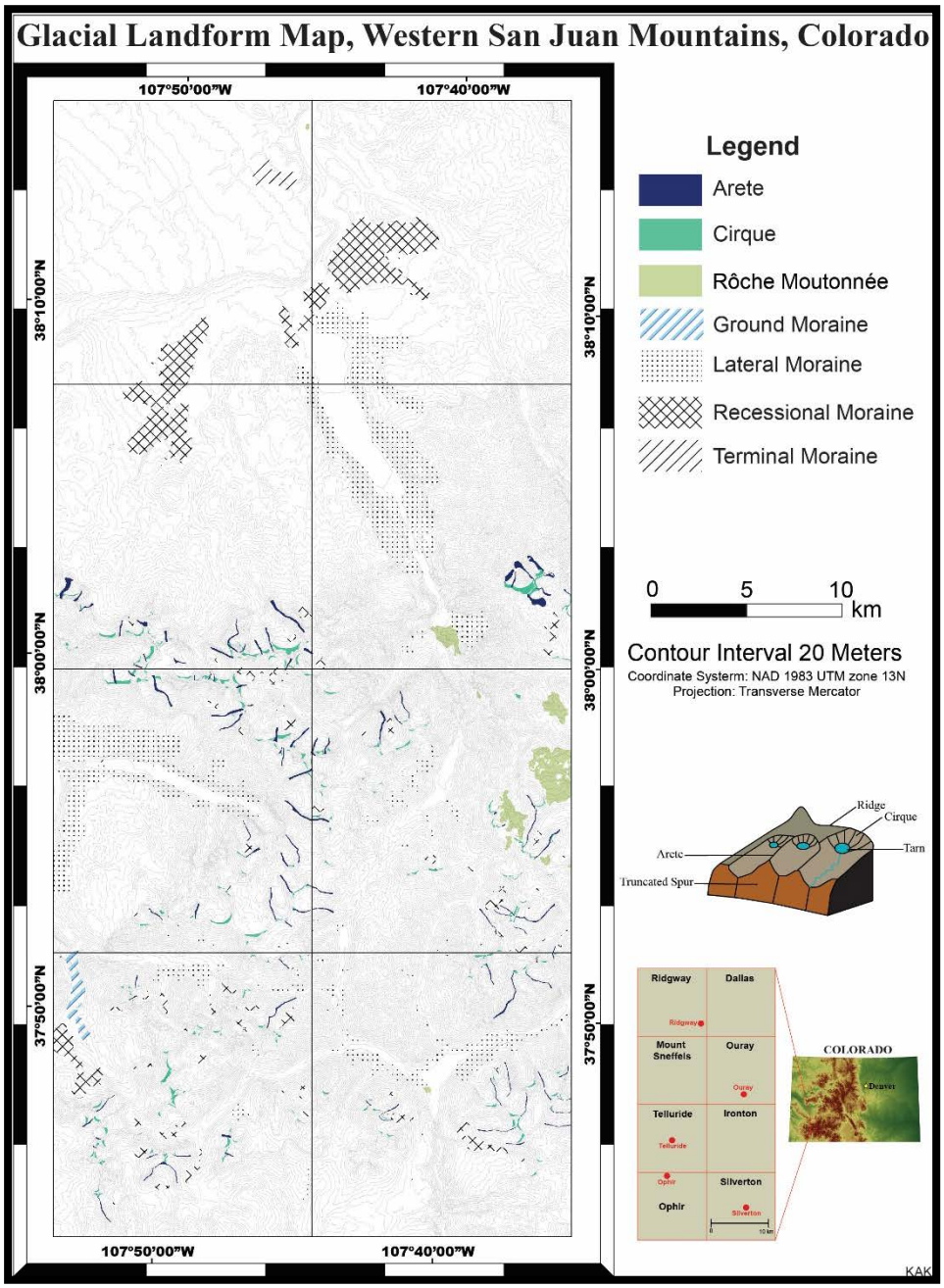

Figure 32: Map displaying glacial activity in the San Juan Mountains.

The alluvium is Quaternary, and encompasses the three major rivers in the area. Alluvium varies in size from silt, sand, gravel, cobbles, rounded to sub-rounded boulders (Luedke, 1996). Modern river channel morphology in the San Juan Mountains is indicative of seasonal changes and anthropogenic alterations of natural fluvial migration.

Fluvial landforms, such as meandering rivers, braided streams, bars, large amounts of bedload, floodplains and incised valleys, are distinguishable. An outwash plain of the former Uncompahgre Glacier was identified in the northern section of the study area (Figure 33). This outwash plain is composed of fine grained sediment and braided streams within nearly flat topography. The surficial extent of valley train deposits were discerned from the limits of the former valley glaciers. Identified valley train deposits are composed of glacial till and fill valley floors. The braided stream networks in valley train deposits were observed, also.

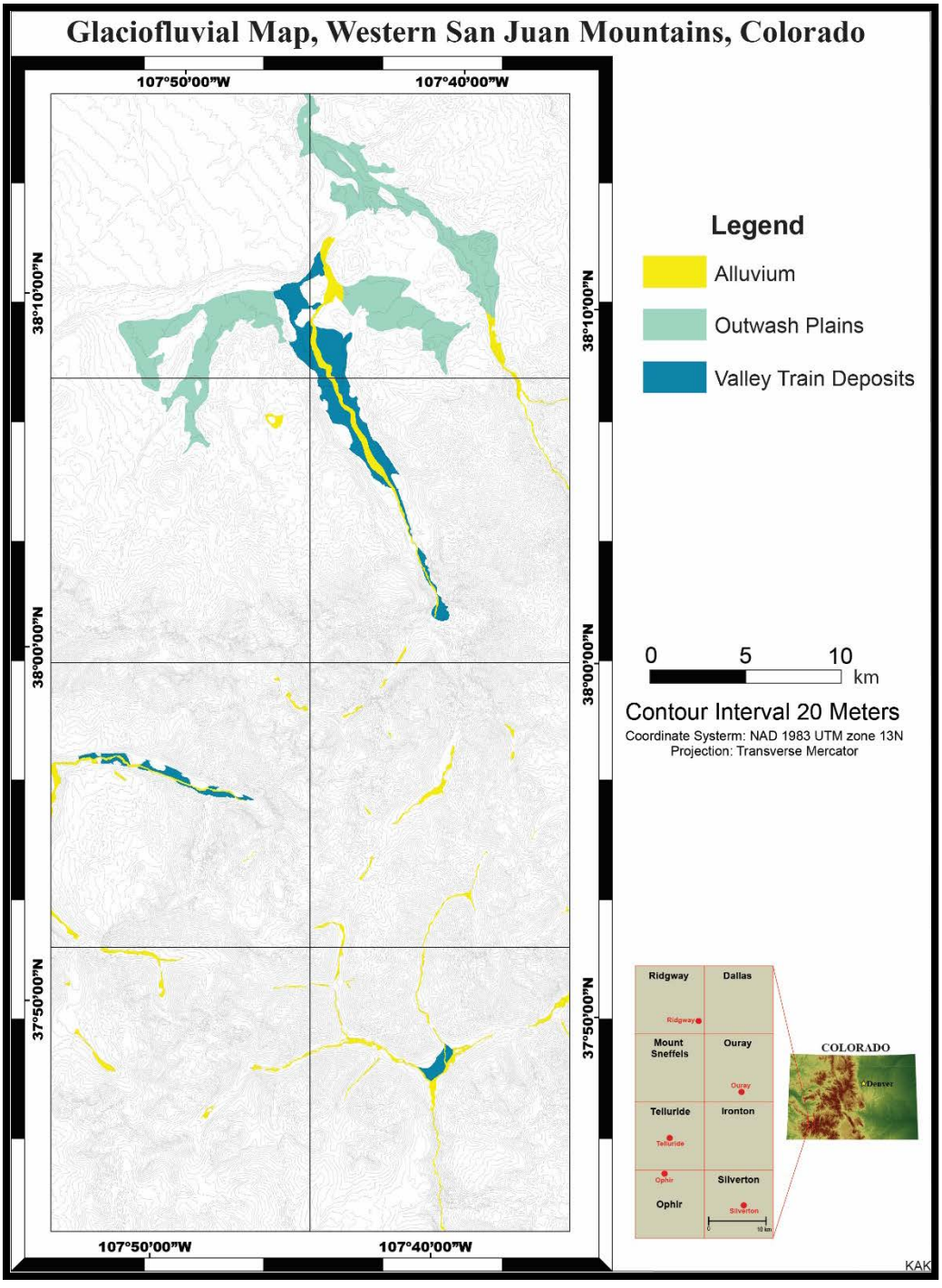

Figure 33: Presence of remnant valley train deposits from valley glaciers.

Mass-movement deposits were differentiated as: avalanche tracks, colluvium, debris-cone deposits, debris-flow deposits, landslide deposits, and talus. Gravitational landforms cover 36.02% of the study area, the greatest area coverage of any of the mapped surficial landforms (Figure 34).

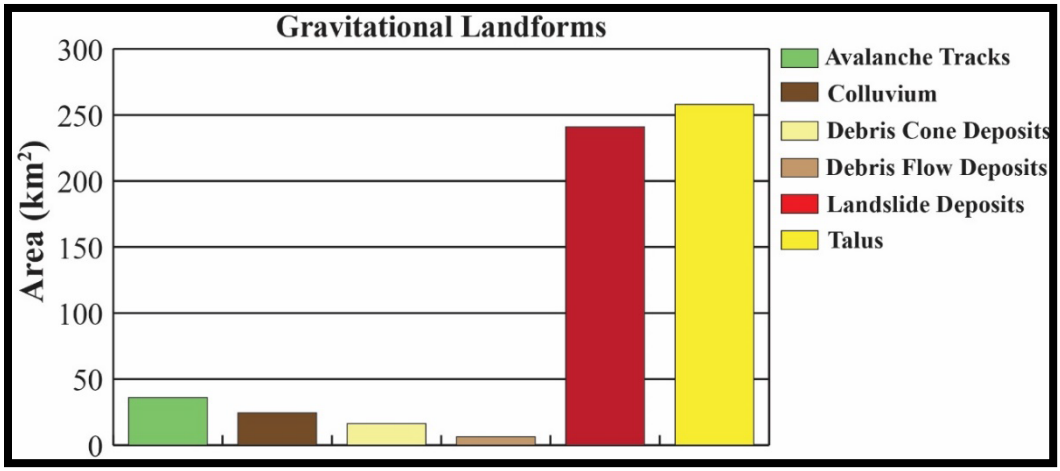

Figure 34: Respective area coverage of gravitational landforms.

The morphology of avalanche tracks is characterized by narrow pronounced paths with minimal vegetation on steep slopes or in the tracks (Figure 35). In general, the avalanche tracks in the area are situated on relatively steep valley sides with a runout zone downslope (Armstrong and Armstrong, 1977). Field documentation of tracks display flattened and uprooted trees, which suggest recent displacements. A total of 276 avalanche tracks were mapped. Colluvium identified at the bottom of slopes varies from unconsolidated silt to boulder-sized debris (Luedke, 1996). In addition to alluvial deposits, displaced slope material, and talus were also mapped as colluvium. Debris-

cone deposits, observed at the foot of slopes, are comprised of unconsolidated gravel, cobbles, and subrounded-angular boulders (Luedke and Burbank, 2000).

The debris-cone deposits are triangular-shaped landforms. A total of 29 debris flows were mapped. Most of the debris flows occur in proximity to Ouray. Debris-flow deposits are loose clast to boulder-sized rubble confined to pre-existing channels. As a side note, it needs to be pointed out that Ouray faces the likelihood of flood and debris flow hazards because the neighboring creeks contain debris derived from local bedrock and mass-movement (Jochim, 1986).

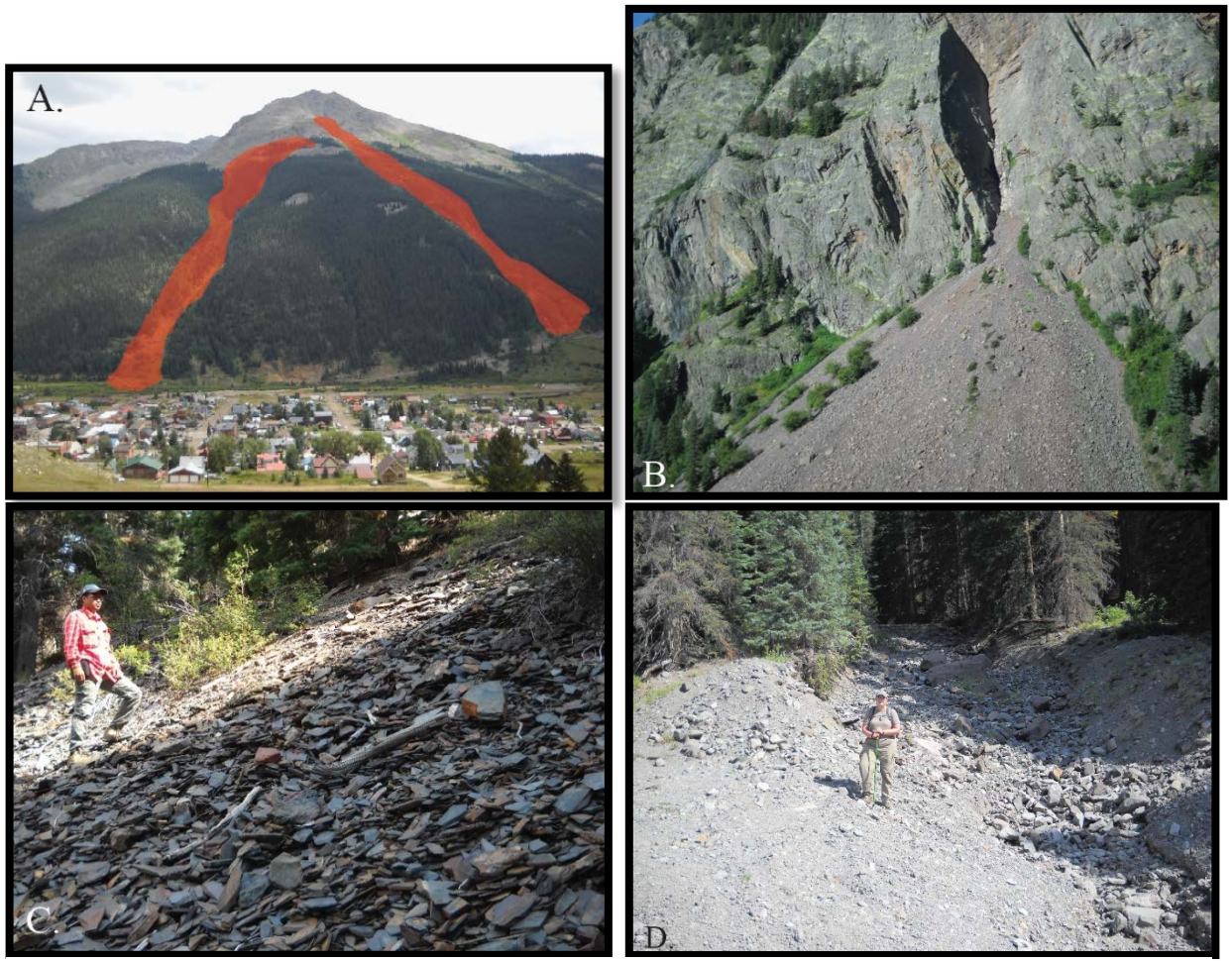

Figure 35: Mass-movement features. A) Avalanche tracks overlooking Silverton (8/13/15); B) Prominent debris cone deposit observed adjacent to U.S. Highway 550 (8/12/15); C) Talus deposit of Uncompahgre Slate (8/20/15); and D) Debris flow deposits near Yankee Boy Basin (8/21/15).

Landslides in the area range from Pleistocene to Holocene and are primarily derived from volcanic and sedimentary bedrock. The various types of mass-movement, such as rockslides, earthflows, and slumps, have contributed to the overall accumulation of landslide debris (Luedke, 1996). The deposits, masses of angular clasts to large boulders, occur on moderately steep gradients (22°- 66° slopes). Some landslide deposits were covered with lichens, which suggests older movement. Notable landslide deposits are the Yellow Mountain Landslide and Silver Mountain Landslide (Howe, 1909). Unfortunately, Telluride is built on the Siver Mountain Landslide deposit. Landslide deposits encompass 241.18 km^2 of the study area.

Talus is observed at the base of slopes and on the floor of several cirques (Figure 36). Field investigations reveal that talus consists of poorly sorted angular rock fragments transported by rockfalls, which commonly form cones. Talus covers the largest area for any landform mapped, encompassing 16 % of the study area.

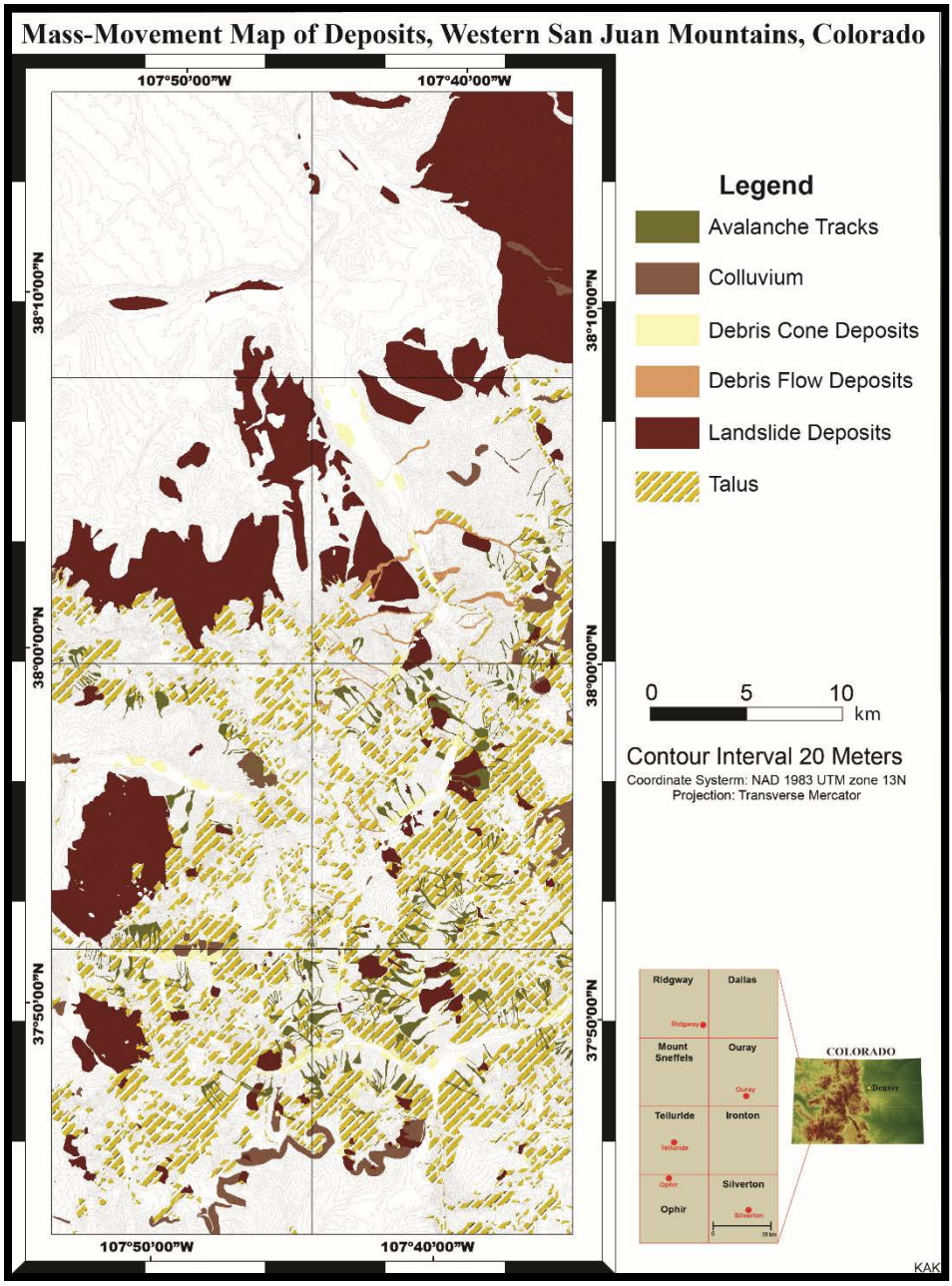

Figure 36: The extent of mass-movement features in the study area.

Hillslopes are the dominant morphological component (Figure 37). Mountain sides with no clear indication of mass movement activity were categorized as hillslopes, as a substantial number of hillslopes are vegetated. A single mesa was mapped in the northwest section of the study area. The mesa has been reworked by stream channels and is sparsely vegetated.

Ridge networks linking mountain peaks and adjoining cirque basins were mapped. Rills and gullies are formed on slopes where surface runoff incises into the topography. Rills were observed on gently sloping hills in the northern portion of the study area.

Scarps were mapped in two categories: bare and vegetated. Scarps were identified as exposed surfaces, which indicate ground displacement on steep slopes. Bare scarps were present within the vertical headwalls of cirques, which potentially may propagate rockfalls (Luedke and Burbank, 1977). Vegetated scarps are present on lower unstable slopes. The most significant scarp mapped is the Ouray amphitheater, east of Ouray. Although, its shape resembles a cirque, the morphology of the Ouray Amphitheatre suggests it originated from a series of repeated landslides (Reed, 2013) (Figure 38).

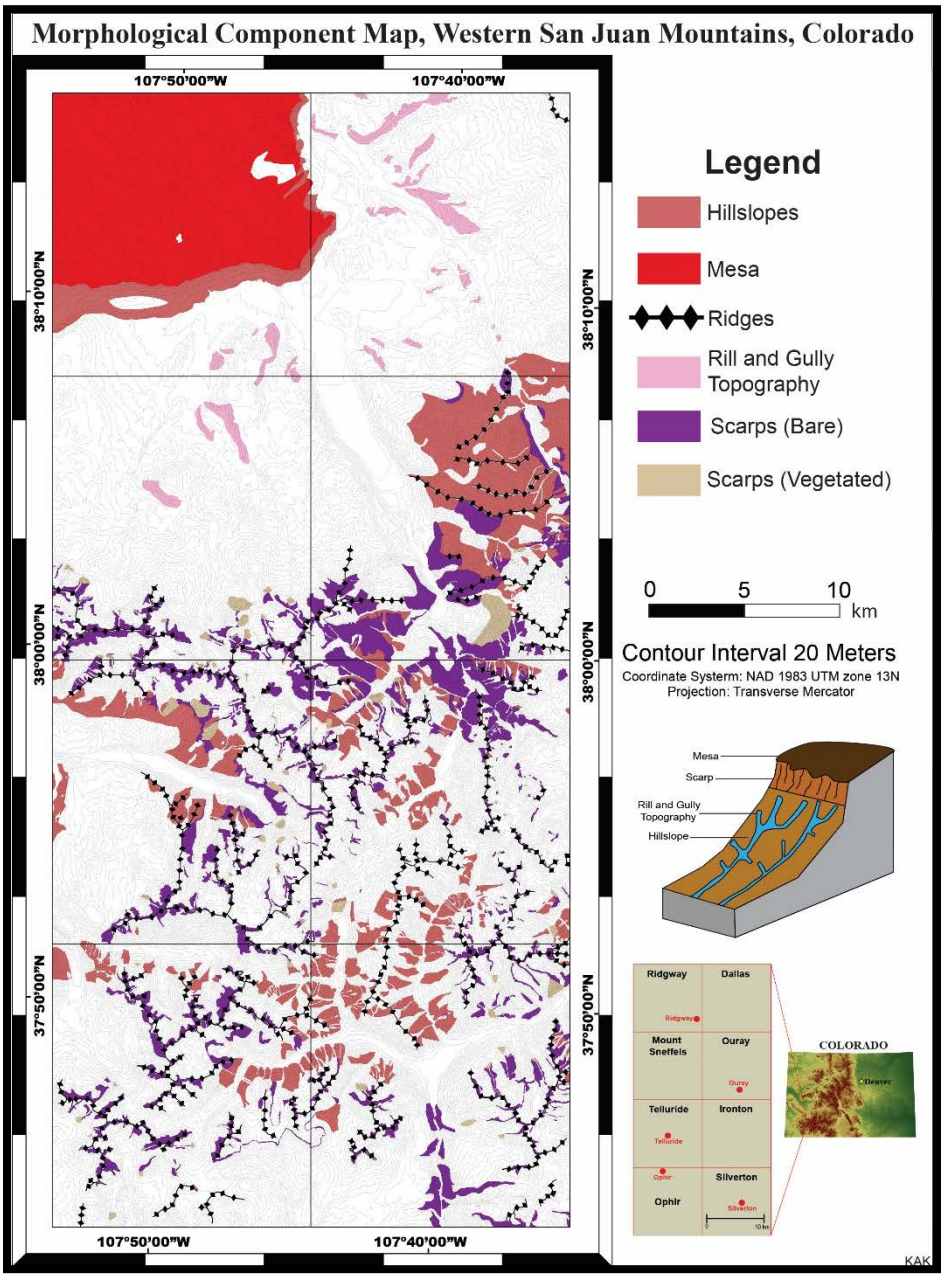

Figure 37: Morphological components mapped within the study area.

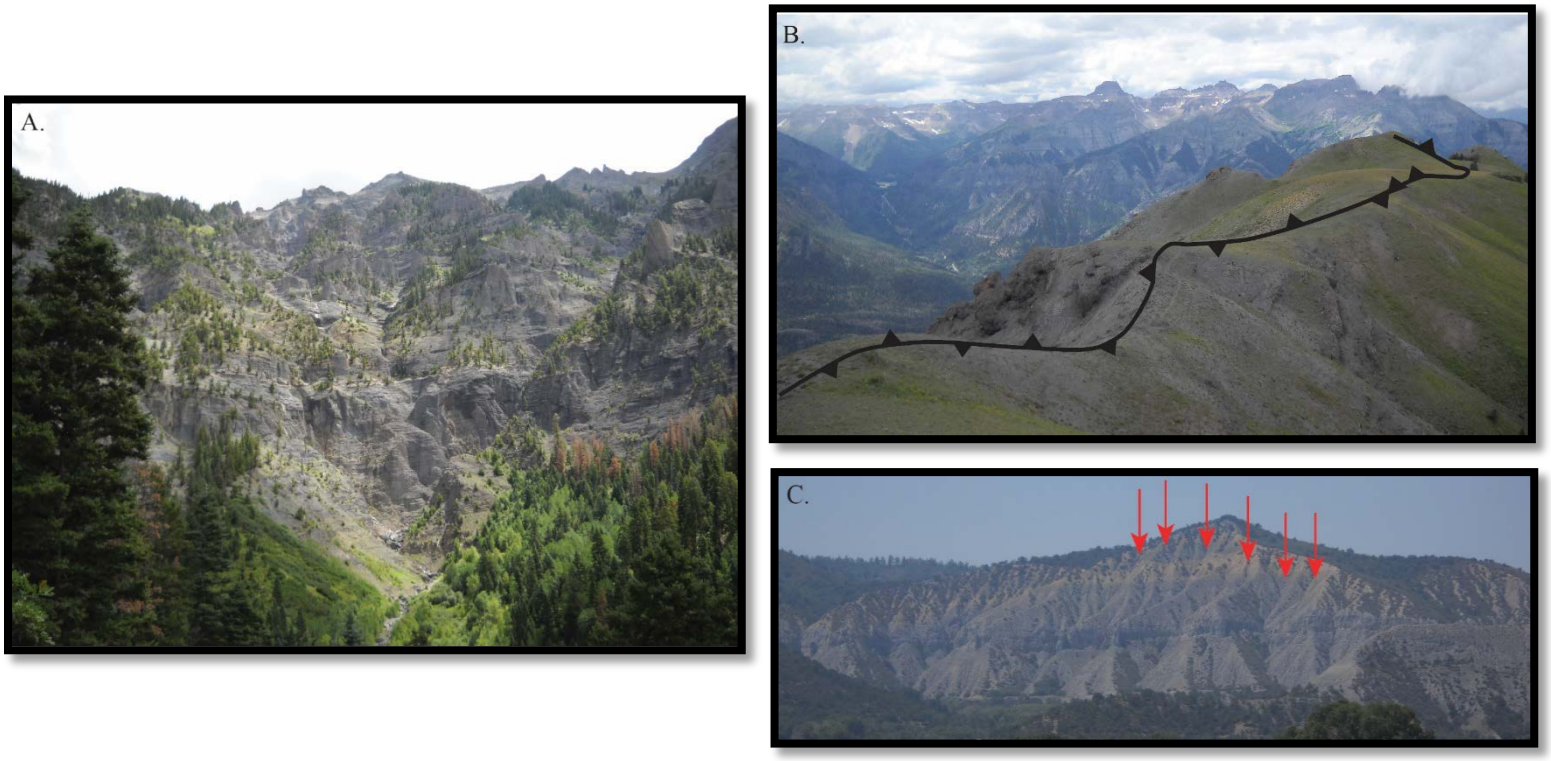

Figure 38: Mapped morphological components. A) Ouray Amphitheater (08/10/15); B) A prominent ridgeline, Bridge of Heaven Trail (08/11/15); and C) Rill and gully topography is denoted by the red arrows (08/19/15).

Exposures of igneous/metamorphic bedrock are present in almost all the alpine valleys (Figure 39). The lithologies identified include: massive-flow breccias, ash-flow tuffs, and granodiorite (Luedke, 1996). Sedimentary outcrops included shales, limestones, siltstones, and sandstones (Luedke, 1996).

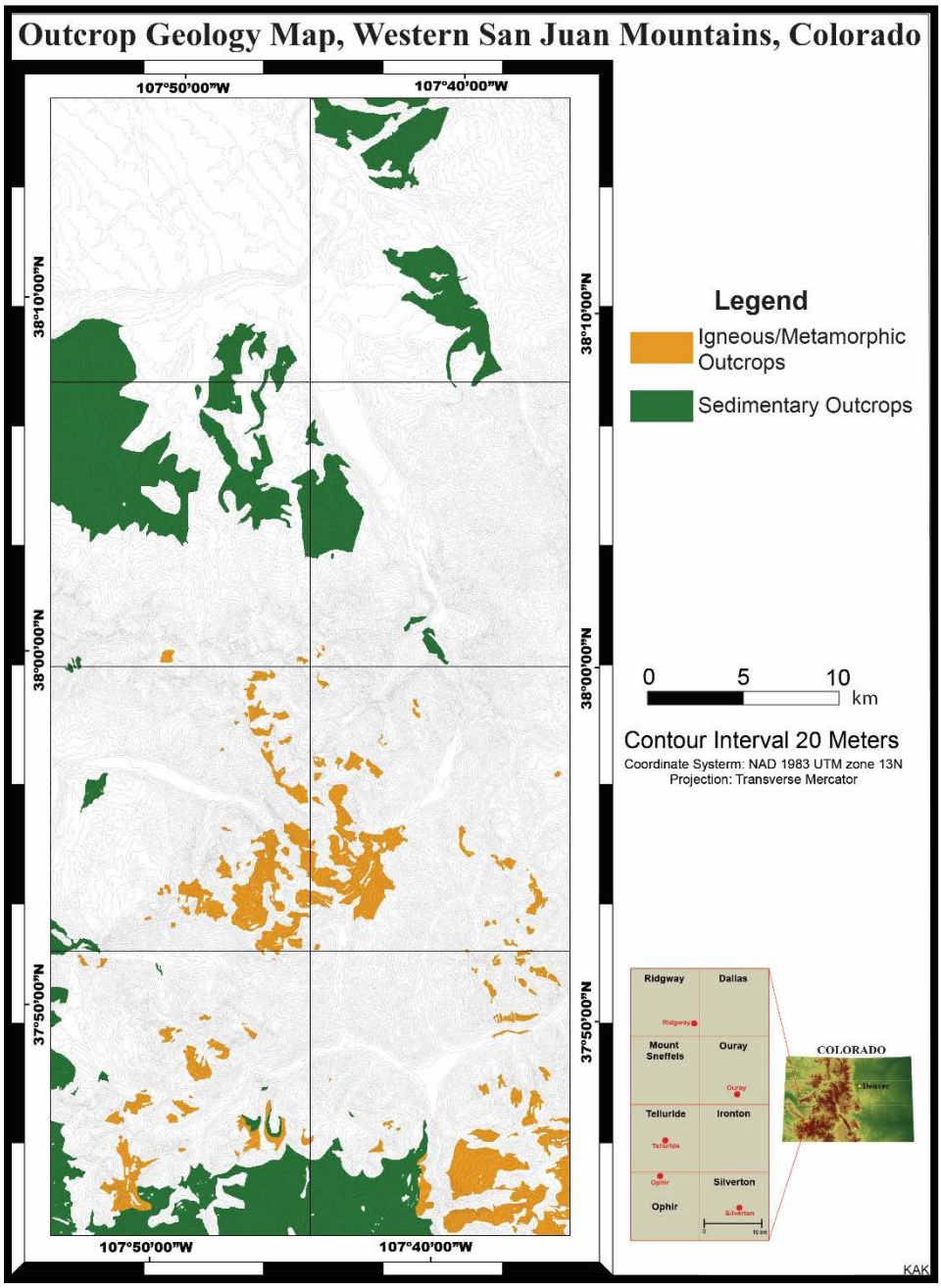

Figure 39: Exposures of volcanic and sedimentary bedrock in the study area.

Periglacial landforms in the area result from cryogenic processes, such as freeze-thaw and solifluction. Three periglacial landforms were observed in the study area: patterned ground, rock glaciers, and solifluction lobes (Figure 40). The most common patterned ground landform in the study area is mounds found at elevations exceeding 3,650 meters. Polygonal patterns resembling stone polygons were observed also (Figure 41).

A total of 258 rock glaciers were identified, which cover approximately 4.81 % of the total area. Typically, rock glaciers are accumulations of angular boulders greater than 1 meter in diameter, which form lobate-shaped tongues with parallel ridges. The rock glaciers in the area, Pleistocene and Holocene in age are observed in cirques and range from 200 meters to 1 kilometer in length (Giardino and Vitek, 1987; Fitzgerald et al., 1988; Luedke and Burbank, 2000; Degenhardt and Giardino, 2003). Several rock glaciers are in the vicinity of persistent snow banks. Solifluction landforms, characteristic of slumping and cryogenic depressions at elevations of 3,650 meters and higher, were mapped.

Hydrologic features were differentiated into the following: streams, rivers, fens, lakes, tarns, and paternoster lakes.

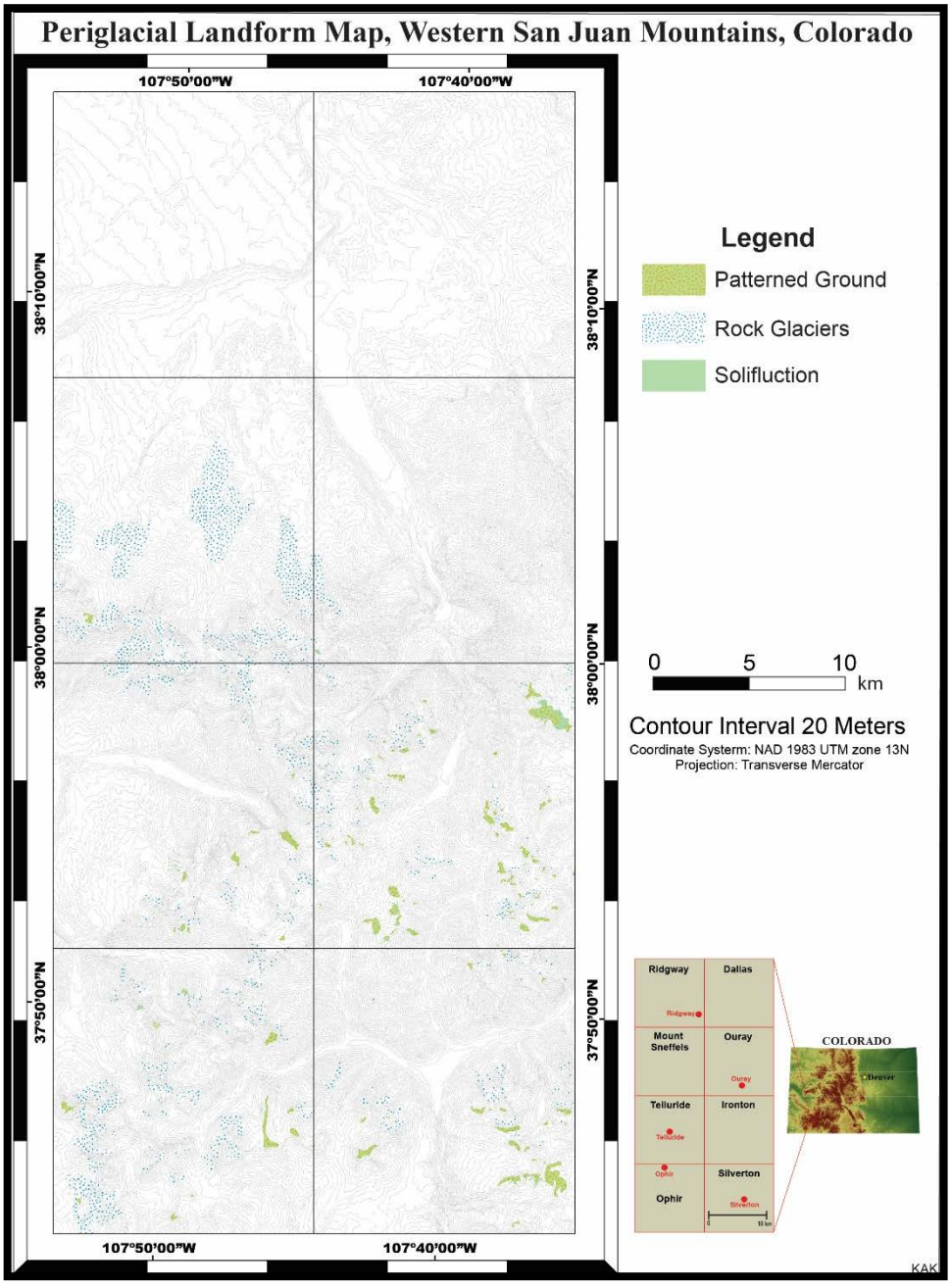

Figure 40: Surficial extent of periglacial landforms in the western San Juan Mountains.

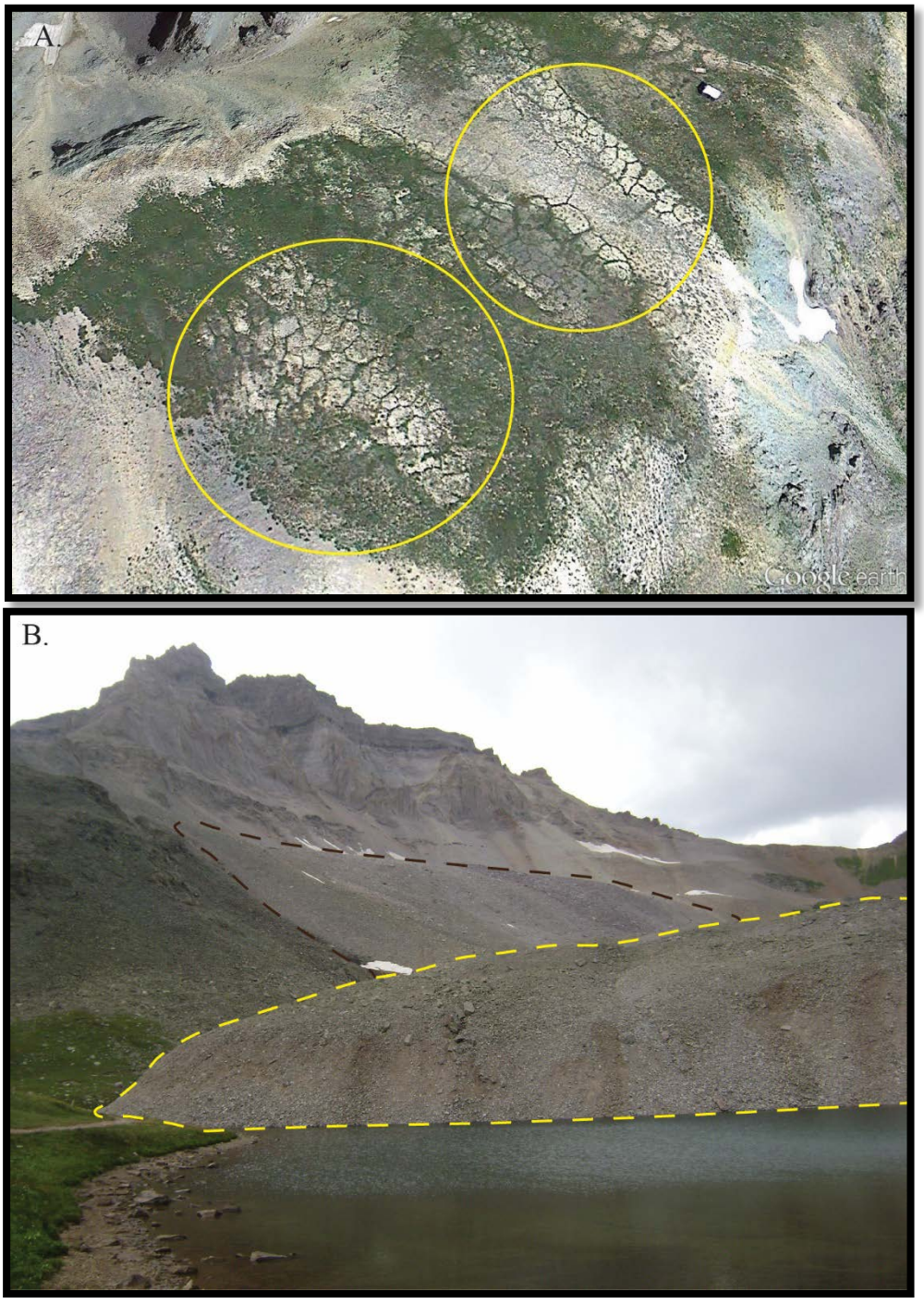

Figure 41: A) A Google Earth® screenshot of stone polygons encircled in yellow (6/01/16); B) The toe of the Gilpin Peak rock glacier is pictured with a dotted yellow line representing the frontal slope and the dotted brown line indicating longitudinal flow structures (8/21/15).

Summary

The San Juan Mountains have a legacy of slope failure (Howe, 1909). The geomorphological map, which was compiled, illustrates the ongoing legacy of slope instability that contributes to the topographic shape of the San Juan Mountains. The complex geologic setting compounded by high-relief topography of the San Juan Mountains results in mass movement being a dominant process. Triggers for slope failure include intense, long-duration precipitations, freeze-thaw processes, human activity, and volcanic lithology overlaying weaker sedimentary formations. Mass movement is the most prevalent process generating widespread surficial deposits in the area. Subsequently, talus and landslide deposits comprise the greatest areal coverage.

The San Juan Mountains contain landforms that demarcate the extents of former valley glaciers (Bandoian, 1968; Small 1995; Guido et al., 2007). Prior to deglaciation, deposits in the area were ice contact features. After the melting of glacial ice, exposed slopes deviated from equilibrium conditions, which resulted in slope instability. With the presence of snowfields at higher elevations in conjunction with alternating seasonality, periglacial processes are currently active.

With growing anthropogenic influence in the area, human-induced modification of steep slopes is occurring. As more people choose to inhabit alpine regions for recreation and acquisition of resources, the risk of injury of death from mass movement will increase. Hence, it is crucial that the public are aware of and understand the hazards associated with a dynamic landscape.

The geomorphological map is the standard for additional analyses of gravitational landforms at various spatial scales in the San Juan Mountains. With a growing need to delineate areas prone to landslides for future development in this mountain terrain, this map can promote efficient land-use practices for planners, developers, and government officials for sustainable land management. Thus, the use of a Geographic Information Systems module based on the compiled maps will illustrate susceptibility to landslides and will lead to improved predictions of landslides. Accurate forecasting of slope instability is a first-step to safeguard economic interests and avert life-threatening conditions in the San Juan Mountains.

CHAPTER IV

SUMMARY

Limitations

The use of geospatial methods allows assessment of landslide susceptibility at varied spatial scales, including: site specific and regional scales. Because this study heavily relied on geospatial data, landslide assessment was limited by the quality of acquired remote-sensed data. Specifically, geospatial functions implemented using terrain variables were greatly restricted to the standard of the study area Digital Elevation Model (DEM). Attention was paid to obtaining detailed remote-sensed data with minimal snow and cloud cover which potentially interfered when employing geospatial functions. ARCGIS® software is pre-programmed to run specific functions not accounting for the input of neural information to delineate complex phenomenon such as the occurrence of landslides. Thus, interpretation of such GIS-based landslide models is confined to the pre-defined controls of ARCGIS®.

This thesis was limited by the short field-season for geomorphological mapping. Unfortunately, it was difficult to ground-truth all surficial geomorphological features in a large study area within one two week summer field season. For instance, inaccessible areas indicative of patterned ground in satellite imagery, were not verified in the field. The digitization of the geomorphological map was greatly limited by the ARCGIS® Editor tool. The limitations encountered when drafting the map included, restricted

utilization of a standardized geomorphic mapping legend and representation of respective landforms as polygons.

Future Recommendations

Landslide propagation is a result of numerous factors working in concert leading to unstable slope conditions. This study examined the role of six parameters contributing to susceptibility to landslides, however, such work can be further modified by assessing the impact of additional parameters on slope instability. The following suggested variables must be considered for future landslide studies in the San Juan Mountains: elevation, distance to faults, downcutting of streams, proximity to population density, precipitation seasonality, temperature variability, and slope concavity/convexity.

As previously mentioned, this thesis was limited to the use of ARCGIS® functions to map susceptibility to landslides. To account for such shortcomings in interpretation of landslide data, prospective studies should employ parallelpiped classifier, machine learning, and artificial neural network applications to better map susceptibility to landslides.

This study has established a GIS-based susceptibility to landslide model for the region, however, the use of Terrestrial Laser Scanning (TLS) would allow terrain analysis at finer scales. Furthermore, such work facilitates the integration of detailed process models into landscape-scale landslide analyses. Working across spatial scales will provide greater advancement in mapping and ultimately forecasting unstable slopes.

Recent accelerated warming observed in alpine regions is destabilizing permafrost-rich slopes. Hence, a study modeling slope instability with respect to permafrost degradation will prove beneficial to predict future landslide susceptibility in the San Juan Mountains.

Although this study demonstrated a 3D susceptibility to landslides map, the implementation of improved 3D modeling software and programming languages will consolidate future models to facilitate enhanced predictions of landslides in the San Juan Mountains.

The establishment of a slope monitoring program within the San Juan Mountains will greatly consolidate landslide studies in the region. This suggested program will comprise the installation of ground motion sensors to detect downslope motion. These sensors will be inspected periodically to record slope movement to inform respective authorities to implement pertinent mitigation measures.

Lastly, the next step for the suggested research is the expansion of the study area to encompass the entire San Juan Mountain Range.

Summary

The San Juan Mountains have a legacy of slope instability as a result of a complex geologic setting and rugged mountain topography. Although, studies documenting the extent of mass movement deposits have been undertaken intermittently throughout the 1900s, inadequate investigation of factors responsible for susceptibility to mass movement in the San Juan Mountains still existed. This research was motivated by

the need to initiate a comprehensive up-to-date mass movement study, addressing the present-day risk from mass movement in the western San Juan Mountains. This thesis strived to answer two research questions: What are the major components that cause slopes to fail in the San Juan Mountains? And what is the distribution of surficial phenomena, which indicate potential hazards from slope failure? To answer these research questions, the first study established a GIS-based model of susceptibility to mass movement and the second study created a surficial geomorphological map of the western San Juan Mountains.

The GIS-based susceptibility to landslide map was constructed using a weighted overlay to determine the role of: slope angle, slope length, aspect, geology, vegetation cover, and soil drainage for slope instability in the western San Juan Mountains. The weighted overlay method was implemented in two phases: heuristic, based on *a priori* knowledge and a Principal Component Analysis (PCA). This completed GIS-based module for susceptibility to landslides was displayed in a dynamic 3D model, also. The findings of this study were: 1) Aspect, slope angle, and geology have the greatest relative weighted influence on slope failure, 2) the study area is experiencing a general uniform rate of erosion, 3) East and west-facing slopes have the greatest areal coverage increasing the likelihood of high and very high susceptibility to landslides, 4) Class 2 slopes (22.01°- 44°) have the greatest areal coverage also increasing the likelihood for high and very high susceptibility to landslides, 5) Class 2, 3, and 4 slopes are highly correlated to high susceptibility, classes 3 and 4 are highly correlated to very high susceptibility 6) Surficial deposits have the greatest mean surface roughness off all

lithologic units, 7) Areas within 50 m from roads are highly susceptible to landslides and, 8) A combination of heuristic, deterministic, and statistical approaches will improve prediction of landslides.

The surficial geomorphological map was prepared at a scale of 1:3,000 to examine the spatial distribution of deposits resulting from geomorphic processes operating in the western San Juan Mountains. Mapped surficial landforms were categorized as 1) glacial landforms; 2) glaciofluvial landforms; 3) fluvial water; 4) gravitational landforms; 5) morphological components; 6) outcrop geology; and 7) periglacial landforms. This study shows that 1) talus and landslide deposits are the most prevalent surficial deposits and 2) landforms that demarcate the extents of former glaciation of the western San Juan Mountains.

This study has employed emerging geospatial techniques, 3D modeling, and geomorphological mapping to better understand mass movement at various spatial scales in the western San Juan Mountains. With growing human development in the area, anthropogenic-induced alteration of steep slopes is ongoing. As more people choose to inhabit alpine regions even with the risk from landslides, delineation of landslide prone areas is required. From an applied perspective, this GIS-based landslide model is a valuable resource for regional planners, government officials, and residents to promote efficient land-use practices in an active landscape. The thesis will serve as a standard for future studies on mass movements in the area, documenting mass movements at various spatial scales. The development of a comprehensive landslide study is the first-step to

accurate forecasting of slope failure to safeguard economic interests and minimize life-threatening conditions in the western San Juan Mountains.

REFERENCES

Alparslan, E., 2011, Landslide susceptibility mapping in Yalova, Turkey, by remote sensing and GIS: Environmental & Engineering Geoscience, v. 17, no. 3, p. 255-265. DOI**:** 10.2113/gseegeosci.17.3.255.

Annaheim, H., 1956, Zur Frage der geomorphologischen Kartierung: Petermanns Geogr. Mitt, v. 103, p. 315-319.

Armstrong, B. R., and Armstrong, R. L., 1977, Avalanche Atlas, Ouray County, Colorado, University of Colorado, Institute of Arctic and Alpine Research.

Atwood, W. W., and Mather, K. F., 1932, Physiography and quaternary geology of the San Juan Mountains, Colorado, USGS Professional Paper 166, U.S. Government Printing Office.

Avtar, R., Singh, C., Singh, G., Verma, R., Mukherjee, S., and Sawada, H., 2011, Landslide susceptibility zonation study using remote sensing and GIS technology in the Ken-Betwa River Link area, India: Bulletin of Engineering Geology and the Environment, v. 70, no. 4, p. 595-606. DOI: 10.1007/s10064-011-368-5.

Ayalew, L., and Yamagishi, H., 2005, The application of GIS-based logistic regression for landslide susceptibility mapping in the Kakuda-Yahiko Mountains, central Japan: Geomorphology, v. 65, no. 1-2, p. 15-31. DOI: 10.1016/j. geomorph.2004. 06.010.

Baeza, C., and Corominas, J., 2001, Assessment of shallow landslide susceptibility by means of multivariate statistical techniques: Earth Surface Processes and Landforms, v. 26, no. 12, p. 1251-1263. DOI: 10.1002/esp.263.

Bandoian, C. A., 1968, Fluvioglacial features of the Animas River Valley, Colorado and New Mexico: Guidebook of San Juan-San Miguel-La Plata region, New Mexico and Colorado Fall Field Conference Guidebook-19, p. 28-32.

Bannari, A., Morin, D., Bonn, F., and Huete, A., 1995, A review of vegetation indices: Remote sensing reviews, v. 13, no. 1-2, p. 95-120. DOI: 10.1080/027572595095 32298.

Barbarella, M., Fiani, M., and Lugli, A., 2015, Landslide monitoring using multitemporal terrestrial laser scanning for ground displacement analysis: Geomatics, Natural Hazards and Risk, v. 6, no. 5-7, p. 398-418. DOI: 10.1080/19 475705.2013.863808.

Bashenina, N. V., 1972, Geomorphologische Kartierung des Gebirgsrelief im Maszstab 1:200,000 auf Grund einer Morphostrucktur Analyse: Z. Geomorphol., NF, v. 16/2, p. 125-128.

Bishop, C. M., 1995, Neural networks for pattern recognition, Oxford university press.

Blomdin, R., Heyman, J., Stroeven, A. P., Hättestrand, C., Harbor, J. M., Gribenski, N., Jansson, K. N., Petrakov, D. A., Ivanov, M. N., Alexander, O., Rudoy, A. N., and Walther, M., 2016, Glacial geomorphology of the Altai and Western Sayan Mountains, Central Asia: Journal of Maps, v. 12, no. 1, p. 123-136. DOI: 10.1080/17445647.2014.992177.

Brunsden, D., 2003, Geomorphology, engineering and planning: Geogr. Pol. , v. 76, p. 185-205.

Burbank, W., and Luedke, R., 1964, Geology of the Ironton Quadrangle, Colorado: U.S. Geological Survey Geol. Quad. Map GQ-291,scale 1:24,000.

Burbank, W. S., and Luedke, R. G., 1966, Geologic map of the Telluride Quadrangle, southwestern Colorado: US Geological Survey, Geologic Quadrangle Map GQ-504, scale 1:24,000.

Carrara, A., 1983, Multivariate models for landslide hazard evaluation: Mathematical geology, v. 15, no. 3, p. 403-426. DOI: 10.1007/BF01031290.

Carrara, P. E., 2011, Deglaciation and postglacial treeline fluctuation in the northern San Juan Mountains, Colorado: U.S. Geological Survey Professional Paper 1782, p. 48. https://pubs.usgs.gov/pp/1782/.

Caterpillar® Tractor Company; 2000 Caterpillar Performance Handbook, Peoria, Illinois.

Cerveny, R. S., and Blair, R., 1997, The Western San Juan Mountains: Their Geology, Ecology, and Human History, JSTOR. http://www.jstor.org/stable/27856786.

Cervi, F., Berti, M., Borgatti, L., Ronchetti, F., Manenti, F., and Corsini, A., 2010, Comparing predictive capability of statistical and deterministic methods for landslide susceptibility mapping: a case study in the northern Apennines (Reggio Emilia Province, Italy): Landslides, v. 7, no. 4, p. 433-444. DOI: 10.1007/s10346-010-0207-y.

Claessens, L., Knapen, A., Kitutu, M., Poesen, J., and Deckers, J. A., 2007, Modelling landslide hazard, soil redistribution and sediment yield of landslides on the Ugandan footslopes of Mount Elgon: Geomorphology, v. 90, no. 1, p. 23-35. DOI: 10.1016/j.geomorph.2007.01.007.

Collins, B. D., and Jibson, R. W., 2015, Assessment of existing and potential landslide hazards resulting from the April 25, 2015 Gorkha, Nepal earthquake sequence: US Geological Survey Open-File Report 2015-1142, p. 50. DOI: 10.3133/ofr20151142.

Colorado Department of Transportation; 2014, US 550 Red Mountain Pass. https://www.cdot.gov/projects/archived-project-sites/us550redmtnpass.

Cooke, R., and Doornkamp, J. C., 1990, Geomorphology in environmental management: a new introduction, Oxford University Press (OUP).

Crosta, G. B., Frattini, P., and Agliardi, F., 2013, Deep-seated gravitational slope deformations in the European Alps: Tectonophysics, v. 605, p. 13-33. DOI: 10.1016/j.tecto.2013.04.028.

Davis, W. M., 1909, Geographical essays, Publisher unknown, Boston, MA, United States, vi, 777 p. https://ia600207.us.archive.org/27/items/geographicaless01davigoog/geographicaless01davidoog.pdf.

Degenhardt, J. J., Jr., and Giardino, J. R., 2003, Subsurface investigation of a rock glacier using ground-penetrating radar; implications for locating stored water on Mars: Journal of Geophysical Research, v. 108, no. E4, p. 17. DOI: 10.1029/2002JE001888.

Demek, J., 1972, Manual of detailed geomorphological mapping, Academia, Publishing House of the Czechoslovak Academy of Sciences 344 p.

Demir, G., Aytekin, M., and Akgun, A., 2015, Landslide susceptibility mapping by frequency ratio and logistic regression methods: an example from Niksar–Resadiye (Tokat, Turkey): Arabian Journal of Geosciences, v. 8, no. 3, p. 1801-1812. DOI:10.1007/s12517-014-1332-z.

Dramis, F., Guida, D., and Cestari, A., 2011, Nature and aims of geomorphological mapping: Geomorphological mapping: Methods and applications, Developments in Earth Surface Processes, edited by: Smith, M., Paron, P., and Griffiths, JS, Elsevier, Amsterdam, the Netherlands, v. 15, p. 39-73. DOI: 10.1016/B978-0-444-53446-0.00003-3.

Erener, A., and Düzgün, H. S. B., 2010, Improvement of statistical landslide susceptibility mapping by using spatial and global regression methods in the case of More and Romsdal (Norway): Landslides, v. 7, no. 1, p. 55-68. DOI: 10.1007/s10346-009-0188-x.

Faraji Sabokbar, H., Shadman Roodposhti, M., and Tazik, E., 2014, Landslide susceptibility mapping using geographically-weighted principal component analysis: Geomorphology, v. 226, p. 15-24. DOI: 10.1016/j.geomorph.2014.07.026.

Fenneman, N.M., 1931, Physiography of Western United States: McGraw- Hill Book Company, Inc., New York.

Fitzgerald, J., Giardino, J., Maggio, R., and Vitek, J., 1988, Mapping and evaluating geomorphic engineering aspects of high mountain terrain using a geographic information system, Sangre de Cristo Mountains, Colorado: Geological Society of America Centennial Celebration, v. 20, no. 7, p. 64-65.

Frodella, W., Morelli, S., Fidolini, F., Pazzi, V., and Fanti, R., 2014, Geomorphology of the Rotolon landslide (Veneto Region, Italy): Journal of Maps, v. 10, no. 3, p. 394-401. DOI: 10.1080/17445647.2013.869666.

Galli, M., Ardizzone, F., Cardinali, M., Guzzetti, F., and Reichenbach, P., 2008, Comparing landslide inventory maps: Geomorphology, v. 94, no. 3, p. 268-289. DOI: 10.1016/j.geomorph.2006.09.023.

Galon, R., 1962, Instruction to the detailed geomorphological map of the Polish Lowland: Geography and Geomorphology Department, Polish Academy of Sciences, Torun.

Gellert, J. F., 1968, Das System der Komplexgeomorphologischen Karten Petermanns Geogr. Mitt, v. 112 (3), p. 185-190.

Gellert, J. F., and Scholz, E., 1974, Bemerkungen zur international vereinheitlichten Legende fur mittelmassstabliche Ubersichtskarten von 1:200,000 zu 1:500,000: Stud. Geograf. Brno, v. 41, p. 32-36.

Giardino, J. R., 2016. Personal Communication, June 5th, 2016.

Giardino, J. R., and Vitek, J. D., 1987, Perspectives on where rock glaciers fit in the landscape continuum: Congress of the International Union for Quaternary Research, p. 172.

Gigli, G., Frodella, W., Garfagnoli, F., Morelli, S., Mugnai, F., Menna, F., and Casagli, N., 2014, 3-D geomechanical rock mass characterization for the evaluation of rockslide susceptibility scenarios: Landslides, v. 11, no. 1, p. 131-140. DOI:10.1007/s10346-013-0424-2.

Gilbert, G. K., 1877, Report on the geology of the Henry Mountains [Utah]: Publication of the Powell Survey, USGS unnumbered series, U.S. Government Printing Office. https://pubs.usgs.gov/unnumbered/70039916/report.pdf.

Görüm, T., Bayrakdar, C., Avdan, U., and Çömert, R., 2017, Geomorphology of the Mount Akdag landslide, Western Taurus range (SW Turkey): Journal of Maps, v. 13, no. 2, p. 165-172. DOI: 10.1080/17445647.2017.1280424.

Griffiths, J. S., and Abraham, J. K., 2008, Factors affecting the use of applied geomorphology maps to communicate with different end-users: Journal of Maps, v. 4, no. 1, p. 201-210. DOI: 10.4113/jom.2008.89.

Guido, Z. S., Ward, D. J., and Anderson, R. S., 2007, Pacing the post–Last Glacial Maximum demise of the Animas Valley glacier and the San Juan Mountain ice cap, Colorado: Geology, v. 35, no. 8, p. 739-742. DOI: 10.1130/G23596A.1.

Gustavsson, M., Kolstrup, E., and Seijmonsbergen, A. C., 2006, A new symbol-and-GIS based detailed geomorphological mapping system: Renewal of a scientific discipline for understanding landscape development: Geomorphology, v. 77, no. 1, p. 90-111. DOI: 10.1016/jgeomorph.2006.01.026.

Hail, W., 1989, Reconnaissance Geologic Map of the Ridgway Quadrangle, Ouray County, Colorado, scale 1:24,000.

Hayden, R., Blair Jr, R., Garvin, J., and Short Sr, N., 1986, Future Outlook; Geomorphology from Space, A Global Overview of Regional Landforms, NASA SP-486: National Aeronautics and Space Administration, Washington, DC. https://ntrs.nasa.gov/search.jsp?R=19870008706.

Hearn, G. J., and Hart, A. B., 2011, Geomorphological contributions to landslide risk assessment: theory and practice: Geomorphological Mapping Methods and Applications. Developments in Earth Surface Processes, v. 15, p. 107-148. DOI: 10.1016/B978-0-444-53446-0.00005-7.

Henaff, A., 2011, Geomorphological Mapping- Case Studies in Coastal Environments, Conference Presentation. https://eost.u-strasbg.fr/omiv/Cerg_documents/09_ FORMOSE-June11-Henaff_Geomorphology.pdf.

Highland, L., Godt, J., Howell, D., and Savage, W., 1998, Landslides-U.S. Geological Survey Fact Sheet 089-98.

Hobson, R. D., Surface roughness in topography; quantitative approach, *in* Proceedings Spatial Analysis in Geomorphology 1972, Harper & Row, New York-London, p. 221-245.

Howe, E., 1909, Landslides in the San Juan Mountains, Colorado, including a consideration of their causes and their classification, U. S. Geological Survey, Reston, VA, United States, U. S. Geological Survey Professional Paper, p. 58.

Huggel, C., Allen, S., Deline, P., Fischer, L., Noetzli, J., and Ravanel, L., 2012, Ice thawing, mountains falling; are alpine rock slope failures increasing?: Geology Today, v. 28, no. 3, p. 98-104. DOI: 10.1111/j.1365-2451.2012.00836.x.

Iverson, R. M., 2000, Landslide triggering by rain infiltration: Water Resources Research, v. 36, no. 7, p. 1897-1910. DOI: 10.1029/2000WR900090.

Ives, J. D., and Bovis, M. J., 1978, Natural hazards maps for land-use planning, San Juan Mountains, Colorado, USA: Arctic and Alpine Research, p. 185-212. DOI: 10.23 07/1550752.

Ives, J. D., and Krebs, P. V., 1978, Natural hazards research and land-use planning responses in mountainous terrain; the town of Vail, Colorado Rocky Mountains, U.S.A: Arctic and Alpine Research, v. 10, no. 2, p. 213-222. DOI: 10.2307/1550 753.

Ives, J. D., Mears, A. I., Carrara, P. E., and Bovis, M. J., 1976, Natural hazards in mountain Colorado: Annals of the Association of American Geographers, v. 66, no. 1, p. 129-144. DOI: 10.1111/j.1467-8306.1976.tb01076.x.

Jenks, G. F., and Caspall, F. C., 1971, Error on choroplethic maps: definition, measurement, reduction: Annals of the Association of American Geographers, v. 61, no. 2, p. 217-244. DOI: 10.1111/j.1467-8306.1971.tb00779.x.

Jochim, C. L., 1986, Debris-flow hazard in the immediate vicinity of Ouray, Colorado, Colorado Geological Survey Special Publication, v. 30, p. 63.

Kayastha, P., Dhital, M., and De Smedt, F., 2013, Application of the analytical hierarchy process (AHP) for landslide susceptibility mapping: a case study from the Tinau watershed, west Nepal: Computers & Geosciences, v. 52, p. 398-408. DOI: 10.10 16/j.cageo.2012.11.003.

Kelkar, K.A., and Giardino, J.R., 2017, The Occurrence and Susceptibility to Mass Movement in the Western San Juan Mountains, Colorado: A 3-D Mapping Approach, in De Graff, J.V., and Shakoor, A., eds., Landslides: Putting Experience, Knowledge and Emerging Technologies into Practice: Proceedings of the 3rd North American Symposium on Landslides, Association of Environmental and Engineering Geologists Special Publication 27, ISBN: 978-0-9897253-7-8, p. 949-957.

Khan, S. F., Kamp, U., and Owen, L. A., 2013, Documenting five years of landsliding after the 2005 Kashmir earthquake, using repeat photography: Geomorphology, v. 197, p. 45-55. DOI: 10.1016/j.geomorph.2013.04.033.

Klimaszewski, M., 1956, The principles of the geomorphological survey of Poland: Przeglad Geograficzny, v. 28, p. 32-40.

Klimaszewski, M, 1963, The principles of the geomorphological map of Poland: Geogr. Stud; v.46, p.60-70.

Klimaszewski, M, 1982, Detailed geomorphological maps: ITC Journal, v.3, p.256-271.

Knight, J., Mitchell, W., and Rose, J., 2011, Geomorphological field mapping: Geomorphological Mapping: methods and applications, Smith MJ, Paron P, Griffiths J (eds.). Elsevier: London, p. 151-188. DOI: 10.1016/B978-0-444-53446-0.00006-9.

Komac, M., 2006, A landslide susceptibility model using the analytical hierarchy process method and multivariate statistics in perialpine Slovenia: Geomorphology, v. 74, no. 1, p. 17-28. DOI: 10.1016/j.geomorph.2005.07.005.

Lardeux, P., Glasser, N., Holt, T., and Hubbard, B., 2016, Glaciological and geomorphological map of Glacier Noir and Glacier Blanc, French Alps: Journal of Maps, v. 12, no. 3, p. 582-596. DOI: 10.1080/17445647.2015.1054905.

Larsen, M., 2008, Rainfall-triggered landslides, anthropogenic hazards, and mitigation strategies: Advances in Geosciences, v. 14, p. 147-153. DOI: hal-00297061.

Lee, S., Choi, J., and Min, K., 2004, Probabilistic landslide hazard mapping using GIS and remote sensing data at Boun, Korea: International Journal of Remote Sensing, v. 25, no. 11, p. 2037-2052. DOI: 10.1080/01431160310001618734.

Lee, S., and Min, K., 2001, Statistical analysis of landslide susceptibility at Yongin, Korea: Environmental geology, v. 40, no. 9, p. 1095-1113. DOI: 10.1007/s00254 0100310.

Lindholm, M. S., and Heyman, J., 2016, Glacial geomorphology of the Maidika region, Tibetan Plateau: Journal of Maps, v. 12, no. 5, p. 797-803. DOI: 10.1080/174456 47.2015.1078182.

Luedke, R., 1996, Geologic Map of the Ophir Quadrangle San Juan, San Miguel, and Dolores Counties, Colorado: US Geological Survey Geologic Quadrangle Series GQ-1760, scale 1:24,000.

Luedke, R. G., and Burbank, W.S., 1962, Geology of the Ouray quadrangle, Colorado: US Geological Survey Geologic Quadrangle Map GQ-152, scale 1:24,000.

Luedke, R. G., and Burbank, W. S., 1977, Map showing potential geologic hazards in the Telluride quadrangle San Miguel, Ouray, and San Juan Counties, Colorado: US Geological Survey Miscellaneous Geologic Investigations Map I-973-B, scale 1:24,000.

Luedke, R. G., and Burbank, W. S., 2000, Geologic map of the Silverton and Howardsville quadrangles, Southwestern Colorado: U.S. Geological Survey, Geologic Investigations Series Map I-2681, scale 1:24,000.

Martínez-Graña, A. M., Goy, J. L., and Zazo, C., 2016, Geomorphological Applications for Susceptibility Mapping of Landslides in Natural Parks: Environmental Engineering & Management Journal (EEMJ), v. 15, no. 2.

Mather, K. F., 1957, Geomorphology of the San Juan Mountains: New Mexico Geological Society v. 8th Annual Fall Field Conference Guidebook, p. 102-108.

McFeeters, S. K., 1996, The use of the Normalized Difference Water Index (NDWI) in the delineation of open water features: International Journal of Remote Sensing, v. 17, no. 7, p. 1425-1432. DOI: 10.1080/01431169608948714.

Meten, M., Bhandary, N. P., and Yatabe, R., 2015, Application of GIS-based fuzzy logic and rock engineering system (RES) approaches for landslide susceptibility mapping in Selelkula area of the Lower Jema River Gorge, Central Ethiopia: Environmental Earth Sciences, v. 74, no. 4, p. 3395-3416. DOI: 10.1007/s12665-015-4377-8.

Mittal, S. K., Singh, M., Kapur, P., Sharma, B. K., and Shamshi, M. A., 2008, Design and development of instrumentation network for landslide monitoring and issue an early warning: Journal of Scientific and Industrial Research, v. 67, no. 5, p. 361-365.

Moore, G. E., 2004, Mines, mountain roads, and rocks: Geologic road logs of the Ouray area, Ouray Historical Society, v. 1.

Nandi, A., and Shakoor, A., 2010, A GIS-based landslide susceptibility evaluation using bivariate and multivariate statistical analyses: Engineering Geology, v. 110, no. 1, p. 11-20. DOI: 10.1016/j.enggeo.2009.10.001.

Otto, J.C., and Smith, M. J., 2013, Geomorphological mapping: Geomorphological techniques (online edition). British Society for Geomorphology, London, ISSN, p. 2047-0371.

Panizza, M., 1978, Analysis and mapping of geomorphological processes in environmental management: Geoforum, v. 9, no. 1, p. 1-15. DOI: 10.1016/0016-7185(78)90020-9.

Parsa Sadr, M., Hassani, H., and Maghsoudi, A., 2014, Slope instability assessment using a weighted overlay mapping method; a case study of Khorramabad-Doroud railway track, W Iran: Journal of Tethys, v. 2, no. 3, p. 254-271.

Pearson, K., 1901, LIII. On lines and planes of closest fit to systems of points in space: Philosophical Magazine Series 6, v. 2, no. 11, p. 559-572.

Perez-Pena, J. V., Azanon, J. M., and Azor, A., 2009, CalHypso; an ArcGIS extension to calculate hypsometric curves and their statistical moments; applications to drainage basin analysis in SE Spain: Computers & Geosciences, v. 35, no. 6, p. 1214-1223. DOI: 10.1016/j.cageo.2008.06.006.

Petley, D., 2010, On the impact of climate change and population growth on the occurrence of fatal landslides in South, East and SE Asia: Quarterly Journal of Engineering Geology and Hydrogeology, v. 43, no. 4, p. 487-496. DOI: 10.1144/1470-9236/09-001.

Petley, D., 2012, Global patterns of loss of life from landslides: Geology, v. 40, no. 10, p. 927-930. DOI: 10.1130/G33217.1.

Pradhan, B., Lee, S., and Buchroithner, M. F., 2010, A GIS-based back-propagation neural network model and its cross-application and validation for landslide susceptibility analyses: Computers, Environment and Urban Systems, v. 34, no. 3, p. 216-235. DOI: 10.1016/j.compenvurbsys.2009.12.004.

Ram Mohan, V., Jeyaseelan, A., Raj, T. N., Narmatha, T., and Jayaprakash, M., 2011, Landslide susceptibility mapping using frequency ratio method and GIS in south eastern part of Nilgiri District, Tamilnadu, India: International Journal of Geomatics and Geosciences, v. 1, no. 4, p. 951-961. www.ipublishing.co.in/jggsvol1no12010/EIJGGS2052.pdf.

Reed, J., 2013, Analysis Of The Mechanics Of The Ouray, CO Landslide [B.S.: Texas A&M University.

Regmi, N. R., Giardino, J. R., and Vitek, J. D., 2010, Modeling susceptibility to landslides using the weight of evidence approach; western Colorado, USA: Geomorphology, v. 115, no. 1-2, p. 172-187. DOI: 10.1016/j.geomorph.2009.10.002.

Reisz, E., 1962, Principles of Cartography, McGraw-Hill Book Company, Inc., New York.

Rose, J., and Smith, M. J., 2008, Glacial geomorphological maps of the Glasgow region, western central Scotland: Journal of Maps, v. 4, no. 1, p. 399-416. DOI: 10.4113/jom.2008.1040.

Sahlin, E. A. U., and Glasser, N. F., 2008, A geomorphological map of Cadair Idris, Wales: Journal of Maps, v. 4, no. 1, p. 299-314. DOI: 10.4113/jom.2008.1011.

Santi, P. M., Russell, C. P., Higgins, J. D., and Spriet, J. I., 2009, Modification and statistical analysis of the Colorado rockfall hazard rating system: Engineering Geology, v. 104, no. 1, p. 55-65. DOI: 10.1016/j.enggeo.2008.08.009.

Schleier, M., Bi, R., Rohn, J., Ehret, D., and Xiang, W., 2014, Robust landslide susceptibility analysis by combination of frequency ratio, heuristic GIS-methods and ground truth evaluation for a mountainous study area with poor data availability in the Three Gorges Reservoir area, PR China: Environmental Earth Sciences, v. 71, no. 7, p. 3007-3023. DOI: 10.1007/s12665-013-2677-4.

Schumm, S. A., 1956, Evolution of drainage systems and slopes in badlands at Perth Amboy, New Jersey: Bulletin of the Geological Society of America, v. 67, no. 5, p. 597-646. DOI: 10.1130/0016-7606(1956)67[597:EODSAS]2.0CO;2.

Schuster, R. L., 1996, Socioeconomic significance of landslides: Landslides: Investigation and Mitigation. Washington (DC): National Academy Press. Transportation Research Board Special Report, v. 247, p. 12-35.

Shahabi, H., Hashim, M., and Bin Ahmad, B., 2015, Remote sensing and GIS-based landslide susceptibility mapping using frequency ratio, logistic regression, and fuzzy logic methods at the central Zab Basin, Iran: Environmental Earth Sciences, v. 73, no. 12, p. 8647-8668. DOI: 10.1007/s12665-015-4028-0.

Sidle, R. C., Ghestem, M., and Stokes, A., 2014, Epic landslide erosion from mountain roads in Yunnan, China–challenges for sustainable development: Natural Hazards and Earth System Sciences, v. 14, no. 11, p. 3093-3104. DOI: 10.5194/nhess-14-3093-2014.

Small, E. E., 1995, Hypsometric forcing of stagnant ice margins: Pleistocene valley glaciers, San Juan Mountains, Colorado: Geomorphology, v. 14, no. 2, p. 109-121. DOI: 10.1016/0169-555X(95)00052-3.

Steven, T., and Hail Jr, W., 1989, Geologic map of the Montrose 30'x 60'Quadrangle, southwestern Colorado: U.S. Geological Survey, Miscellaneous Investigations Series Map I-1939, scale 1:24,000.

Stoffel, M., Tiranti, D., and Huggel, C., 2014, Climate change impacts on mass movements - Case studies from the European Alps: Science of the Total Environment, v. 493, p. 1255-1266. DOI: 10.1016/j.scitotenv.2014.02.102.

Strahler, A. N., 1952, Hypsometric (area-altitude curve) analysis of erosional topography: Bulletin of the Geological Society of America, v. 63, no. 11, p. 1117-1141. DOI: 10.1130/0016-7606(1952)63[1117:HAAOET]2.0CO;2.

Stroeven, A. P., Hättestrand, C., Heyman, J., Kleman, J., and Morén, B. M., 2013, Glacial geomorphology of the Tian Shan: Journal of Maps, v. 9, no. 4, p. 505-512. DOI: 10.1080/17445647.2013.820879.

Teza, G., Galgaro, A., Zaltron, N., and Genevois, R., 2007, Terrestrial laser scanner to detect landslide displacement fields: a new approach: International Journal of Remote Sensing, v. 28, no. 16, p. 3425-3446. DOI: 10.1080/01431160601024234.

Thornbury, W. D., 1965, Regional geomorphology of the United States, John Wiley and Sons, Inc., 609 p.

Toney, J. L., and Anderson, R. S., 2006, A postglacial palaeoecological record from the San Juan Mountains of Colorado USA: fire, climate and vegetation history: The Holocene, v. 16, no. 4, p. 505-517. DOI: 10.1191/0959683606hl946rp.

Van Westen, C. J., Van Asch, T. W. J., and Soeters, R., 2006, Landslide hazard and risk zonation - Why is it still so difficult?: Bulletin of Engineering Geology and the Environment, v. 65, no. 2, p. 167-184. DOI: 10.1007/s10064-005-0023-0.

Vandewater, C. J., Dunne, W. M., Mauldon, M., Drumm, E. C., and Bateman, V., 2005, Classifying and assessing the geologic contribution to rockfall hazard: Environmental & Engineering Geoscience, v. 11, no. 2, p. 141-154. DOI: 10.2113/11.2.141.

Varnes, H. D., 1949, Landslide problems of southwestern Colorado: U.S. Geological Survey Circulation, v. 31, p. 13. https://pubs.usgs.gov/circ/1949/0031/report.pdf.

Verstappen, H. T., 2011, Old and new trends in geomorphological and landform mapping: Geomorphological Mapping: methods and applications, v. 15, p. 13-38. DOI: 10.1016/B978-0-444-53446-0.00002-1.

Vitek, J. D., Giardino, J. R., and Fitzgerald, J. W., 1996, Mapping geomorphology: A journey from paper maps, through computer mapping to GIS and Virtual Reality: Geomorphology, v. 16, no. 3, p. 233-249. DOI: 10.1016/S0169-555X(96)80003-1.

Warrick, J., and Ritchie, A., 2017, Preliminary Mapping of the Mud Creek Landslide with 4D Photogrammetry: U.S. Geological Survey. Preliminary Report. https://walrus.wr.usgs.gov/remote-sensing/USGS_RSCC_MudCreek_CACoast_2017_June13_LoRes.pdf.

Western Regional Climate Center, 2016. https://wrcc.dri.edu/cgi-bin/cliMain.pl?co8204.

Wilson, P., 2009, Rockfall talus slopes and associated talus-foot features in the glaciated uplands of Great Britain and Ireland: periglacial, paraglacial or composite landforms?: Geological Society, London, Special Publications, v. 320, no. 1, p. 133-144. DOI: 10.1144/SP320.9.

Yilmaz, I., 2009, GIS based statistical and physical approaches to landslide susceptibility mapping (Sebinkarahisar, Turkey): Bulletin of Engineering Geology and the Environment, v. 68, no. 4, p. 459-471. DOI: 10.1007/s10064-009-0188-z.

Youssef, A. M., Pradhan, B., Jebur, M. N., and El-Harbi, H. M., 2015, Landslide susceptibility mapping using ensemble bivariate and multivariate statistical models in Fayfa area, Saudi Arabia: Environmental Earth Sciences, v. 73, no. 7, p. 3745-3761. DOI: 10.1007/s12665-014-3661-3.

Yusof, N. M., and Pradhan, B., Landslide susceptibility mapping along PLUS expressways in Malaysia using probabilistic based model in GIS, *in* Proceedings 7th IGRSM International Conference and Exhibition on Remote Sensing and GIS, IGRSM 2014, April 21, 2014 - April 22, 2014, Kuala Lumpur, Malaysia, 2014, Volume 20, Institute of Physics Publishing, p. Antaragrafik Systems Sdn. Bhd.; Geospatial Media and Communications Sdn. Bhd.

Zhu, A., Wang, R., Qiao, J., Qin, C., Chen, Y., Liu, J., Du, F., Lin, Y., and Zhu, T., 2014, An expert knowledge-based approach to landslide susceptibility mapping using GIS and fuzzy logic: Geomorphology, v. 214, p. 128-138. DOI: 10.1016/j.geomorph.2014.02.003.

APPENDIX A

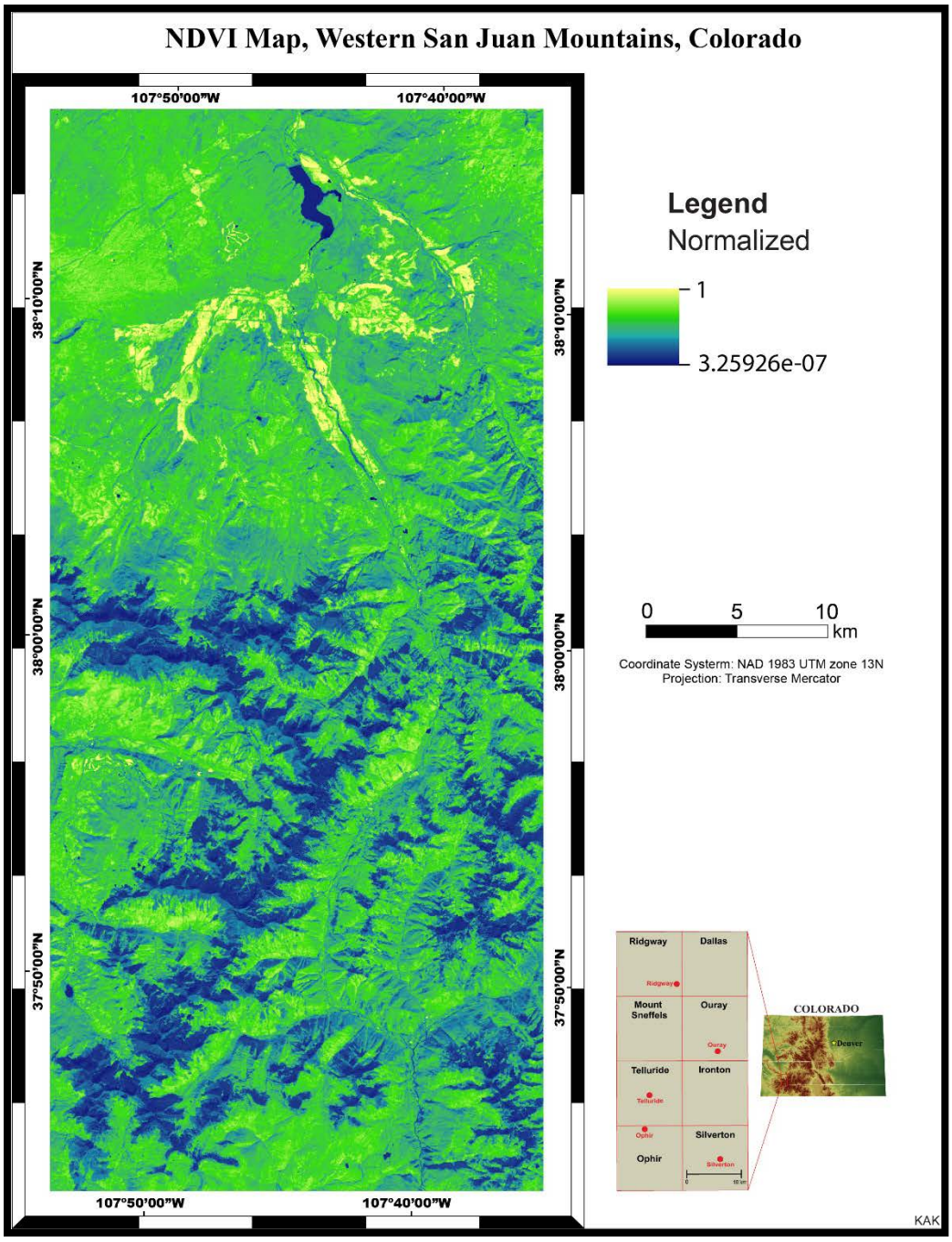

Figure A-1: NDVI map of the western San Juan Mountains.

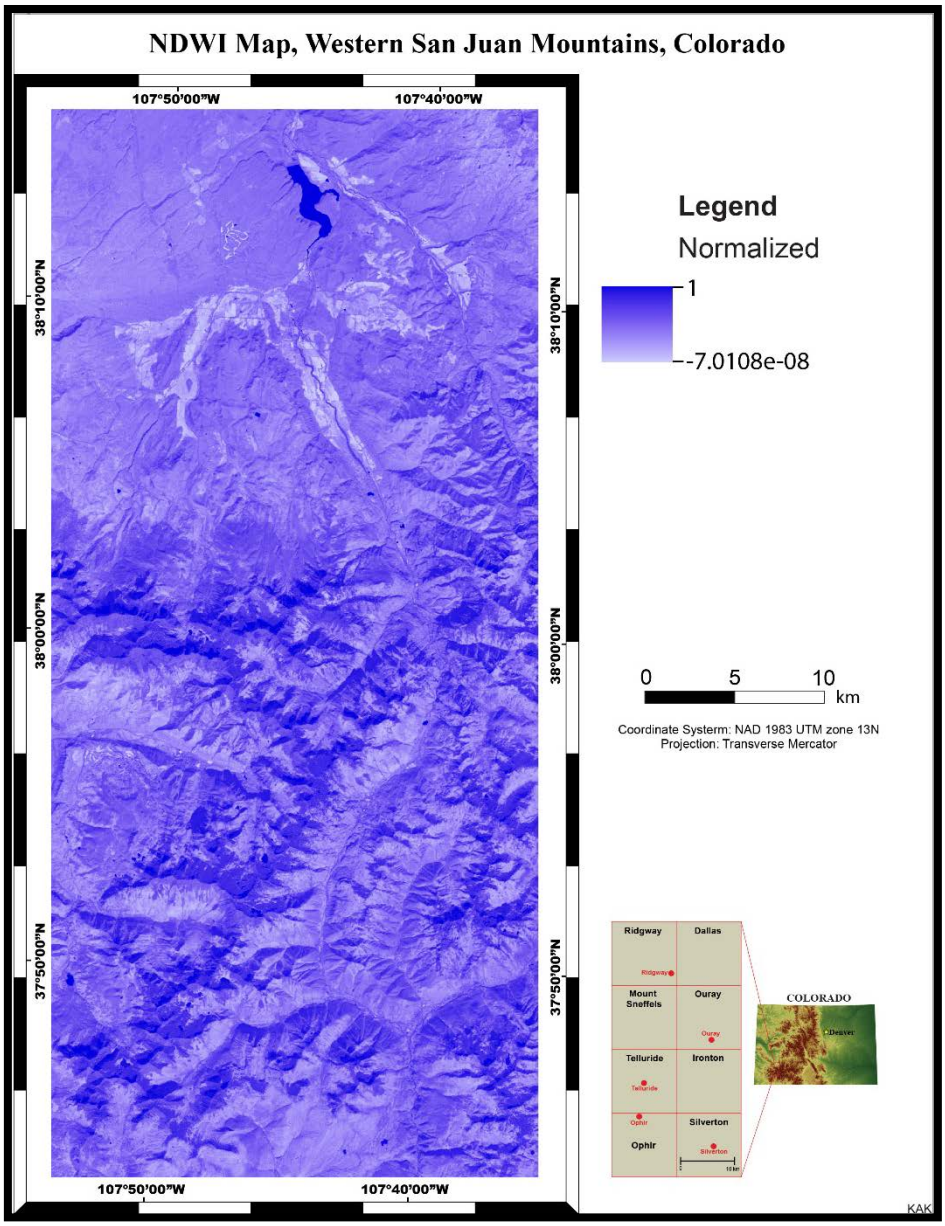

Figure A-2: NDWI map of the western San Juan Mountains.

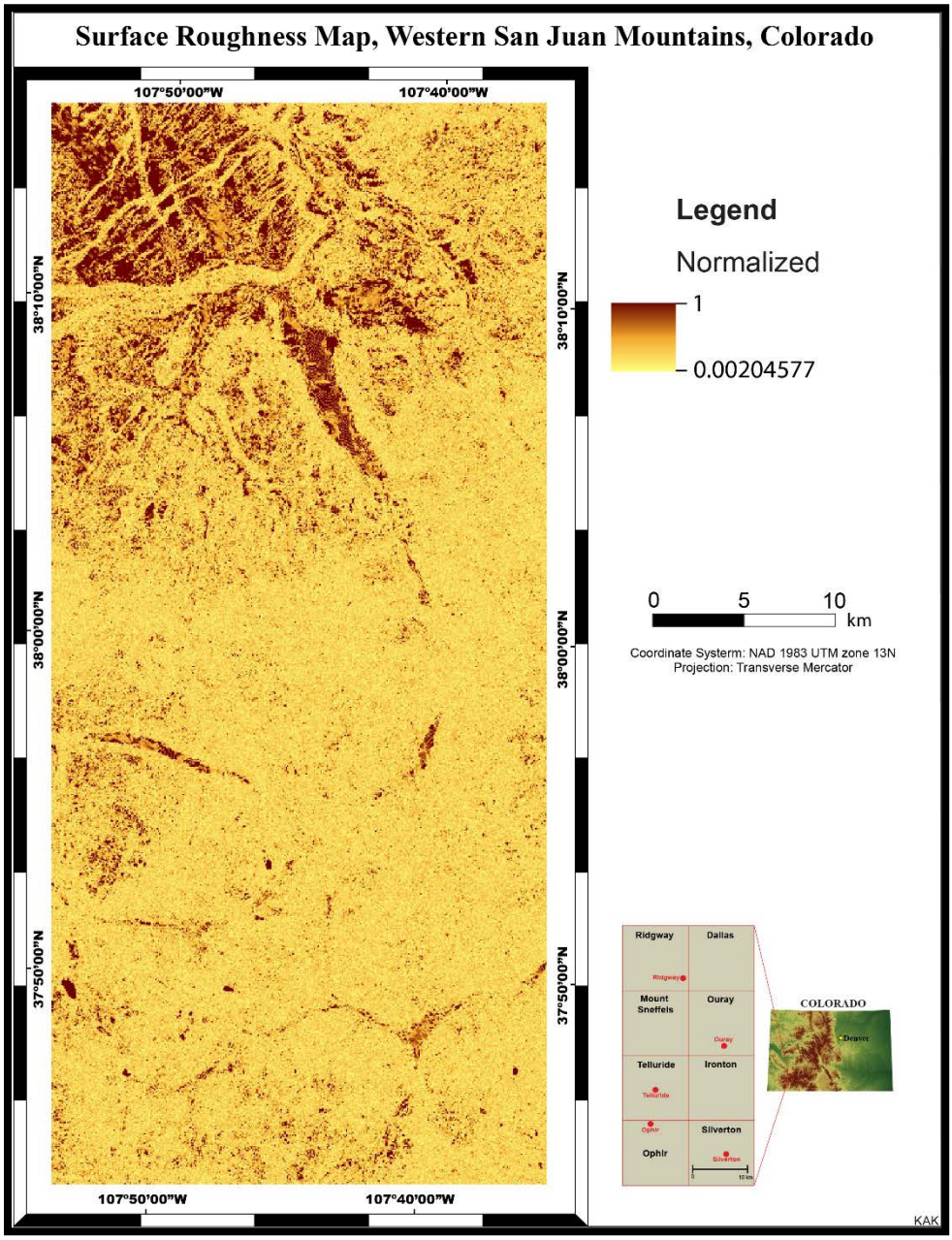

Figure A-3: Surface roughness map of the western San Juan Mountains.

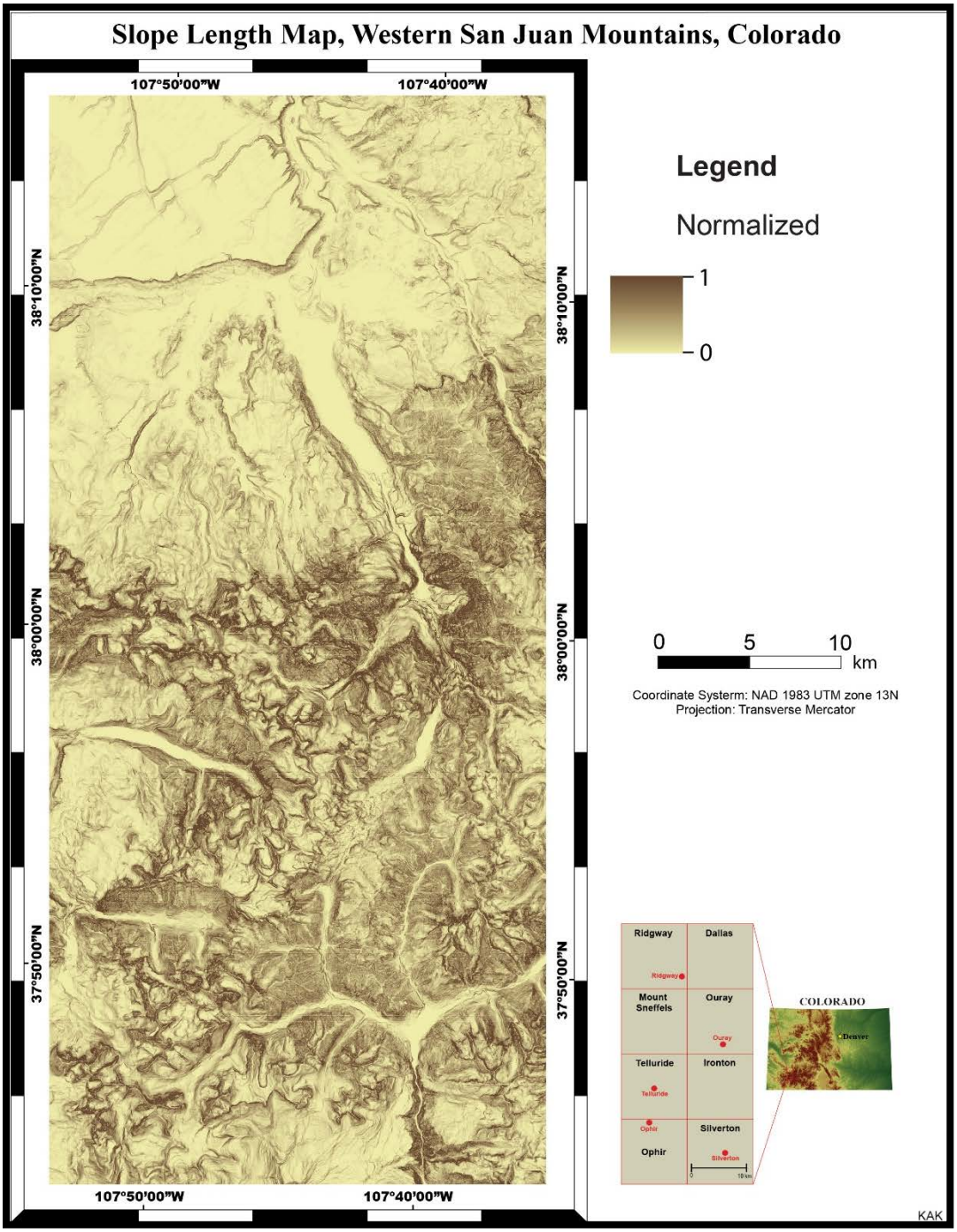

Figure A-4: Slope length map of the western San Juan Mountains.

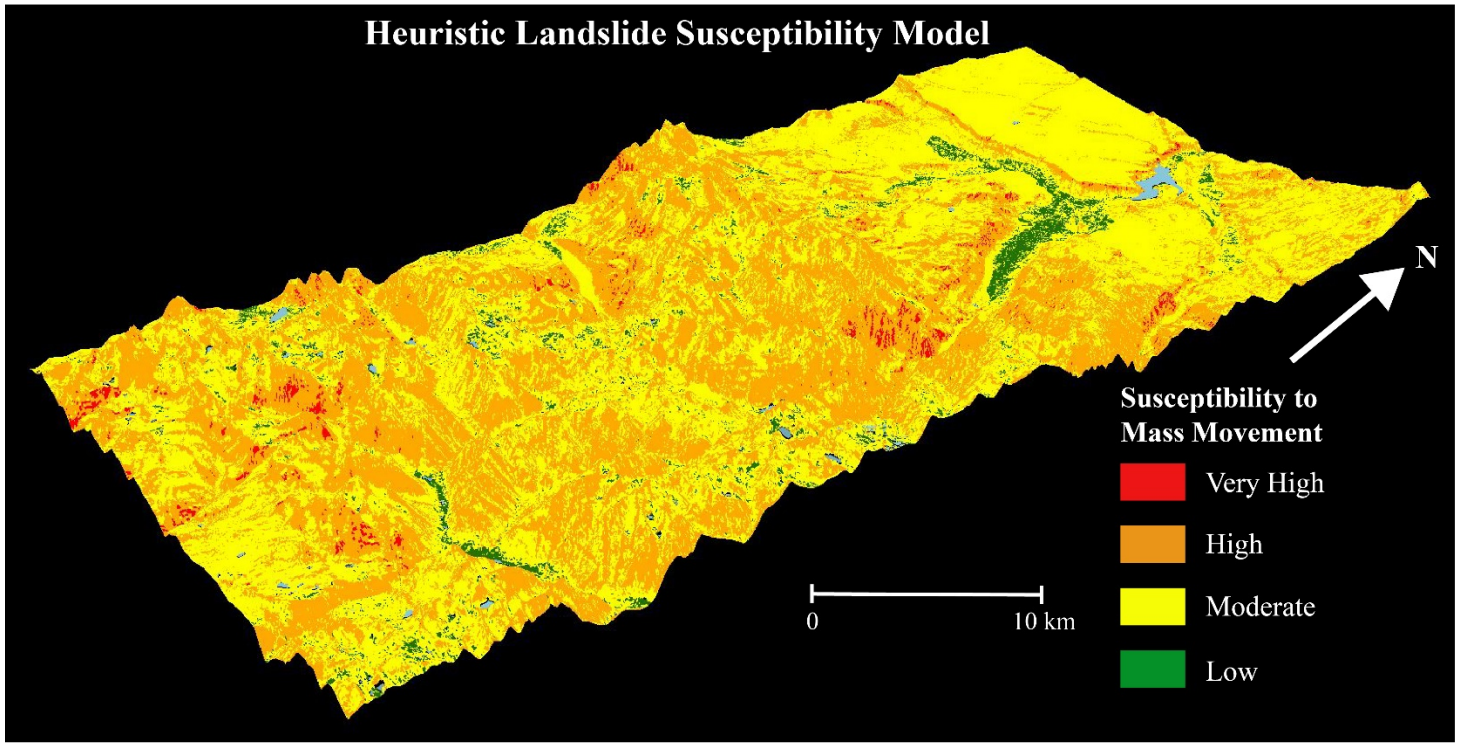

Figure A-5: Heuristic-based map in 3-D of susceptibility to landslides.

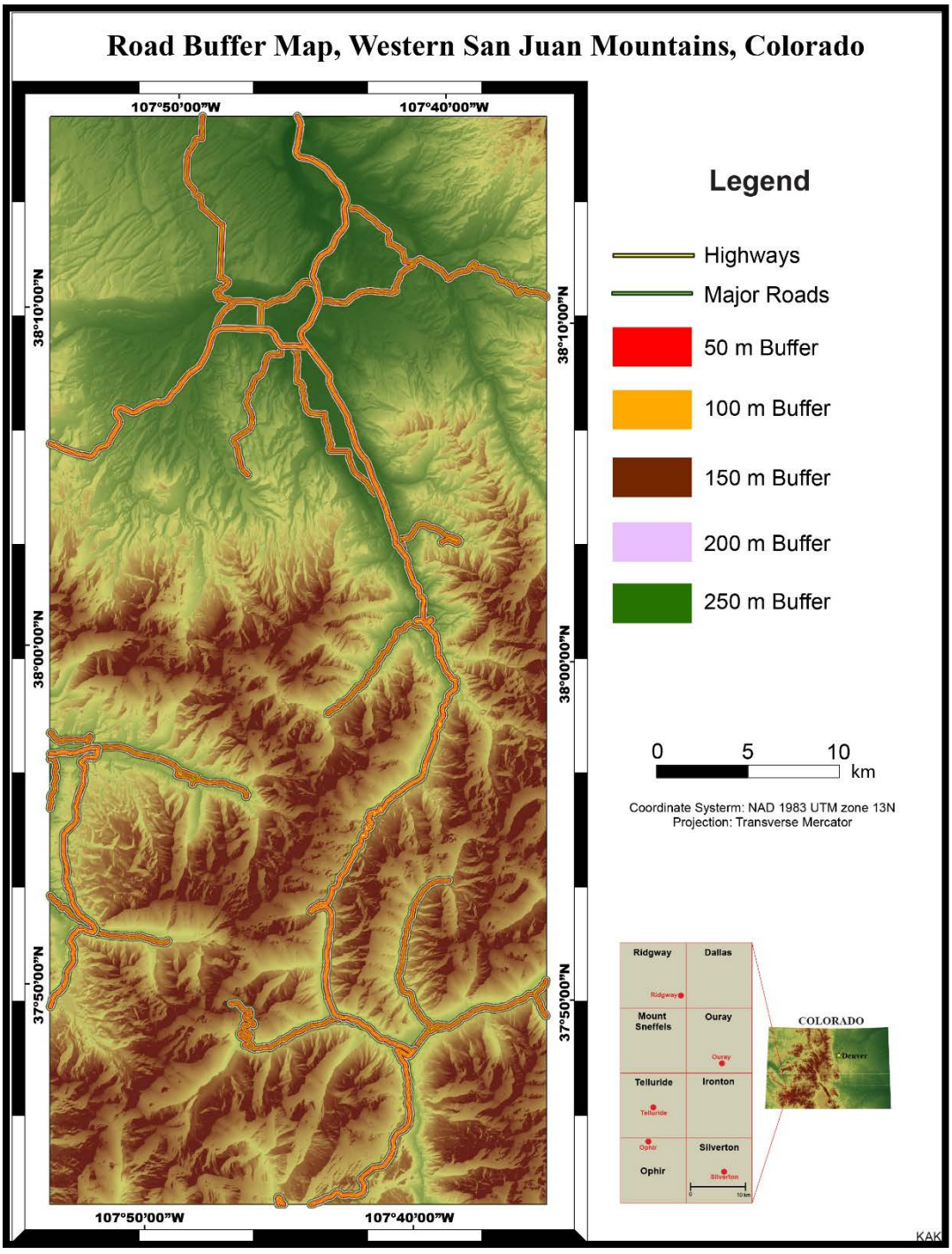

Figure A-6: Road buffer map used to identify potential damage to roads.

APPENDIX B

Figure B-1: Screenshot of video simulating the deglaciation on the San Juan Mountains.

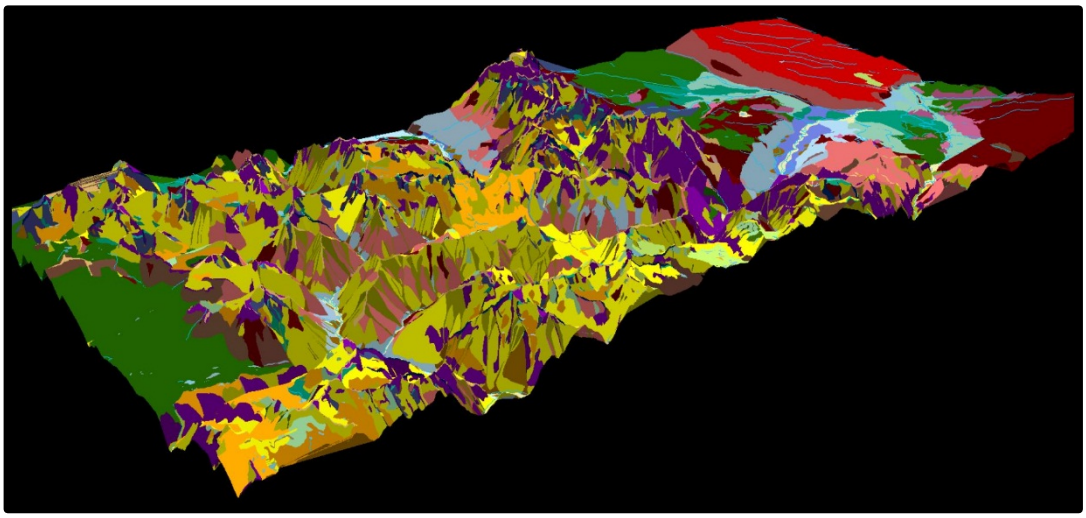

Figure B-2: The geomorphological map of the western San Juan Mountains in 3D.

APPENDIX C

Figure C-1: Avalanche shed on U.S. Highway 550 (08/13/15).

Figure C-2: Image of rock mesh installed on U.S. Highway 550 to prevent rockfall (08/07/15).

Figure C-3: Cascade creek flume built to divert and minimize hazards from debris flows.

APPENDIX D

Supplemental Video Files Information

- Kelkar_SJM_PCA.mp4: A 360 degree panorama of the PCA-based landslide susceptibility map.
- Kelkar_SJM_flyby.mp4: A virtual fly-by of the study area provides the viewer a dynamic true-to-life perspective of the active landscape.
- Kelkar_SJ_heuristicvideo.avi: 360 degree perspective of the heuristic-based landslide susceptibility map.
- Kelkar_SJ_Geomorphic.avi: A 3-D rendition of the mapped surficial and geomorphic features in the study area.
- Kelkar_SJ_Deglaciation.avi: An animation displaying the deglaciation of the area which led to the over steepening of slopes in the region.

APPENDIX E

Name: Kaytan Anand Kelkar

Address: Texas A&M University
Department of Geology and Geophysics
College Station, Texas 77843-3115

Email Address: kaytank@tamu.edu

Education: B.S., Geology, University of California, Riverside, USA, 2011
M.S., Geology, Texas A&M University, USA, 2017